The Streamwise Development of Two-Dimensional Wall Jets and Other Two-Dimensional Turbulent Shear Flows

By

Ian S. Gartshore

A thesis submitted to the Faculty of Graduate Studies and Research in partial fulfilment of the requirements for the degree of Doctor of Philosophy.

Department of Mechanical Engineering

McGill University

Montreal, P.Q.

August, 1965

SHORT TITLE

STREAMWISE DEVELOPMENT OF TWO-DIMENSIONAL TURBULENT SHEAR FLOWS

Ian S. Gartshore August 1965

SUMMARY

This thesis presents the formulation, evaluation and application of a method for predicting the streamwise development of turbulent shear flows, and the three chapters relate respectively to these three aspects of the work.

The theoretical analysis of Chapter I is based on the energy equilibrium hypothesis and relates the turbulent shear stress to the mean rates of strain in the flow. The streamwise developments of wall jets, free jets, wakes and other similar shear flows can be predicted using this analysis.

Two groups of measurements are presented in Chapter II: the first provides verification of the energy equilibrium hypothesis through intermittency measurements in a variety of shear flows; the second supplies measured mean flow developments which can be compared directly with the theoretical predictions of Chapter I.

Chapter III presents an application of the wall jet analysis in predicting the point of separation of a boundary layer, augmented by blowing, on an aerofoil with a trailing edge flap. The effects and requirements of a blowing slot located near the leading edge or, alternatively, near the flap wing junction, have been examined theoretically and the minimum blowing momentum required to suppress separation completely has been found for a variety of flap deflection angles.

.../iii

PREFACE

The author would like to thank Dr. B.G. Newman for his continuing interest, his valuable suggestions and for the thoughtful criticism which he has offered during the course of this work. Messrs. Gustavsen and Hansen were responsible for the excellent construction of the apparatus used and for many practical suggestions concerning its design.

Mr. E.R. Funke of the National Research Council (Ottawa) designed one of the electrical circuits used for measuring intermittency and gave expert advice during the associated calculations; his help is gratefully acknowledged. Thanks are also due to Mr. L. Vroomen of McGill University for his assistance with various instrumentation problems, and to Miss V. Quinlan for typing the text of this thesis.

Financial support has been provided by a National Research Council studentship and by the Defense Research Board under Grant Number 9551-12.

.../iv

TABLE OF CONTENTS

			Page
	Summary		
	Preface		
	Nomenclature for main text		
Chapter I		The Basis for Predictions of the Streamwise Development of Turbulent Shear Flow	
	1.1.1	Introduction	1
	1.1.2	Methods of Analysis	3
	1.2	The Turbulent Shear Stress in the outer region of a turbulent shear flow	
		1.2.1 Energy equilibrium of the large eddies	7
		1.2.2 The scale of the large eddies	11
		1.2.3 A discussion of the theory for the outer region	18
	1.3	The inner region of a turbulent wall jet	24
	1.4	The application of the double integral method	30
Chapter II		Experimental Investigations and Comparisons of Measured and Calculated Results	
	2.1	Introduction	33
	2.2	Intermittency measurements and the verification of large eddy equilibrium	
		2.2.1 The measurement of intermittency	36
		2.2.2 The experimental verification of large eddy equilibrium and a discussion of intermittency results	40

.../v

	2.3	Wall jets in streaming flow	50
	2.4	The self-preserving wake	53
	2.5	The free jet in uniform streaming flow	57
	2.6	The asymmetric jet in uniform streaming flow	60
	2.7	The mixing layer	68
	2.8	Concluding summary for Part II	73
Chapter III		An Application of the Wall Jet Analysis: Separation Control on an Aerofoil with Trailing Edge Flap	
	3.1	Introduction	77
	3.2	The external pressure distribution	78
	3.3	The initial conditions for the calculations	80
	3.4	Results and discussion	86
	3.5	Summary and Conclusions	94

Tables I to III

List of References

Appendices 1 to 8

Figures A1 to A14

Figures 1 to 37

Note: due to an error in pagination, pages numbered 42 and 44 do not appear in the main text.

NOMENCLATURE FOR MAIN TEXT

Coordinates x, y, z with corresponding mean velocities U,V,W and turbulent velocities u,v,w

A, B - mean rates of strain $\frac{\partial U}{\partial y}$ and $\frac{\partial U}{\partial x}$ respectively

b - slot width

C - constant in equation (12)

c - chord of aerofoil

C_p - pressure co-efficient $\frac{p-p_{\infty}}{1/2 \rho U_{\infty}^2}$; equation (41)

d - dimension of wake forming body

H - shape factor δ^*/θ

k - natural logarithm of 2

k_1, k_2 constants defined following equation (21)

L_o - length scale of mean motion

L - length scale of large eddies in turbulent motion

L_U, L_L - mean motion length scales of asymmetric jet; see equation (31) and Fig. 1.

m - exponent in variation of velocity scale for self-preserving flow

n - exponent of equations (13) or (48)

p - mean static pressure

p_{∞} - mean total pressure in the free stream

p_{atm} - atmospheric pressure

R_T - $\left\{(U_o L_o)/\nu_T\right\}_{@ L_o}$

R_{T_o} - value of R_T when B = 0

R_T^* - non-dimensional shear stress in inner region; equation (14)

T - life of large eddy; equation (10^A)

.../vii

U_o - velocity scale of mean motion

u' - velocity scale of large eddies in turbulent motion

U_1 - local velocity outside turbulent shear region

U_M - maximum or minimum velocity; see Figure 1

U_∞ - free stream velocity

U_τ - $(\frac{\tau_o}{\rho})^{1/2}$

U_j - velocity on centre-line of jet at slot

x_o - virtual origin of mean flow development

$Y(t)$ - instantaneous position of viscous super layer

y_s - nominal thickness of boundary layer just upstream of a blowing slot

y_M - value of y at which the mean velocity is a maximum

$y_{M/2}$ - value of y at which the mean velocity is the average of U_1 and U_M

GREEK LETTERS

β - constant defined by equation (10^A)

γ - intermittency factor

δ_M^* - displacement thickness defined in equation (14)

δ^* - usual displacement thickness based on velocity U_1

δ - nominal thickness of boundary layer

η - y/L_o or $\frac{y-y_M}{L_o}$ if $y_M \neq 0$.

η_1 - flap angle measured from main chord of aerofoil

θ - usual momentum thickness based on velocity U_1

θ' - co-ordinate angle defined by equation (42)

Λ - parameter for evaluating rate of change of equilibrium; equation (13)

.../viii

λ - defined by equation (39)

ν_{T_m} - mean value of eddy viscosity in outer part of flow

ν_T - virtual or eddy viscosity; $\nu_T = - \frac{\overline{uv}}{\partial U/\partial y}$

ξ - variable defined in equation (21)

ρ - density, assumed constant throughout the thesis

σ - standard deviation of free viscous superlayer position

τ_o - shear stress at y = 0

$\Phi = \left\{\frac{\overline{uv}}{U_\tau^2}\right\}_{@\, L_o}$ in equation (15)

$\omega_x, \omega_y, \omega_z$ - vorticity components in x, y, z, directions, respectively.

ω_{x_1}, etc. - value of ω_x etc. when B = 0

ω_{x_o}, etc. - value of ω_x etc. when t = 0

Subscripts:

M - refers to values at point of maximum velocity for jets and wall jets or minimum velocity for wakes

$@\, L_o$ - refers to values at $y = y_M + L_o$ (or $y = L_o$ if $y_M = 0$).

$@\, y_M$ - refers to values at $y = y_M$

1,2 in section 3.3 refer to original and fully developed profiles respectively.

CHAPTER I. THE BASIS FOR PREDICTIONS OF THE STREAMWISE DEVELOPMENT OF TURBULENT SHEAR FLOW

1.1.1 INTRODUCTION

Although much effort has been expended during the past half century in attempts to predict the streamwise development of turbulent shear flows, no confident predictions can yet be made for a general shear flow without recourse to experimental information obtained from a nearly identical situation. An exception to this statement may perhaps be made for a particular group of shear flows, the so-called self-preserving or self-similar cases, for which exponents can be found which describe the variation of mean quantities with the streamwise co-ordinate. One self-preserving flow cannot be related to another however, and experimental information is still necessary in each case to complete the description of streamwise development. In consequence this facility with particular cases, although valuable for fully and nearly self-preserving flows, has not yet led to a broad basis from which a general flow development can be predicted.

It is encouraging to find, however, that whenever a self preserving form of the equation of motion is physically possible, a self preserving flow does occur. This observation implies a tendency in real flows towards self preservation and suggests that a technique for determining the streamwise development of a general case might be based on the assumption of local self preservation or local moving equilibrium. The

.../2

validity of this approach clearly depends on the rates of change of external conditions in comparison with the rate at which the flow can adjust to these conditions.

The assumption of local energy equilibrium is made in the analysis presented in Chapter I of this thesis (see section 1.2 in particular) where the restrictions to this method are also discussed. The parameter which describes a particular local equilibrium condition and the variable against which this parameter can most usefully be correlated, will appear in the analysis. These are neither unique, nor are they obvious. One might suspect however that a non-dimensional form of the shear stress could be used to compare the fully self-preserving cases and therefore to identify the local equilibrium at some streamwise station in a non-self-preserving case.

Many of the ideas in the first chapter are contained in, or stem from, the monograph of Townsend "The Structure of Turbulent Shear Flow" (ref. 7). Reference should also be made to the previous reports by the present author (refs. 8, 9, 10) of which this thesis is intended to be a summary and extension.

The analysis of Chapter I is evaluated in Chapter II, first by an experimental examination of the energy equilibrium hypothesis and second by comparison between measured and calculated mean flow developments of wall jets, free jets, self-preserving wakes, and asymmetric free jets.

The final chapter of this thesis, Chapter III, applies the analysis to predict the streamwise development of the wall jet which forms on an aerofoil on which blowing is used for

.../2a

boundary layer control. A flat plate with trailing edge flap is used to represent the aerofoil in the calculations and various slot sizes and flap angles are investigated for zero angle of incidence of the main chord.

Constant fluid density and temperature are assumed throughout this thesis.

1.1.2. METHODS OF ANALYSIS

The success of the self-preservation concept in the analysis of the few flows to which it applies tempts one to force the form of self preservation onto flows which neither satisfy the assumptions nor exhibit the features of full self preservation. For example, it might be thought that a free jet in a uniform streaming flow (a non-self-preserving case) might be "transformed" to a free jet in still air (a self-preserving case) by viewing the flow from a co-ordinate system moving with the external stream velocity. Although initially attractive it is clear that the flow of a jet in a uniform stream, viewed from such co-ordinates, is unsteady and is not self-preserving. The analyses presented by Kucheman and Weber (ref.1), Abramovich (ref.2) Ribner (ref.3) and Eskinazi (ref.4) do not formally transform co-ordinates, but all use relative velocities or relative distances in order to place the data from non-self-preserving flows within the more successful framework of self preservation.

As an example, the reasoning of Abramovich (ref.2) for the analysis of a free jet in uniform streaming flow, is summarized below. It extends the arguments given by Schlichting for the analysis of a free jet in still air.

The rate of increase of jet width is assumed to be proportional to a transverse turbulent velocity intensity, provided that a total derivative, or derivative following the motion, is used in defining the rate of increase. The total derivative is put equal to $\frac{1}{2}(U_1 + U_M)\frac{d}{dx}$ where U_1 and U_M are

.../4

the external and maximum flow velocities respectively, and $\frac{1}{2}(U_1 + U_M)$ is therefore an average streamwise velocity in the jet. By assuming that the transverse turbulent intensity is proportional to $(U_M - U_1)$, Abramovich completes his equation, which now relates the rate of increase of the jet width (using a usual derivative $\frac{d}{dx}$) to the ratio $\frac{U_1}{U_M}$. The final equation adequately describes certain experimental data (see ref. 2^A) but its usefulness should not disguise the apparently insecure foundation on which it is built.

These techniques, although possible useful, ultimately amount to data correlations. The present work is directed as much toward a greater understanding of turbulent shear flows as toward a more adequate correlation of their principal features.

Squire and Trouncer (5) have presented an analysis of a jet in uniform streaming flow. For this non-self-preserving flow, they used momentum integral methods and were able to predict the streamwise variation of width and maximum velocity by assuming a mixing length proportional to the width of the flow. Unfortunately, subsequent experimental measurements (ref.6) indicated that the analysis of ref. 5 oversimplifies the physical situation.

Bradbury (ref.14) has made measurements of a jet in uniform streaming flow and, independently of the present work, compared these measurements with values calculated on the basis of local energy equilibrium. He concluded that the turbulent structure was not able to respond rapidly enough to approach local equilibrium in this non-self-preserving flow. Bradbury's

objections to this concept, as applied to a jet in uniform streaming flow, are considered in section 2.5 together with his measured data.

The distributions of the streamwise component of mean velocity in all two dimensional free turbulent shear flows, differ very little from each other. Reichardt's well known theory of turbulence is based on this observation. The close similarity of these velocity profiles suggests the use of an integral approach to the problem. The method used by Squire and Trouncer (5), that of writing several momentum integrals each with different limits, has an advantage over other integral approaches in that the shear stress must be known only at the limits of the integrals used and not throughout the flow. This method has been used in the analysis outlined in section 2 of this thesis, and is hereafter designated at the "double integral" approach, as a means of identification. Its application to free shear flows is discussed in section 1.4, and to boundary layers in Appendix III. The analysis of sections 1.2 and 1.3 derives expressions for the shear stress at the limits of the integrals used in the double integral approach.

The two major postulates of the analysis to be presented are:

i. that the shear stress in the flow may be related to the scale of the largest eddies by the energy equilibrium hypothesis (see ref.7).

ii. that the scale of the largest eddies may be predicted by a consideration of the effect of the mean rates of strain $\frac{\partial U}{\partial y}$

and $\frac{\partial U}{\partial x}$ on the vorticity in a typical large eddy. This second assumption results in an analysis which is similar to the rapid distortion theory for isotropic turbulence described in ref. 7, and requires additional assumptions in order that a practical relationship be obtained.

These two steps in the analysis are considered in the next two subsections of this thesis.

1.2 THE TURBULENT SHEAR STRESS IN THE OUTER REGION OF A TURBULENT SHEAR FLOW

1.2.1 ENERGY EQUILIBRIUM OF THE LARGE EDDIES

Townsend (ref.7) has proposed a model for the structure of turbulent shear flow which is based upon the division of the turbulent scales of the flow into "large eddies" comparable in width to the dimension of the mean flow, and the "remaining eddies" which contain most of the turbulent energy. The distortion of the large eddies by the mean flow was postulated as the chief mechanism whereby energy is transferred from the mean to the turbulent motion, and the transfer of energy to the smaller eddies may be pictured as a repetition of the initial process but on a different scale and with increasingly random orientation.

A further proposal, that of large eddy energy equilibrium, suggested that the large eddies are in energy equilibrium through a significant part of their lives, gaining energy from the mean motion and losing energy at an equal rate to the remaining turbulent motion. The large eddies in this theory control the flow since the energy which they receive from the mean motion governs the remaining turbulent motion. Slight changes in the large eddies may result in significant changes in turbulent intensity and shear stress although the large eddies contain only a small fraction of the total turbulent energy.

Consider a large eddy with time-averaged velocity components u", v", w" in a mean velocity field whose components are U, V. The rate of gain of energy by the large eddy is given

primarily by the term $\overline{u"v"} \frac{\partial U}{\partial y}$. The loss of energy to the remaining turbulent motion may be expressed by terms like $\nu_{T_M} \cdot (u" \frac{\partial^2 u"}{\partial y^2})$ where ν_{T_M} is a mean value (averaged over a long time and over the eddy itself) of the eddy viscosity arising from the action of the remaining turbulent motion on the large eddy.

If u" and v" are characterized by a velocity scale u' and the eddy size by a length scale L, (i.e. if a self similar large eddy flow is postulated with its own length and velocity scales) the energy equilibrium hypothesis may be written as:

$$\frac{\partial U}{\partial y} (u')^2 \propto \nu_{T_M} (\frac{u'}{L})^2 \qquad (1)$$

Since ν_{T_M} is $\frac{\tau}{\rho \frac{\partial U}{\partial y}}$, this relationship is:

$$\frac{\tau}{\rho} \propto L^2 (\frac{\partial U}{\partial y})^2 \qquad (2)$$

which is equivalent to Prandtl's mixing length hypothesis except that L is now identified as the scale of the large eddies in the flow, and therefore is likely to be of the same magnitude as the length scale associated with the mean motion, L_o. For L to be proportional to L_o, an assumption commonly made in the use of the mixing length in free turbulent flows, the large eddy scale must remain a constant fraction of the mean velocity scale. This is true only of self preserving flows and even for these cases the constants of proportionality may change from one self preserving flow to another.

If the velocity scale of the mean flow is U_o, the

.../9

energy equilibrium hypothesis may then be written as:

$$\frac{\nu_{T_M}}{U_o L_o} \propto \left(\frac{L}{L_o}\right)^2 \qquad (3)$$

if $\frac{\partial U}{\partial y}$ may be represented by $\frac{U_o}{L_o}$.

Equation (3) will be used hereafter, since in all regions in which equation (1) is applied, the non-dimensionalized mean-velocity profile may be represented by a single function of y/L_o.

Equation (3) may be checked experimentally in the following manner: the scale of the largest eddies is assumed to be proportional to the standard deviation of the laminar superlayer (σ) and σ in turn is calculated from measured intermittency distributions. ν_{T_M} is represented by a value of ν_T at a typical non-dimensional ordinate Y/L_o = const., and this value of ν_T is calculated from the measured flow development. Measurements of several fully or approximately self preserving cases show that an approximately linear relationship exists between $\frac{\nu_T}{U_o L_o}$ = const., and $\left(\frac{\sigma}{L_o}\right)^2$ as anticipated by the energy equilibrium hypothesis. (See section 2.2 and fig.3 for the experimental results of this examination and for a discussion of the assumptions involved). The cases which have been investigated experimentally are:

a) wall jet in still air

b) three approximately self preserving wall jets in streaming flow

c) free jet in still air

d) small deficit wake (Townsend, ref. 11)

.../10

e) smooth wall flat plate boundary layer (Klebanoff ref.12)

f) mixing layer between uniform stream and fluid at rest.

All these are discussed in section 2.2.2.

.../11

1.2.2 The Scale of the Large Eddies

Using the vorticity equations, the interaction between a mean velocity field and a small vorticity perturbation may be calculated. The perturbation represents the large eddy motion and, with a few assumptions, the effect on the eddy vorticity of a mean shear rate of strain $\frac{\partial U}{\partial y}$ and a mean lateral rate of strain $\frac{\partial U}{\partial x}$, may be found. The derivation is summarized in the next paragraphs.

Consider a steady mean velocity field U, V, W with the properties:

$$\frac{\partial U}{\partial x} = -\frac{\partial V}{\partial y} = B$$

$$\frac{\partial U}{\partial y} = A, \quad \frac{\partial V}{\partial x} = 0$$

$$W = 0 \qquad (4)$$

where A and B may be considered constant and $\frac{A}{B} \gg 1$.

Add a small vorticity perturbation with components ω_x, ω_y, ω_z. These may also be represented by the perturbation velocity components u, v, w where $u \ll U$, $v \ll V$, $\omega \ll V$. Because the perturbation will represent a large eddy, ω_z is assumed to be an order of magnitude smaller than A, which is the only vorticity component in the mean flow. Retaining only first order quantities, the instantaneous vorticity equations become:

$$\frac{D\omega_x}{Dt} = B\,\omega_x + A\,\omega_y - A\,\frac{\partial u}{\partial z} + \nu(\nabla^2\omega_x)$$

$$\frac{D\omega_y}{Dt} = -B\,\omega_y - A\,\frac{\partial v}{\partial z} + \nu(\nabla^2\omega_y)$$

$$\frac{D\omega_z}{Dt} = -A\,\frac{\partial w}{\partial z} + \nu(\nabla^2\omega_z) \qquad (5)$$

.../12

where

$$\frac{D}{Dt} = \frac{\partial}{\partial t} + U \frac{\partial}{\partial x} + V \frac{\partial}{\partial y} + w \frac{\partial}{\partial z}$$

The terms $\frac{\partial u}{\partial z}$, $\frac{\partial v}{\partial z}$ and $\frac{\partial w}{\partial z}$ appearing in equation (5) are determined by the form of the large eddy and, for a solution to the equations, it is necessary either to assume expressions for u, v and w in terms of x, y, z and t, or to place specific restrictions on the velocity components. For simplicity and greater generality, the latter approach has been followed.

To describe the fluid motions associated with a large eddy, using equations (5), it will be assumed that at any stage in its development the large eddy may be described as a body of fluid rotating about an axis but not as a rigid body and with its particle paths not necessarily in planes normal to the axis. The inclination of the axis and the velocity components in the eddy will vary as the eddy is strained by the mean flow. The vorticity and the gradients of the velocity components on the axis itself will be assumed to represent the motion as a whole so that equation (5) will be applied specifically to the large eddy axis.

From extensive double velocity correlations measured in a small deficit wake, Grant (15) concluded that large simple eddies of the type described above could exist provided they contained no v-component of velocity. This conclusion will be applied to the other flows considered in this report since all these flows are considered to be basically similar to the wake.

For present purposes therefore, it will be assumed

that the particle paths of the large eddy are circles lying in the x-z plane. (The eddies may occur in pairs as Grant has postulated.) A direct test of this assumption would require knowledge of the large eddy form at various stages of its existence. As such information would be very difficult to obtain, the assumption will be tested only insofar as the final expression derived by its use is compared with measured data.

From the restriction which has been placed on the form of the large eddy, the following simplifications to equation (5) may be introduced:

$$\frac{\partial u}{\partial z} = \frac{1}{2}\,\omega_y,$$

$$\frac{\partial v}{\partial z} = 0,$$

$$\frac{\partial w}{\partial z} = 0.$$

(If the particle paths of the large eddy motion in the x-z plane are not exactly circular, but still retain geometric similarity throughout the life of the eddy, one may write $\frac{\partial u}{\partial z} = \alpha\,\omega_u$, where α is a constant. The following analysis is not affected by the magnitude of α provided that $\frac{A}{B}(1-\alpha)$ is large c.f. unity. The term $\frac{\partial w}{\partial z}$ is zero on the axis of any large eddy whose particle paths in the x-z plane are symmetrical about the z-axis.)

Assuming the diffusion terms (represented by $\nu(\nabla^2\omega_x)$ etc.) are negligible, equations (5) become:

$$\frac{D\omega_x}{Dt} = B\,\omega_x + \frac{1}{2}A\,\omega_y$$

$$\frac{D\omega_y}{Dt} = -B\,\omega_y$$

.../14

$$\frac{D\omega_z}{Dt} = 0. \tag{6}$$

For $\omega_y = \omega_{y_o}$, $\omega_x = \omega_{x_o}$ and $\omega_z = \omega_{z_o}$ for $t = 0$, the results (following the motion) are:

$$\omega_x = \left\{ \frac{A}{2B} (\omega_{y_o}) + \omega_{x_o} \right\} \sinh Bt + \omega_{x_o} \cosh Bt$$

$$\omega_y = \omega_{y_o} e^{-Bt}$$

$$\omega_z = \omega_{z_o} \tag{7}$$

With the same initial conditions, but $B = 0$, the vorticity components, denoted now by ω_{x_1} and ω_{y_1} are:

$$\omega_{x_1} = \frac{1}{2} A \omega_{y_o} t + \omega_{x_o}$$

$$\omega_{y_1} = \omega_{y_o}$$

$$\omega_{z_1} = \omega_{z_o}$$

Since $\frac{A}{B} \gg 1$, and assuming that ω_{x_o}, ω_{y_o} and ω_{z_o} are of the same order of magnitude, the total vorticity magnitudes become:

$$\omega = (\omega_x^2 + \omega_y^2 + \omega_z^2)^{1/2}$$

$$\approx \omega_x$$

$$\approx \frac{1}{2} \frac{A}{B} \omega_{y_o} \sinh (Bt) \tag{8}$$

and $\omega_1 = (\omega_{x_1}^2 + \omega_{y_1}^2 + \omega_{z_1}^2)^{1/2}$

$$\approx \omega_{x_1}$$

$$\approx \frac{A}{2} \omega_{y_o} t$$

The average of the vorticity during time T is:

$$\bar{\omega} = \frac{1}{T} \int_0^T \omega dt \text{ and } \bar{\omega}_1 = \frac{1}{T} \int_0^T \omega_1 dt$$

or, more crudely (considering the assumptions made, a sophisticated mean is unnecessary)

$$\bar{\omega} \propto \frac{1}{2} \frac{\sinh BT}{B} \text{ and } \bar{\omega}_1 \propto \frac{T}{2}$$

These are respectively, average vorticities over time T with and without a lateral rate of strain. Then:

$$\frac{\bar{\omega}}{\omega_1} = \frac{\sinh BT}{BT} \qquad (9)*$$

If the same initial conditions for the vorticity components are used in the presence or absence of mean lateral rate of strain, then the circulation is the same in both cases. Thus it is possible to define an average large eddy size by L or L_1 where:

$$\Gamma \propto \bar{\omega} L^2 = \bar{\omega}_1 L_1^2 = \text{const.}$$

and where subscript 1 indicates the condition wherein B = 0.

* This result differs from that of ref. 9. The change makes no difference to the calculated values because of a further approximation (equ.(12)) and is thought to represent a more correct average over time T. Ref. 9. contains the result:

$$\left(\frac{\bar{\Omega}}{\omega_1}\right) = \frac{1}{2}\left\{1 + \frac{\sinh BT}{BT}\right\}.$$

.../16

Finally then:

$$\frac{L^2}{L_o^2} = \frac{L_1^2}{L_o^2} \frac{BT}{\sinh BT}$$

or, by the energy equilibrium hypothesis of equation (3):

$$\left(\frac{\nu_{TM}}{U_o L_o}\right) = \left(\frac{\nu_{TM}}{U_o L_o}\right)_1 \frac{BT}{\sinh (BT)} \qquad (10)$$

The time T is now assumed to be a representative time scale of the large eddy and is hereafter called the "life of the large eddy". Because the diffusive mechanism has been dropped from the vorticity equations, the vorticity perturbation can increase indefinitely in the simple model. No calculation of the time T is possible from the present result; therefore, following a suggestion of Townsend's (ref.8), the time T is made inversely proportional to the derivative $\left(\frac{\partial U}{\partial y}\right)$. Thus:

$$T = \beta \left|\frac{1}{A}\right| \qquad (10\ a)$$

where β is a constant.

In order to apply equation (10) to a real shear flow, the derivatives designated by the constants A and B in equation (4) must be evaluated at some representative non-dimensional ordinate $\frac{y}{L_o}$ = constant, since obviously the derivatives $\frac{\partial U}{\partial y}$ and $\frac{\partial U}{\partial x}$ are not generally constant across a real shear flow. similarly it is convenient to use ν_T evaluated at the same non-dimensional ordinate, rather than ν_{TM}, the average value of ν_T across the flow. Finally then:

$$R_T = R_{T_o} \cdot \frac{\sinh (\beta \cdot B/|A|)}{\beta \cdot B/|A|} \qquad (11)$$

.../17

where $R_T = \frac{U_o L_o}{\nu_T}$, $R_{T_o} = \left[\left(\frac{U_o L_o}{\nu_T}\right)\right]_{B = 0}$ and both B and A are understood to be values of $\frac{\partial U}{\partial x}$ and $\frac{\partial U}{\partial y}$ respectively at the non dimensional ordinate y/L_o = constant.

For calculation purposes, it is convenient to replace the expression for R_T in equation (11) by an approximately equivalent linear expression:

$$\frac{1}{R_T} = \frac{1}{R_{T_o}} \left(1 - C \frac{B}{A}\right) \qquad (12)$$

where C is a constant.

A further discussion of the significance of the ratio $\frac{B}{A}$ and of the choice of co-ordinate system, is given in Appendix I, where a model incorporating an idealized mean flow distribution is used to illustrate the processes just described.

In the final expressions for R_T (equations 11 or 12), the two constants R_{T_o} and C, or R_{T_o} and β, must be determined experimentally. A summary of the values found for R_{T_o} and C in the various cases is given in table 1.

1.2.3 A DISCUSSION OF THE THEORY FOR THE OUTER REGION

Some of the advantages and limitations of the theory in the outer region will be presented in this section by listing and discussing the major assumptions which have been made.

i) Division of the flow into "large eddies" and the "remaining turbulent motion". The total energy of the turbulent motion at a particular point in a turbulent shear flow can, in theory at least, be divided into fractions corresponding to various length scale intervals, so that a certain fraction of the total turbulent energy is associated with motions whose scales lie between certain limits. In practice this division involves the use of Taylor's hypothesis in order to transfer from length to time scales and the use of spectral analysis by means of suitable electrical circuits.

An alternative definition and one which is more compatable with the large eddy equilibrium hypothesis, is that the "large eddies" are those associated with a certain fraction (say one tenth) of the total turbulent shear stress in the flow. By measuring the shear stress at a point with and without suitable electrical filters, one can quickly determine the frequency range which delineates the "large eddies" according to this definition. The frequency range can then be transferred to a length scale range by use of Taylor's hypothesis.

This alternative definition may depend on the axis system used to define the shear stress. It would make no difference however to the analysis of section 2.1 since the shear stress arising from the action of the "smaller eddies" would

.../19

become proportional to, instead of equal to, the total shear stress, and the final relationship (equation 3) would be unchanged.

(ii) Description of the turbulence and the energy transfer mechanisms in terms of vorticity and velocity interactions. Just as the equation of motion may be written in terms of velocity and pressure or velocity and vorticity, so the physical processes may be thought of in terms of various combinations of these quantities. The description of the turbulence in terms of vortex lines and the energy transfer in terms of vortex stretching is therefore only one of a number of possible views. The vorticity model does illustrate the present theory however and has, in large measure, formed the basis for the development outlined in the previous two sections (sections 1.2.1 and 1.2.2).

(iii) The assumption of local self preservation in a non-self-preserving flow.

As stated in the introduction (section 1.1) the validity of the assumption of local equilibrium depends on the rate of change of the conditions affecting the large eddies in comparison with the rate at which the large eddy can adapt to these changes. It is very difficult to evaluate the maximum rate at which a large eddy can respond. However, in the cases for which the analysis succeeds, it is possible to evaluate the rates of response of the large eddy which are apparently not too rapid to cause serious error. For this comparison, the parameter Λ will be used, as defined below:

$$\Lambda = \frac{\left(\frac{U_1 + U_M}{2}\right) \cdot \beta}{\left|\frac{\partial U}{\partial y}\right|_{@L_o}} \cdot \frac{\frac{d}{dx}\left(\frac{1}{R_T}\right)}{\frac{1}{R_T}} \qquad (12^A)$$

.../20

Physically Λ may be described as the fractional change in $\frac{1}{R_T}$ which would result from the continued application of the local rate of change of $\frac{1}{R_T}$ over a length $\left[U\beta/|A|\right]_{@L_o}$ This length is representative of the distance through which the large eddies travel during their existence; thus, in conditions in which local equilibrium is present, Λ represents the change in $\frac{1}{R_T}$, and therefore in the proportional large eddy size, during the life of a typical eddy. This parameter is therefore a measure of the response of the eddy during its lifetime.

The non-dimensionalized shear stress $\frac{1}{R_T}$ forms a better basis for the present comparison than would a simpler quantity such as a profile shape parameter $\Lambda^{(H)}$, although a simpler quantity would be more convenient. The shear stress is related through the equations of motion to both the profile shape and the rate of change of profile shape and therefore provides a relatively complete identification of the flow. The parameter Λ is used in section 2.5.

Mention must also be made of the possibility that other forms of equilibrium can develop as a result of the energy transfer due to turbulent normal stresses. These normal stresses are usually neglected in the equation of motion in the direction parallel to the streaming flow, but can become important in certain circumstances. (See, for example, Reynolds, ref. 13.)

(iv) The assumptions and restrictions concerning the form of the large eddy.

The close similarity for different self preserving shear flows of the mean velocity distributions suggests that the

.../21

organization of the larger scales of the turbulent motion (which are those most directly affected by the organization of the mean rates of strain) is similar from one self preserving case to another. Provided that the assumption of local equilibrium is valid, the self similarity of the turbulent motion should be a reasonable approximation for non self preserving cases as well. This assumption, together with the restrictions placed on the form of large eddy motion (section 1.2.2) are intended to be as general as possible and yet sufficiently specific to obtain a result. The restrictions placed on the large eddy motion do not explain all of the velocity correlations observed by various authors in self preserving shear flows, but they are not incompatable with any of these correlations. (An example of extensive velocity correlations in a small deficit wake and a flat plate boundary layer may be seen in Grant, reference 15).

(v) The neglect of the mean rate of strain $\frac{\partial V}{\partial x}$ in the analytical formulation.

The velocity gradient $\frac{\partial V}{\partial x}$, when it is combined with $\frac{\partial U}{\partial y}$ to form the shear rate of strain $\frac{1}{2}\left(\frac{\partial U}{\partial y} + \frac{\partial V}{\partial x}\right)$, can usually be neglected in comparison with $\frac{\partial U}{\partial y}$. However, its effect in other ways is not necessarily small since it may rotate the vorticity of the large eddy and place it progressively more or less nearly parallel to the direction of the principal mean rate of strain. In order to demonstrate the effect of this addition, the simple model flow of Appendix I is extended in Appendix II to include the velocity gradient $\frac{\partial V}{\partial x}$. Reference should be made to Appendix II for this discussion.

.../22

The results of the present analysis i.e. that neglecting $\frac{\partial V}{\partial x}$ entirely, will be most suitable for an axis system in which $\left[\frac{\partial V}{\partial x}\right]_{@L_o}$ is zero. This criterion allows a consistent choice of co-ordinate axes to be made for a comparison of different self preserving shear flows. For reasons given in Appendix II, the calculated results contained in Chapter II of this thesis have employed the usual convenient axes, oriented as shown in Figure 1, and were based on the assumption that $\frac{\partial V}{\partial x}$ was negligible. The present work could be usefully extended therefore by a more consistent orientation of these axes and recalculation of the analytic results to include the effect of $\frac{\partial V}{\partial x}$.

(vi) The neglect of vorticity diffusion in the calculation of the large eddy vortex strength.

When the vorticity equations are written for the entire turbulent motion, the diffusion terms represented by $\nu(\nabla^2\omega_x)$ etc. may be large because of the large gradients of ω which occur in the small scale motion. If these equations are used to represent only a part of the turbulent motion, for example the large scale motion, the diffusion terms may still be large, not because of the gradients of ω , which are probably small, but because the molecular viscosity ν must now be replaced by an effective viscosity, which represents the action of all smaller scales on the motions of largest scale for which the equation is written.

However, we do not know either the value of the effective viscosity or the vorticity gradients which should be used to represent the vorticity diffusion, and the inclusion of this

.../23

effect necessitates a direct appeal to experimental information, in the present state of knowledge. In the theory presented in section 1.2.2 of this thesis, the effect of diffusion is represented by the assumption of a finite life for the eddy, using an empirical constant, in equation(10^{A}). In a more accurate analysis the effects of diffusion might be added to the effects of distortion, an approach described by Townsend (ref.7) in his discussion of the distortion of homogeneous turbulence. Even in the simpler case however, experimental information is necessary, and the results obtained so far, experimentally and theoretically, are not conclusive.

1.3 THE INNER REGION OF A TURBULENT WALL JET

For purposes of discussion, the wall jet will be divided into an inner layer $y < y_M$ (i.e. values of y less than that for which the mean velocity is a maximum) and an outer or jet layer. The outer or jet layer has a non-dimensionalized velocity profile which is very similar to that of free turbulent shear flows, and it is plausible to assume that a similar turbulent structure is present in both cases. On these grounds, the analysis of sections 1.2.1 and 1.2.2 will be used for the outer layer of a wall jet, and attention is now given to the inner layer.

Consider first the point which divides the outer and inner layers where the mean velocity is a maximum. The shear stress at $y = y_M$, particularly for a wall jet in still air, is not zero (see, for example, ref. 22). However, the ratio of this stress to τ_o (the value of the shear stress at the wall) decreases as U_1/U_M increases (ref.19). (See Figure 1 for definition of the terms used). Calculations of the inner layer development have been based on two alternative assumptions. In the earliest work (ref.9) it was assumed that $\tau_M \neq 0$; y_M was then prescribed by assuming $\frac{dy_M}{dx}$ to be a function of $\frac{U_j b}{\nu}$ only and the function was found from experiment (b is the slot width and U_j the jet velocity at the slot). The results of these calculations are shown in Figures 7 to 10 of reference 9, where the calculated maximum velocity and total width of four wall jet flows are compared with experimental values. Later calculations (ref.10) assumed that $\tau_M=0$;

.../25

the growth of y_M was then calculated using a "double integral" technique (see section 1.1). The results of these calculations are shown in figures 2 and 3 of reference 10 where calculations of the same four wall jet flows are compared with measured values. Because of the convenience and versatility of the assumption $\tau_M = 0$, and because it gives reasonably accurate results, this assumption has been used for all wall jet calculations described in this thesis.

With reference to the sketch of figure 1, the velocity profile for $y < y_M$ has been represented by a power profile of the form:

$$\frac{U}{U_M} = \left(\frac{y}{y_M}\right)^n \tag{13}$$

where n is a function of x, the streamwise co-ordinate. The description of the inner layer of the wall jet requires only that the quantities y_m and n be known. To calculate these two quantities, use is made of two integral equations of motion (the "double integral" technique) having the following limits: $y = 0$, $y = y_M$; and $y = 0$, $y = \frac{y_M}{2}$.

For use in the second of these integral equations, the shear stress at $y = \frac{y_M}{2}$ must be known. It may be represented by:

$$\frac{1}{R_T^*} = \left[\frac{\nu_T}{U_M\ \delta_M^*}\right]_{@\ \frac{y_M}{2}} \tag{14}$$

where $\delta_M^* = \int_0^{y_M} \left(1 - \frac{U}{U_M}\right) dy$

and $\nu_T = -\frac{\overline{uv}}{\frac{\partial U}{\partial y}}$

.../26

A parameter similar to R_T* was found by Clauser (ref. 17) to be essentially constant in boundary layers in equilibrium pressure gradients. (Clauser averaged R_T* over the outer part of the boundary layer by using a mean ν_T; if $y_{\frac{m}{2}}$ is representative of this outer part however, the parameters are equivalent). In boundary layers in non-equilibrium pressure gradients, the value of R_T* probably varies, but a mean value has been chosen, as described in Appendix III, from comparison with a measured boundary layer development near separation in an adverse but not equilibrium pressure gradient. The mean value chosen was R_T*= 50. In reference 10, the mean value of R_T* was chosen as R_T* = 30 since this is its value in a flat plate boundary layer. The present choice of R_T* = 50, since it is based on a pressure gradient more like that for which the calculations are expected to apply, should provide more accurate results.

The difference between $\frac{1}{R_T^*}$ in a boundary layer without external layer (i.e. when $U = U_1$ for $y > y_M$) and a wall jet inner layer will be primarily due to the inter-action of the jet layer with the inner layer. The effect of the outer layer can be described by the magnitude of some turbulent property of the outer flow. Since the variation of shear stress is being sought, it is important to choose a turbulent property which is relevant to the shear stress. The turbulence intensity $\overline{u^2}$ for example is probably not acceptable, since it includes motions which do not contribute to the shear stress. That $\overline{u^2}$ can include such irrelevant motion is pointed out by the fact that the turbulent intensity distributions in pipes, channels and boundary layers

.../27

differ from each other whereas the mean velocity distributions (and by implication the shear stress distributions) all conform to the same logarithmic law of the wall throughout much of the flow width.

The turbulent property of the outer layer that has been chosen for this correlation is the shear stress at $y_{M/2}$, partly because of its obvious relevance to the shear stress in the inner layer through convection of sheared fluid from one layer to another and partly because it is a turbulent property of the outer layer which is known from previous analysis. Thus it has been assumed that $\frac{1}{R_T^*}$ varies with $\overline{uv}$ measured at $y_{M/2}$ and non-dimensionalized in a suitable way.

The non-dimensionalizing velocity that has been chosen is $U_\tau = (\frac{\tau_o}{\rho})^{1/2}$. This is the velocity scale used in the defect law which represents the mean velocity distribution in the ordinary flat plate boundary layer and is therefore an appropriate non-dimensionalizing parameter in that case. In self-preserving boundary layers, the significant non-dimensionalizing velocity is still U_τ. Thus it has been assumed that:

$$\frac{1}{R_T^*} = g\left\{\frac{(\overline{uv})_{yM/2}}{U_\tau^2}\right\} = g(\Phi) \qquad (15)$$

Since $\overline{uv}$ can be calculated from equation (12), when the mean velocity in the outer layer is known, Φ can be calculated once U_τ is known. As described in a later paragraph, U_τ is assumed to obey a Ludweig-Tillman type of relationship and can therefore be calculated. The function $g(\Phi)$ has been found empirically from the self preserving cases of Patel and Newman (ref.16) and

.../28

the boundary layer value $R_T^* = 50$ (which is discussed in Appendix III) for $\Phi = 0$. A suitable function was found to be:

$$\frac{1}{R_T^*} = .033(1 - .67\,\Phi - .039\,\Phi^2) - .013\,e^{-\Phi} \qquad (16)$$

where

$$\Phi = \left[\frac{\overline{uv}}{U_\tau^2}\right]_{@\,y_{M/2}}$$

This empirical formulation is intended only as a method of estimating the shape of the inner layer. It is by no means the only such correlation which could be developed but is based on measured values in a variety of cases and should therefore produce reasonably realistic results.

The Ludweig-Tillman relation for wall shear stress in a boundary layer may be written as

$$C_f = \frac{\tau_o}{\frac{1}{2}\rho U_1^2} = 2\left(\frac{U_\theta}{C_1 U_1}\right)^{\frac{2}{m+1}} \cdot R_\theta^{-\frac{2m}{m+1}} \qquad (16^A)$$

where $\frac{U}{U_\tau} = C_1\left(\frac{yU_\tau}{\nu}\right)^m$ is the form of the law of the wall for $y \ll \theta$, θ is the usual momentum thickness of the layer, U_θ is the value of U at $y = \theta$ and R_θ is $\frac{U_1\theta}{\nu}$. By replacing U_1 by U_M and by redefining θ as:

$$\theta = \int_o^{y_M} \frac{U}{U_M}\left(1 - \frac{U}{U_M}\right) dy$$

this form may be used for the wall jet as well.

The relation for C_f will be forced to conform with the wall shear stress beneath a wall jet in still air by evaluating C_1 and m from known measurements in this case. From the measurements of Patel (ref. 18)

$$C_f = .0257\left(\frac{U_\theta}{U_1}\right)^{11/6} R_\theta^{-1/6} \quad \text{(still air wall jet)}$$

.../29

where a variation of $\pm$ 10% in the numerical constant was found and an average is given in the equation. This variation is not surprising in the light of the large variations in wall shear stress which can occur across a "two dimensional" boundary layer downstream of wire screens. (references 20 and 21)

A relation between $\frac{U_\theta}{U_1}$ and H may be found using equation (13). This relation is:

$$\frac{U_\theta}{U_1} = \left\{ \frac{(H-1)}{H(H+1)} \right\}^{\frac{H-1}{2}}$$

so that finally,

$$C_f = .0257 \left\{ \frac{H-1}{H(H+1)} \right\}^{\frac{11}{12}(H-1)} R_\theta^{-1/6} \qquad (17)$$

Since it has been assumed in all cases that the velocity distribution for $y < y_M$ is given by equation (13), H may be related to the exponent n of equation (13) by the expression $H = 1 + 2n$, while θ is related to y_M by:

$$\theta/y_M = \left[(n + 1)(2n + 1)\right]^{-1} \cdot n$$

.../30

1.4 THE APPLICATION OF THE DOUBLE INTEGRAL METHOD

The mean velocity profiles of all free turbulent shear flows, even in adverse pressure gradients, can be expressed for most practical purposes as a single function of a scaling length L_o and a scaling velocity U_o. These two scaling parameters are identified in Figure 1 for each flow; U_o is the maximum velocity deficit (or increment) in the outer layer and L_o is the width of this layer measured to the ordinate where $U = U_1 \pm \frac{U_o}{2}$. The single function of U_o and L_o also describes the non-dimensional profile of the outer or jet layer of a wall jet. To determine the complete velocity field, one needs only to find the two scaling dimensions. Two equations are required for the calculation, and, as already mentioned in section 1.1, these are provided by two momentum integrals with limits $y = 0$, $y = \infty$ and $y = 0$, $y = L_o$ respectively. The shear stresses at $y = 0$ and $y = \infty$ are assumed to be zero, and that at $y = L_o$ can be found from equation (12), with empirically determined values of the constants R_{T_o} and C (see Table 1).

A wall jet also possesses an inner layer, so that the analysis of the outer layer in this case uses integrals whose lower limits are $y = y_M$ and whose upper limits are $y = y_M + L_o$ or $y = \infty$. (See Figure 1). The inner layer is represented, albeit somewhat crudely, by a mean velocity profile which is a function of a velocity scale, a length scale, and a shape parameter (equation 13), the velocity scale being already determined by the outer layer analysis. The double integral technique is again employed, as described in section

.../31

1.3.

For a free turbulent flow, three differential equations must be solved simultaneously (the two momentum integral equations and an equation for the variation of the external velocity) to determine the three unknowns U_o, L_o and U_1. For a wall jet, five equations are solved, the additional unknowns being y_M and the shape of the inner layer, represented in this analysis by the non-dimensional exponent n of equation 13.

Except in a few exceptional cases, the equations must be solved numerically and for this purpose a four-point Runge Kutta technique has been written in the Fortran 4 language for the IBM 7040 computer. A derivation of the complete equations for a wall jet analysis is given in Appendix IV and the computer programme for solution of these equations is given in Appendix V.

For a solution of the differential equations describing a particular flow, the initial values of all variables must be known. In almost all cases, this requirement poses severe difficulties and, as shown in sections 3.3 and 3.4, the initial values which are used can critically affect the downstream results.

In ref. 9, which dealt only with jets and wall jets in a uniform streaming flow (zero pressure gradient), the initial values for wall jet calculations were determined by an analysis of the mixing layer immediately downstream of the slot. The comparison between theory and experiment presented in Figures 6, 9 and 10 of ref. 9, suggests that this type of

analysis can be useful for the zero pressure gradient case.

No attempt has been made to calculate the initial values for free turbulent flows. In these cases initial values have been taken from the measured values at a particular station and the calculated development of the flow downstream of that station compared with further measured values. For purely theoretical predictions, where no experimental values are available, some technique must be developed to calculate the initial conditions. For example, section 3.3 of this thesis is devoted almost entirely to a calculation of the initial values for a wall jet in an adverse pressure gradient including the effect of large upstream boundary layers.

The double integral method is also applied, in Appendix III, to the plane turbulent boundary layer, primarily to determine the value of $\frac{1}{R_T^*}$ applicable for $\Phi = 0$ in equation 16, and secondly as a useful means of calculating the streamwise development of turbulent boundary layers for the analysis of Chapter III of this thesis.

.../33

CHAPTER II EXPERIMENTAL INVESTIGATIONS AND COMPARISONS OF MEASURED AND CALCULATED RESULTS

2.1 INTRODUCTION

In this chapter, the analysis of Chapter I will be applied to a wide variety of shear flows in order to determine, by direct comparison with experimental values, the limitations and the accuracy of the theoretical predictions. The following two-dimensional turbulent shear flows have been examined: wall jets in streaming flow, self preserving wakes, free jets in uniform streaming flow, asymmetric jets (jets with uniform streaming flow on one side and still air on the other), the mixing layer between a uniform stream and fluid at rest. Each flow is considered in a separate subsection. The measurements in almost all cases have been made by the present author.

Because of the variety of flows investigated, the particular experimental arrangements will be described in each individual subsection. A general description of the measurement technique and of the tunnel used, is given in the following paragraphs.

A majority of the measurements were made in a special working section constructed for the McGill Cascade Blower tunnel. This tunnel, whose calibration and description are reported in ref. 28, is used with a working section of dimensions 17 in. x 30 in. The working section which was designed for this investigation, is described in ref. 8. It incorporates a blowing slot for jet and wall jet measurements and has

.../34

moveable slats for one (and sometimes both) of its 30 inch sides. The slats, in combination with perforated plates or screens fastened over the downstream end of the section, can be positioned to create a wide variety of adverse pressure gradients in the working section. The working section is similar to that used in ref. 16, but is longer and incorporates a more carefully designed blowing slot.

Mean velocities were measured by pitot tubes in combination with static taps located in one of the tunnel walls. For measurements near a solid boundary, as in wall jets, a flattened pitot tube was used (outside height 0.014 in.), whereas a round tube was used for measurements in the free turbulent flows. Both probes had sharpened lips to decrease their sensitivity to flow inclination. The pitot probes were mounted on a double ended dial gauge so that they could be traversed across the flow. The static pressure was assumed to be constant across the flow.

Turbulent intensities and shear stresses were measured with a DISA constant-temperature hot-wire anemometer. Slanting and normal wires were traversed across the flow using the dial gauges just described, and the results were reduced according to the equations outlined in Appendix VI and in more detail, in ref. 29. Appendix VI describes measurements of the shear stress in fully developed pipe flow. This investigation, which is similar to that of ref. 29, was undertaken in order to gain familiarity with the hot wire anemometer, and to establish the accuracy of measurement.

.../35

Flow visualization of a wall jet in uniform streaming flow and in both favourable and adverse pressure gradients was undertaken in a preliminary investigation. This work was carried out in the 10 inch x 13 inch working section of the N.R.C. water tunnel and a description of the apparatus used together with examples of the photographs taken is presented in Appendix VII. Measurements of the intermittency factors can be made directly from a series of pictures such as these, as described in the Appendix. A 35 mm slow motion film taken of the flow provided strong evidence of the existence of large, temporarily coherent regions of the flow which are described in this thesis as "large eddies".

The measurement of intermittency from the wind tunnel measurements is described in the following section (section 2.2.1).

.../36

2.2 INTERMITTENCY MEASUREMENTS AND THE VERIFICATION OF LARGE EDDY EQUILIBRIUM

2.2.1 THE MEASUREMENT OF INTERMITTENCY

The phenomenon of intermittency near the free stream boundary of a turbulent shear flow is easily observed from an oscillograph trace of the voltage from a hot wire placed in the flow. Two reasonably distinct processes appear to be represented in such a trace, one having larger frequencies and amplitudes than the other, and occurring in distinct bursts.

A useful and accurate definition of intermittency is more difficult to obtain. The usual definition, stating that intermittency is the alternating presence and absence of vortical flow, is of little practical use in most cases, since fluctuating vorticity is seldom measured. (The measurements of Corrsin and Kistler in ref. 31 are an exception to this statement). The differences between one process and another, as represented in the usual oscillograph trace, may be quite easy to recognize by eye, but are not easy to define with accuracy and generality. A study of this mixed process from the standpoint of communication theory might reveal more realistic and perhaps more fundamental differences between the bursts, loosely called "turbulent", and the background noise in which they occur.

Two methods of measuring the intermittency were adopted:

i. The construction of a constant voltage or "δ" signal which had a positive value when the wire was in a fully turbulent

.../37

region, but a negative value of equal magnitude at all other times.

ii. The visual examination of trace recordings made of the signal from the hot wire.

The first method is based on a technique used by Corrsin and Kistler (ref. 31) and involves differentiation, rectification and smoothing of the original signal to produce a "processed signal". A discrimination level is then set so that the presence of voltages above this level in the processed signal produce a certain positive output while lower voltages produce a negative output of equal magnitude. The outputs are summed over a time which is sufficiently long to produce results which are essentially independent of sample length. A further description of this technique and an example of the original, processed and output signals is given in Appendix I of ref. 9.

The chief difficulty with this method is that the discrimination level (and, although less critical, the smoothing time constants) must be set by a visual comparison of the original and output signals. The method is therefore dependent on the ability of the operator to set a proper, or at least a consistent, criterion for discrimination.

Analyses using the first technique were carried out on the N.R.C. Pace Analog computer (model 16-131R). The accuracy of the amplifiers in this computer are described by their frequency response which cuts off at 1 kc (3 db down) for gains less than 10. Since the analyses were performed on samples which were slowed down considerably (by recording on magnetic tape) this frequency response is considered adequate.

.../38

Since a subjective element could not apparently be avoided, it was decided to try the second, essentially more simple method of analysis, wherein the discrimination is made directly by examining trace recordings of the differentiated signal from the hot wire unit. For this method, a differen - tiating circuit was constructed with 3db frequency response limits of 16 and 5,000 cps. A high speed recorder was used to obtain the trace records, the stated frequency limit of the galvanometer in the apparatus being 5000 cps. By suitably adjusting the recording and replaying speed of the original magnetic tape records, this frequency range was found to be quite adequate.

Although differentiation of the hot wire signal emphasizes the high frequency fluctuations associated with the turbulent motion, it may also mask the entire signal by selectively amplifying any very high frequency noise which is present. This difficulty always arises when differentiating low amplitude signals from a constant temperature anemometer, which is inherently a noisy instrument, and requires the deletion of high frequencies through filter circuits, with the obvious risk of deleting some of the original signal as well, or the analysis of the hot wire signal without differentiation.

The two methods itemized previously as numbers i and ii were checked by measurements in a smooth wall flat plate boundary layer and in a small deficit wake. These measurements are compared with other published results in Appendix VIII. Intermittency measurements are presented as distributions of

.../39

the intermittency factor, which is usually defined as:

$$\gamma(y) = \text{prob } (y < Y(t)) \tag{18}$$

where $Y(t)$ is the instantaneous position of the boundary between vortical and non-vortical fluid. It will be assumed that the processes presently identified as distinct from one another in the trace records, represent vortical and non-vortical fluid. A substantiation of this assumption may be found by reference to ref. 31, where the intermittency calculated from instantaneous vorticity measurements compares very favourably with intermittency measured through the construction of a "δ" signal. (method i, above).

In practice, $\gamma(y)$ may be approximated by a curve of Gaussian form. The probability density $P(y)$ of $Y(t)$ may be defined as $P(y) = -\frac{d\gamma}{dy}$, so that a convenient measure of the distortion of Y from its mean position is the standard deviation σ defined as:

$$\sigma^2 = \int_{-\infty}^{\infty} P(y)\ (y - \overline{Y})^2\ dy \tag{19}$$

where $\overline{Y}$ is the mean value of Y chosen so that

$$\int_{-\infty}^{\infty} P(y)\ (y - \overline{Y})\ dy = 0.$$

.../40

2.2.2 THE EXPERIMENTAL VERIFICATION OF LARGE EDDY EQUILIBRIUM AND A DISCUSSION OF INTERMITTENCY RESULTS

The experimental evaluation of equation (3) is based on the assumption that the standard deviation of the laminar superlayer (the name usually applied to a free boundary of the turbulent fluid) is directly proportional to the scale of the large eddies present in the turbulence. The standard deviation, defined by equation (19), has been obtained from measured distributions of the intermittency factor.

Attention must first be given to the conditions which limit the lateral extent of the large eddies. Since the large eddies exist only through constant extraction of energy from the mean flow, they will be bounded by regions in which this energy supply cannot continue, as well as by solid boundaries. Thus, as Townsend (ref. 7) has pointed out, the large eddies will not extend into regions in which $\frac{\partial U}{\partial y}$ is zero or of opposite sign to $\frac{\partial U}{\partial y}$ in the region where the large eddy originated. The eddy will be most sharply bounded by a solid surface, as exists in a boundary layer (the thickness of the viscous sublayer is not likely to affect this condition significantly), less sharply by a change in sign of $\frac{\partial U}{\partial y}$, and least sharply by a region in which $\frac{\partial U}{\partial y}$ is zero. In flows in which a lateral limit is set by a change in sign of $\frac{\partial U}{\partial y}$, the magnitude of the derivative $\frac{1}{U}\frac{\partial^2(U)}{\partial(y/L_o)^2}$ evaluated where $\frac{\partial U}{\partial y} = 0$, would probably provide a criterion for the relative sharpness of the large eddy boundary. If this last refinement is ignored for the moment however, it is clear that the large eddies in wall jets, wakes and jets have qual-

.../41

itatively similar lateral boundaries and may therefore be compared directly with each other. The examination of large eddy equilibrium will therefore be restricted primarily to these types of flow. Intermittency measurements in two other cases are discussed at the conclusion of the section.

All of the quantities in equation (3) have been evaluated in five different two dimensional shear flows of which four are approximately self preserving wall jets (see ref. 16) and one is the free jet in still air. To these results have been added values calculated from the small deficit wake, measured by Townsend (ref. 11). In all these cases, the mean velocity profile over a major part of the flow may be represented by an expression of the form:

$$\pm (U - U_1) = U_o \exp \left\{ - k \left(\frac{y - y_M}{L_o} \right)^2 \right\} \qquad (20)$$

where U_1 is the free stream velocity, L_o is the width to the point where $U = U_1 \pm \frac{1}{2} U_o$, and k, in consequence of these definitions, is $\log_e 2$ (see also Figure 1 for identification of symbols. y_m is zero for symmetrical flows). As a consequence of self preservation, the ratio U_1/U_o is essentially constant, and the pressure gradient is of the form $\frac{dU_1}{dx} = \frac{U_1}{x + x_o} .m$ where x_o is a virtual origin and m is a constant (see ref. 16).

This examination was restricted to approximately self preserving jets and wall jets in order to ensure that the turbulence at the point of measurement had had a sufficiently long and uniform history so that the large eddies of the flow were a product of equilibrium types and orientations of the

mean flow rate-of-strain tensors. It appears from Townsend's measurements of intermittency in a small deficit wake (ref. 7,11) that the intermittency at $\frac{x}{d} = 160$ is distinctly different from that at $\frac{x}{d} = 1000$, the difference being due presumably to the persistence of large eddies formed near the wake-producing body. Since no such large eddies are formed in the initial stages of a jet or wall jet, these flows approach complete similarity much more quickly than the wake, and their investigation therefore requires shorter streamwise lengths to ensure definitive results.

The experimental arrangements for the wall jet measurements are described in section 2.3, where the mean velocity results are given. Table II summarizes the slot Reynolds numbers and other pertinent data for all the 5 tests.

The free jet measurements were made 100 slot widths downstream of a carefully constructed symmetrical slot 0.180 inches in width and 24 inches in length. Large end plates were used to help maintain two dimensionality of the flow.

Results of the intermittency measurements are plotted in Figure 2 and the values of $\frac{\sigma}{L_o}$ are listed in Table III (the numbers on the curves of Figure 2 correspond with those of Table II). Curves of the form:

$$\gamma = \frac{1}{2} (1 - \text{erf } \xi) \qquad (21)$$

have been drawn through the measured results, where $\xi = k_1 \cdot (\frac{y - y_M}{L_o} - k_2)$ and k_1, k_2 are listed in Table III. The curves may be located by means of k_2 which is the value of $\frac{y - y_M}{L_o}$ at which $\gamma = \frac{1}{2}$. The use of these curves does not imply that the

.../45

distributions of intermittency are precisely ~~Gaussian.~~ error functions. Much more uniform results are obtained when a curve is fitted to the measured data however, since values of $\frac{\partial\gamma}{\partial y}$ are required, and equation (21) has an appropriate and convenient form for this purpose.

The quantity $\frac{U_o L_o}{\nu_{T_M}}$ appearing in equation (3) may be calculated by assuming a mean value of ν_T over the outer part of the layer or by choosing a single non-dimensional ordinate to represent the shear stress in the outer region. For the present evaluation the latter approach has been used, $y = y_{M/2}$ + y_M being chosen as a convenient and yet typical point for the calculation. Use of the subscript "@L_o" designates evaluation at this value of y. The values of $(\frac{U_o L_o}{\nu_T})_{@L_o}$ versus $(\frac{L_o}{\sigma})^2$ should plot as a straight line, since σ is assumed to be proportional to (L), the large eddy scale. Figure 3 shows these quantities for the five flows listed in Table II together with values calculated from Townsend's self preserving small deficit wake (ref.11). The numbers of the points in Figure 3 correspond with those in Table II, and the values of $\frac{\sigma}{L_o}$ and $(\frac{U_o L_o}{\nu_T})_{@L_o}$ are listed in Table III.

Despite some scatter, the points in Figure 3 do display the expected linear trend and thereby substantiate the form of relationship predicted by the large eddy energy equilibrium hypothesis.

The weak or degenerate wall jet (flow number 4), as may be seen from Table III, has large values of y_M/L_o and

.../46

therefore is likely to have small values of $\frac{1}{U}\frac{\partial^2 U}{\partial(y/L_o)^2}$ at or near the point of maximum velocity. This is expected to produce abnormally large eddies, i.e. large σ compared with the usual mean velocity scale L_o. From Figure 3, it can be seen that the value of $\frac{L_o}{\sigma}$ is too small in the flow designated as number 4, qualitatively justifying this expectation.

Measurements of intermittency have also been made in the smooth-wall flat-plate boundary layer and in the shear layer between moving fluid and fluid at rest. As described in Appendix VIII, the present measurements of γ in a flat-plate boundary layer are almost identical with those of Klebanoff (ref. 12) (a plot of y/δ vs. γ is shown in Figure A 12, and the measurements are discussed in Appendix VIII). It is interesting to note that Klebanoff's measurements of shear stress and mean velocity profile, together with his value of $\frac{\sigma}{\delta}$, yield results which can be compared with those of Figure 3 once allowance has been made for the change of shape in the velocity profile. The comparison is possible in terms of equation (2) which, after substitution of σ for L as before, may be written as:

$$-\frac{\overline{uv}}{U_1^2} \propto \left(\frac{\sigma}{\delta}\right)^2 \left\{\frac{\partial(U/U_1)}{\partial(y/\delta)}\right\}^2 \qquad (22)$$

where δ is a nominal boundary layer thickness.

From Klebanoff's measurements, at the representative point $\frac{\delta}{2}$, $\frac{\overline{uv}}{U_1^2} = -.00082$, $\frac{\partial(U/U_1)}{\partial(y/\delta)} = .366$, and $\frac{\sigma}{\delta} = .14$ (the value of $\frac{\sigma}{\delta}$ found in the present measurements was 0.13). Using

.../47

these figures, the constant of proportionality in equation (22) would be 0.312.

Similarly, for the jets, wakes and wall jets already considered, equation (2) may be written as:

$$\left(\frac{\nu_T}{U_o L_o}\right)_{L_o} \propto \left(\frac{\sigma}{L_o}\right)^2 k \qquad (23)$$

where $k = \log_e 2$. From Figure 3 the relationship between $\left(\frac{\sigma}{L_o}\right)^2$ and $\left(\frac{\nu_T}{U_o L_o}\right)_{@L_o}$ is approximately

$$\left(\frac{\nu_T}{U_o L_o}\right)_{@L_o} = \frac{1}{5.40}\left(\frac{\sigma}{L_o}\right)^2 \qquad (24)$$

The constant of proportionality predicted by these values is 0.268, c.f. the value of 0.312 for the boundary layers. A comparison between these two values suggests that the large eddies of the boundary layer are proportionally smaller than those in jets or wakes. The sharpness with which a solid wall bounds the large eddies, as discussed already in this section, explains this result.

The distributions of intermittency factor in a plane mixing layer are shown in Figure 14. (The mean velocity distribution associated with the measurements is presented in section 2.7). Two intermittent regions are present in this flow and the measurements indicate that they are not identical. Values of $\frac{\sigma}{x}$ are shown for each curve in Figure 14. The difference between the values of $\frac{\sigma}{x}$ on the two sides of the plane mixing layer cannot be explained by the present theory but its appearence is not surprising in view of the fact that the mean velocity distribution is not asymmetrical about $y_{M/2}$.

.../48

Because the non-dimensionalized distribution of mean velocity in the mixing layer is quite similar to that of jets or wakes (see section 2.7) it is possible to include the mixing layer in the comparison of Figure 3. Two problems arise in this case however: the mean velocity scale L_o is no longer as clearly defined as in previous cases, and there is no longer one unique value of σ for the mixing layer. The former difficulty can be avoided, albeit somewhat crudely, by assuming the usual form of velocity distribution for the mixing layer, i.e.

$$U = U_o \exp \left\{ -k \left(\frac{y - y_M}{L_o} \right)^2 \right\} \qquad (25)$$

and determining both L_o and y_M from a best fit with the experimental data. The latter difficulty, that of having two intermittent regions, can be ignored by choosing one or other of the intermittent regions in the mixing layer as a basis for comparison with the other flows. In this regard, the mixing layer is most closely comparable to the free jet in still air, and this observation prompts the use of the intermittent region on the zero velocity side of the mixing layer for comparison with other flows.

The value for L_o at the station where the intermittencies were measured, was determined as described above (see section 2.7) and the value for $\left[\frac{U_o L_o}{\nu_T}\right]_{@L_o}$ was calculated from the mean flow development and the equation of motion for the mean flow. The value of this ratio was found to be 58.4. From the measured value of $\frac{\sigma}{x}$ for the zero velocity side, the

.../49

ratio of σ/L_o was determined as 0.37. A point in Figure 3 representing these values lies off the straight line drawn through the other data, the value of σ/L_o being larger than would be required for good agreement with the other points. This trend was anticipated in the discussion of the lateral limits for the large eddies, since the large eddies in the mixing layer are bounded differently, and in particular less sharply, than the other cases represented in Figure 3.

A paper by the present author, covering the work described in sections 2.2.1 and 2.2.2 of this thesis, will be published shortly in the Journal of Fluid Mechanics.

.../50

2.3 WALL JETS IN STREAMING FLOW

In the course of the presentwork, the streamwise developments of nine wall jets were examined, of which three were approximately self-preserving cases, four were uniform streaming flow cases (of which one, the wall jet in still air, was also approximately self preserving) and two were non-self-preserving wall jets in adverse pressure gradients. The measurements from all of these groups will be considered in this section.

The tunnel, working section and measurement technique used for these measurements are described briefly in section 2.1 and in greater detail in references 8 and 28. The slot, which was located in one of the 30 inch sides of the tunnel, was varied in width from .200 to .302 inches so that the slot "aspect ratio" was never less than about 100. Two-dimensionality tests of the flow from the slot, reported in reference 8, showed that mean velocities at equal levels across a twelve-inch centre lane were within $\pm$ 1%. The total momentum thickness of both internal slot boundary layers was always less than 4% of the slot width, which was constant across the central 12 inch lane to within $\pm$ .001 inch. The static pressure was measured through static taps .015 inch diameter located in the 30-inch wall beneath the wall jet.

Chapter I of this thesis describes a method for predicting the streamwise development of wall jets. Before calculations can be made however, the two empirical constants R_{r_o} and C appearing in equation (12) must be evaluated. These

.../51

have been found by trial and error from the two following cases: wall jet in still air and wall jet in uniform streaming flow in which $\frac{U_1}{U_j} = 0.487$. Both of these cases are included with other experimental and theoretical results discussed in the next paragraph. The values of R_{T_o} and C are listed in Table 1. Once found, these values were used for all the wall jet analyses. As the present results demonstrate, the introduction of these two experimental values provides a remarkably general method for the prediction of wall jet mean flow development. Initial values for the calculations were chosen from experimental values in all cases.

Experimental and theoretical results are shown in figures 4 and 5 for the uniform streaming flow cases ($\frac{U_1}{U_j}$ =0,.197, 0.333 and 0.487) and in figures 6 and 7 for three approximately self-preserving cases. Two non-self-preserving cases are presented in figures 8 to 10, the measured pressure distributions being shown in figure 8 and the measured and calculated values of $y_{M/2}$ and U_M in figures 9 and 10.

Four further self preserving cases are shown in figures 11 and 12, the data being that of Patel and Newman (ref. 16). A summary of all the self preserving cases is presented in fig. 13 as a plot of the rate of growth of the outer layer $\frac{dy_{M/2}}{dx}$, against the velocity ratio $\frac{U_1}{U_M}$, which is essentially constant in these flows.

In all these cases the agreement between theory and experiment is satisfactory.

The analysis proposed by Abramovich (ref. 2) was

.../52

described in section 1.1.2 and results in an equation for the growth of a free jet which may be written as:

$$\frac{\frac{d\ y_{M/2}}{dx}}{\left[\frac{d\ y_{M/2}}{dx}\right]_{U_1=0}} = \frac{U_M - U_1}{U_M + U_1}$$

This equation may be adapted to wall jet analysis by replacing the quantity $y_{M/2}$ by the wall jet outer length scale, $y_{M/2} - y_M$. The resulting equation can be applied directly to the self preserving wall jets whose rate of growth is plotted in figure 13. By adding the measured values of $\frac{dy_M}{dx}$ to the growth rate of the outer length scale predicted by Abramovich's analysis, the total growth rate $\frac{dy_{M/2}}{dx}$ can be compared directly with the measured values in figure 13. As can be seen from this figure, the present method of analysis provides distinctly better predictions of $\frac{dy_{M/2}}{dx}$ than does the analysis of Abramovich.

.../53

2.4 THE SELF PRESERVING WAKE

The results derived by Patel and Newman (ref. 16) show that wakes or jets may be made self preserving if they are subjected to adverse pressure gradients of the form:

$$U_1 \propto (x + x_i)^m$$

where m is a negative constant which can be related to the constant ratio U_M/U_1, and x_i is a virtual origin of the flow development. (Figure 1 defines the velocities U_1 and U_M for the jet and wake). It can easily be shown from the momentum integral equation that the quantity $\theta \cdot U_1^{H+2}$ is a constant, as a result of self preservation, where H is the ratio of the displacement thickness to the momentum thickness, δ^*/θ. The constancy of this quantity in the experimental values is a measure of the two dimensionality of the flow and of the unimportance of the normal stress turbulence terms ($\overline{u^2}$ and $\overline{v^2}$).

Two self-preserving wakes were examined in the McGill cascade blower tunnel; they are designated as wakes A and B. For these tests both the 30 inch sides of the tunnel consisted of slats adjusted so that air could be bled from the tunnel to provide a mean flow symmetrical about a plane parallel to the free stream and midway between the 30 inch sides. The 1/4-inch square rod forming the wake was mounted with its centreline in the plane of symmetry just described and with one flat face normal to the oncoming stream.

The static pressure was measured through static holes 0.015 inches in diameter, located along the plane of symmetry in a false wall at the side of the tunnel working section.

.../54

For both wakes the Reynolds numbers were approximately 7×10^3 based on model dimension d (1/4 inch). No evidence of a periodic wake was observed probably because the investigation was limited to $x/d > 20$ (see ref. 7).

The theoretically invariant quantity $\theta \cdot U_1^{H+2}$, calculated from experimental values, was found to vary by 22% in the first case (wake A). Investigation showed that the wake producing body was set at a slight angle (1/4°) to the cross stream direction and correction of this slight mis-orientation resulted in nearly constant values of $\theta\, U_1^{H+2}$ for the second wake (wake B). The small cross flows present in most "two dimensional" experiments are often sufficient to cause large variations in theoretically invariant quantities. The recent work of Bradshaw (ref. 20) and Patel (ref. 21) also emphasizes this point.

The mean velocity profile is represented by an equation of the form:

$$U_1 - U = U_o \exp \left\{ -k \left(\frac{y}{y_{M/2}} \right)^2 \right\}$$

and $y_{M/2}$ (which is equal to L_o in this case) and U_o are defined in Figure 1. A comparison between this equation and measured values of the mean velocity is shown in Figure 10 of reference 10.

Because of the difference in boundary conditions between the wake and the wall jet, the values of R_{T_o} and C used in connection with equation (12) for the solution of wall jet flows will not carry over to the present analysis. However, on the assumption that the theory may be applied equally to wakes

.../55

and jets, the constants required by the analysis have been calculated for the wake flows from the following well known cases:

i. free jet in still air

ii. small deficit wake in uniform stream.

The value of the constants used are shown in Table I.

The streamwise distributions of U_o and $y_{M/2}$ for wakes A and B are shown in Figures 15 and 16. Linearity of growth of $y_{M/2}$ is associated with self preservation of the flows and may be predicted from the equation of motion (see ref. 16). The experimental growth is approximately linear in each case and the ratio of maximum velocity deficit to free stream velocity is nearly constant, as required for self preservation.

The values of U_o and $y_{M/2}$ calculated with the double integral method described in section 1.4 are also shown in Figures 15 and 16. Agreement between theory and experiment is fairly good, despite the variation of the "invariant" $\theta \cdot U_1^{H+2}$ in wake A and a slight lack of linearity of $y_{M/2}$ in wake B.

Although the mean velocity profiles in a wake may appear self preserving, it is usual to find that the distribution of turbulent velocities is not self preserving until some further distance downstream (see for example ref. 7, in connection with small deficit wakes). ~~This gradual~~ The gradual approach toward complete self preservation is more ~~pronounced~~ in wakes than in jets or wall jets, as discussed in section 2.2.2. Intermittency measurements were made in wake B at the station $\frac{x}{d} = 140$, and the result, described by the standard deviation of the vis-

.../56

cous superlayer σ, is $\sigma/y_{M/2} = .345$, a value of $\gamma = \frac{1}{2}$ occurring at $y/y_{M/2} \approx 1.8$. These values were not used in section 2.2.2 since it is almost certain that complete turbulent self preservation was not reached at $x/d = 140$.

Distributions of longitudinal turbulence intensity and turbulent shear stress were made in the two wakes. For the results of these measurements, see ref. 10, section 4.3. The intensity distributions, made at several streamwise stations in each wake, illustrate the slow approach to complete self preservation in the flows. The shear stress measurements are compared in ref. 10 (Figures 16 and 17) with the distribution of shear stress calculated from the equations of motion and the measured flow development. The agreement between the measured and calculated values provides a measure of confidence in the turbulence measurements.

2.5 THE FREE JET IN UNIFORM STREAMING FLOW

The development of a free jet in uniform streaming flow has been measured by Bradbury, (ref. 14) for the following three values of $\frac{U_1}{U_j}$: 0.07, 0.162 and 0.58. Although a $\pm$ 7% spanwise variation in total head is reported in conjunction with these measurements, the streamwise variation of the total momentum thickness is less than 4% in each case so that the overall two dimensionality of the flow is thought to be acceptable. Other measurements of a plane jet in uniform streaming flow have been made by Weinstein et al (ref. 49) but Bradbury's measurements are reported in a more convenient form and his data will be compared with calculated values in this section.

As in section 2.4, the scaling length L_o is taken as $y_{M/2}$ and the scaling velocity U_o as the maximum velocity increment. The calculations of section 4.3 were based on the assumption that the theory may be applied equally well to wakes or free jets and this same assumption and hence the same two constants for equation (12) are used for calculation of the jet flows.

The measured and calculated values are shown in Figures 17 to 19. Agreement between them is not good. It is of practical interest to note that if one of the constants appearing in the theory (that constant corresponding to the small increment case) is specified by trial and error for best fit with the present data, a reasonably accurate analytical technique is again obtained. However, the new value for R_{T_o} for the small increment jet is about 20.5 c.f. 12.1 for the small deficit

.../58

wake, which is surprising (see Table I). The results of the calculations using the "adjusted" value of the constant R_{T_o} are also given in Figures 17 to 19.

The assumption of local self preservation has been questioned by Bradbury (ref. 14) in connection with this non-self-preserving flow, and a parameter for examining this assumption was constructed in section 1.2.3. The parameter Λ was defined in equation (12^A) as:

$$\Lambda = \frac{\left(\frac{U_1 + U_M}{2}\right) \frac{d(1/R_T)}{dx}}{\frac{1}{R_T}} \cdot \left|\frac{\beta}{\frac{\partial U}{\partial Y}}\right|_{@Y_{M/2}}$$

The following table gives some values for Λ from the zero pressure gradient cases indicated:

FLOW	U_1/U_j	x/b	Λ
WALL JET	.487	142	.190
	.197	80.75	.295
	0	44.7	.085
FREE JET	.58	50.5	.066
	.162	31.4	.156
	.07	25.0	.080

The magnitudes of Λ are similar in the jet and wall jet cases and show that the local rate of change of $1/R_T$, if maintained for a distance representative of the length travelled by a large eddy during its existence, would result in a change of $1/R_T$ of up to 30%. However, the analysis provided good agreement with measured values for the wall jet: (1) in uniform streaming flow and <u>also</u> (2) in pressure gradients

.../59

which provided approximate self preservation. The change of $1/R_T$ is small in the second case and is apparently not large enough to cause serious error in the first case. It can be concluded tentatively therefore that a change in $1/R_T$ at a rate given by $\Lambda < .30$ cannot be a reason for failure of the analysis. If this conclusion is correct, the rate of change of $1/R_T$ is not responsible for the discrepancy in Figures 17 to 19 between predicted and measured values.

Note that the definition of Λ in ref. 10 was based on the rate of change of $\left[\frac{\partial U}{\partial x}/\frac{\partial U}{\partial y}\right]_{@L_o}$ instead of the rate of change of $1/R_T$. The values of Λ are therefore different from those presented here although the same conclusion was reached in both cases.

No explanation has been found for the apparent dissimilarity between the small deficit wake of Townsend and the small increment jet of Bradbury. This conflict emphasizes the need for further measurements in two dimensional free jets, preferably at large distances from the slot, in uniform streaming flow and also in pressure gradients in which the jets are self preserving.

.../60

2.6 THE ASYMMETRIC JET IN UNIFORM STREAMING FLOW

The asymmetric jet in uniform streaming flow describes the flow produced by a jet bounded on one side by a uniform streaming flow and on the other by still air.

The arrangement of the test section for measurements in this flow is shown in Figure 20. Particular care was taken to ensure smooth entry of entrained air into the test section by installing the circular arc fairings shown in the sketch. In the limiting case of the two dimensional jet in still air, in which no primary or tunnel flow is used, the slats used as one of the 30 inch sides of the tunnel were removed and circular arc fairings attached to the tunnel, again to direct entrained air more smoothly into the flow. Without any of the fairings, the total momentum flux of the jet in still air decreased at an unacceptable rate with increasing x, although the rate of growth of the jet was approximately equal to that finally measured with the fairings. The section was used without a floor for all these asymmetric jet tests, and the traversing mechanism was supported from the laboratory floor on a suitable stand. Only pitot pressures were measured in these experiments, in every case with a round pitot tube having sharpened lips.

An important property of this asymmetric flow is that its two limiting conditions, i.e. the symmetric jet wherein $\frac{U_1}{U_j} = 0$ and the mixing layer wherein $\frac{U_1}{U_j} = 1$, are fully self preserving flows. In both of these limiting cases, the mixing region grows linearly with streamwise distance x, and

.../61

from values given by Schlichting (ref. 34) on these two well known flows, it appears that the rate of growth of the mixing layer is very nearly equal to that of one side of the free jet in still air. It is likely therefore that the zero velocity side of the asymmetric jet will grow at a practically constant rate regardless of the ratio of $\frac{U_1}{U_j}$. This linearity of growth suggests partial or total self preservation and the next few paragraphs show the conditions for which one side of the asymmetric jet can be fully self preserving.

Consider in general a flow U(x, y) which can be described as follows:

$$
\begin{aligned}
U &= U_1 + U_o f\left(\frac{y}{L_o}\right) \\
\overline{u^2} &= U_o^2 \, g_1 \left(\frac{y}{L_o}\right) \\
\overline{v^2} &= U_o^2 \, g_2 \left(\frac{y}{L_o}\right) \\
\overline{uv} &= U_o^2 \, g_{12} \left(\frac{y}{L_o}\right) \\
V &= V_M \text{ at } y = 0
\end{aligned}
\tag{26}
$$

This description includes, but is more general than, that for the asymmetric jet insofar as no restriction has been placed on the velocity U_1 above whereas U_1 is constant in the asymmetric jet. It can easily be shown that the flow of equation 26 is self-preserving if: (see ref. 16)

$$
\begin{aligned}
L_o &\propto (x + x_o) \\
U_1 &\propto (x + x_o)^m \\
U_o &\propto (x + x_o)^m
\end{aligned}
\tag{27}
$$

.../62

$$V_M \propto (x + x_o)^m \qquad (27^A)$$

If $\tau = 0$ at $y = 0$ and at $y = \infty$, the momentum integral equation can be written as:

$$\frac{d}{dx}\int_o^\infty U(U - U_1)dy - V_M(U_M - U_1) + \frac{dU_1}{dx}\int_o^\infty (U - U_1)dy = 0 \qquad (28)$$

and using equations (27)and (28),but not (27^A) :

$$\frac{V_M}{U_o} = \left\{\frac{U_1}{U_o}(3m + 1)\int_o^\infty f d\eta + (2m + 1)\int_o^\infty f^2 d\eta\right\}\frac{dL_o}{dx} \qquad (29)$$

where $\eta = y/L_o$.

Thus if $\frac{dL_o}{dx}$ = constant and $\frac{U_1}{U_o}$ = constant, then $\frac{V_M}{U_o}$ = constant, and the flow satisfies all the conditions for self preservation. In other words, the conditions $\frac{dL_o}{dx}$ = constant and $\frac{U_1}{U_o}$ = constant are sufficient conditions for self preservation of the mean flow in this case. Note that it has been tacitly assumed that $y = 0$ is a straight line (although certainly not a stream line).

An example of this type of self preserving flow is found (approximately) in the outer layer of the self preserving wall jet in streaming flow (ref. 16) in which, if the locus of maximum velocity points grows linearly with x and if the shear stress on this line can be neglected, the cross velocity V_M conforms to the requirements of self preservation. The same result can be shown by assuming a mean velocity profile of the form $U = U_1 + U_o f\left(\frac{y - y_M}{L_o}\right)$; a requirement for self preservation then becomes that both y_M and L_o be linear functions of x, i.e. that the line of maximum velocity be straight.

In the asymmetric jet, the streaming flow velocity

.../63

side is clearly not self preserving unless the ratio $\frac{U_1}{U_o}$ is constant, a condition satisfied only in the two extreme cases of the mixing layer or the jet in still air. The other side however, on which the external stream velocity is zero, can satisfy the requirements for self preservation if a line joining points of maximum velocity is straight, and if the shear stress at the point of maximum velocity is negligible.

If the zero velocity side is completely self preserving then the exponent m describing the streamwise variation of maximum velocity, is given by:

$$m = \frac{1}{2}\left\{ \frac{V_M/U_o}{\int_o^\infty f^2 d\eta \, \frac{dL_o}{dx}} - 1 \right\} \qquad (30)$$

where $U_M \propto (x + x_o)^m$ and $U = U_M \; f(y/L_o) = U_M \; f(\eta)$.

Equation (30) reduces to the exponent for the jet in still air (- 1/2) when $V_M = 0$ and gives the value for V_M/U_o for the plane mixing layer when m = 0, in co-ordinates oriented along the line of maximum velocity.

In practice, the degree to which the lower side of the asymmetric jet will be self preserving depends on the shear stress at the velocity maximum and on the history of the fluid entering the layer with velocity V_M. If the shear stress at the velocity maximum is small (compared with some other shear stress in the layer, say at the point of maximum shear) and if the fluid entering the layer has not already been influenced by a relatively large rate of strain, then the flow will be approximately self preserving. The last requirement is probably not

.../64

met for most asymmetric jet flows, and the function g_{12} in equation (26) will probably not be the same at various streamwise locations in the zero velocity side of the flow.

Calculations of the present asymmetric jet flow were based on the assumption of exponential velocity profiles for each side, i.e.

$$\text{streaming flow side: } U = U_1 + U_o \exp\left\{-k\left(\frac{y}{L_U}\right)^2\right\} \qquad (31)$$

$(y \gg o)$

$$\text{zero velocity side: } U = U_M \exp\left\{-k\left(\frac{y}{L_L}\right)^2\right\}$$

$(y \ll o)$

where $U_1 + U_o = U_M$ for continuity of velocity at $y = 0$, $k = \log_e 2$, and L_u and L_L are defined in Figure 1.

Five unknowns are present: U_M, L_U, L_L, V_M and τ_M, the latter being the shear stress at $y = 0$. The cross velocity V_M is an unknown since no obvious boundary condition for V exists. Four equations can be constructed on the basis of the present double integral technique. All are momentum integrals of the boundary layer equations of motion in the x direction, and the limits used are:

i. $y = -\infty$, $y = 0$

ii. $y = -L_L$, $y = 0$

iii. $y = 0$, $y = \infty$

iv. $y = 0$, $y = L_U$

Since τ_M is zero in the two extreme cases (the still air and the mixing layer) it appears reasonable to neglect its effect in intermediate cases. The equation (31) makes the

.../65

assumption that the locus of the maximum velocity points lie along a straight line, the line y = 0. With these two assumptions, complete self preservation of the zero velocity side is assumed.

For calculations, the shear stress at the points $y = L_U$ and $y = - L_L$ can be found from equation (12) with values for the constants R_{T_o} and C the same as those found necessary by examination of free jets in uniform streaming flow (section 2.3). By assuming $\tau_M = 0$, the number of equations equals the number of unknowns.

The calculated and measured values of L_U and L_L are shown in figures 21 to 25. Initial values for the calculation were chosen from experimental measurements in all cases.

The width scale L_L on the zero velocity side grows linearly in all calculations and predicts the measured values with fair accuracy (the width scale in Figure 25 could be measured only approximately for $x/b > 140$ since the point of maximum velocity is not well defined experimentally as the asymmetric jet flow becomes a mixing layer).

The calculated distributions of L_U do not describe the measured values at all well, the differences between the two increasing with increasing $\frac{U_l}{U_j}$. Apparently the assumption that the two sides of the jet are independent is approximately valid for the major side, i.e. the zero velocity side, but not for the other or minor side. The effect of the ratio $\frac{L_u}{L_L}$ might be taken into account by choosing mean-velocity length scales for each side which are a combination of the dimensions L_U and

.../66

L_L or a function of $\frac{L_U}{L_L}$. It is clear that the smaller or minor side must be significantly affected by the major side and that the analysis has omitted such interdependence.

For sufficiently large x, the virtual origin of the flow (represented by x_o in equations (27)) can be assumed zero. Thus, using measured values as starting conditions, the calculated values of U_M should vary as x^m, because of the theoretical self preservation of the zero velocity side. This was found to be the case in all calculations as evidenced by the approximately linear plots on logarithmic scales of $\frac{U_M}{U_j}$ vs. x/b in figure 26.

Some divergence is evident between calculated and measured values of U_M however, as shown in figure 26. The differences between experimental points and calculated curves can probably be attributed to the unrealistic independence of the two sides assumed in the calculations.

The experimental results indicated a nearly linear streamwise distribution of the maximum velocity location except for large values of $\frac{U_1}{U_M}$ when L_U is decreasing. To relax the assumption of linearity in the development of y_M (the value of y at which $U = U_M$), a condition by which V_M can be calculated must be found. In this connection, the transverse equilibrium condition has been used by Kuethe (ref. 36) in his analysis of the mixing layer between two parallel streams of velocity U_1 and U_2. This condition was suggested by Von Karman and was stated as:

$$U_2V_2 + U_1V_1 = 0 \qquad (32)$$

.../67

where V_1 and V_2 are the values of V which accompany the uniform velocities U_1 and U_2 at large positive and negative values of y respectively.

Equation (32) is not applicable to the asymmetric jet in uniform streaming flow. Since $U_2 = 0$, it reduces to $V_1 = 0$ for all cases, a condition which is not even approximately correct for small values of $\frac{U_1}{U_M}$.

The complete transverse momentum integral equation may be given by:

$$V_{+H}^2 - V_{-H}^2 + \frac{d}{dx} \int_{-H}^{H} (UV)dy = 0 \qquad (33)$$

where H is assumed to be large c.f. the width of the shear layers. Equation (33) could be applied to the present problem, using an iterative technique, but has not been used in the calculations presented in this thesis.

With the present analytical method, it appears that one must be content with a fairly accurate prediction of the development of the dominant side of the asymmetric jet. The further improvements suggested - manipulation of the mean flow length scales to account for the interdependence of the two sides and the use of the transverse equilibrium condition - might well provide a framework for more accurate predictions of the entire flow development.

.../68

2.7 THE MIXING LAYER

Although a limiting case of the asymmetric jet in uniform streaming flow, the plane mixing layer between a uniform stream and fluid at rest is of particular interest because of its completely self-preserving nature. Measurements in a mixing layer were made in the test section configuration described in the previous section (2.6) and measurements of intermittency in this flow have already been described in some detail (sections 2.1 and 2.2). The value of $\frac{U_1}{\nu}$ in the present experiments was 40.2×10^4 FT^{-1}.

Two mean velocity profiles are shown in Figure 28 together with a mean line from the measurements of ref. 37. The boundary layer just upstream of the origin was measured and can be described by the two integral parameters θ and δ^* together with a nominal thickness $\delta_{.99}$ measured to the ordinate where $\frac{U}{U_1} = .99$. The values for the present case were: $\theta = .031$ in., $\delta^* = .039$ in., $\delta_{.99} = .350$ in.

The measured development of the mixing layer, in terms of the points where $\frac{U}{U_1}$ is 0.5, 0.1 and 0.95, is shown in Figure 27. Mean lines drawn through the data indicate a virtual origin for the flow which is both above and downstream from the nominal origin of mixing. This effect is discussed in ref. 38 and is a result of the turbulent upstream boundary layer.

For comparison with other shear flows, it was found convenient in section 2.2.2 to approximate the mean velocity distribution in a mixing layer by the equation (25), that is:

$$U = U_1 \exp \left\{ - k \left(\frac{y - y_M}{L_o} \right)^2 \right\} \qquad (34)$$

.../69

where $L_o = y_{M/2} - y_M$. A curve of the form:

$$U = U_1 \exp \left\{ - 50 \left(\frac{y - y_M}{x}\right)^2 \right\}$$

has been drawn on figure 28, fairly describing the data, from which the approximate relation

$$\frac{y_{M/2} - y_M}{x} = \frac{L_o}{x} = 0.118 \qquad (35)$$

may be found for the present results. In equations (34) and (35), y_M is the value of y at which $U = U_1$. Since y_M is uncertain in the measured data, its value has been found by fitting the best curve of the form of equation (34) to the experimental points of figure 28. As described in ref. 9, the theoretical solution of Tollmein for the mixing layer, used with the data of ref. 37 provides a value for $\frac{y_{M/2} - y_M}{x}$ of 0.114.

When the analysis of the preceeding section is applied to the mixing layer, only two equations and two unknowns remain. The unknowns are L_o of equation (34) and V_M, the magnitude of V at $y = y_M$. The equations may be combined to eliminate V_M and the resulting single equation is:

$$\frac{dL_o}{dx} = \frac{1}{C + .1455\ R_{T_o}} \qquad (36)$$

where the mean velocity profile of equation (34) has been used and C and R_{T_o} are defined by equation (12).

Choosing the values for R_{T_o} and C found in section 2.5 in connection with the free jet in uniform streaming flow, (as was done in the previous section), the predicted value for $\frac{dL_o}{dx}$ becomes 0.108. This compares favourably with the measured value of 0.118 described by equation (35). (For large x, the

.../70

effect of a virtual origin may be neglected and $\frac{dL_o}{dx} \approx \frac{L_o}{x}$). In this analysis, as in that for the asymmetric jet in uniform streaming flow (section 2.6) the co-ordinate system has been chosen so that the x axis lies along (or parallel to) the line joining points of maximum velocity, in this case defined by $y = y_M$ in equation (34).

The use of equation (34) to describe the mixing layer is convenient, in view of other analyses carried out, but is not the best approximation to the data which could be found. (See, for example, ref. 7). Nevertheless, the agreement between predicted and measured values of $\frac{dL_o}{dx}$ provides evidence that the constants R_{T_o} and C found in connection with the free jet in uniform streaming flow, have value for predictions of other mean flow developments.

The analysis of this section may be readily extended to the mixing layer between two streams of constant velocity U_1 and U_2 ($U_1 > U_2$). No new variable enters the problem, both U_1 and U_2 being presumed known, and no new equations or constants are required. The velocity profile is assumed to be given by:

$$U - U_2 = (U_1 - U_2) \exp \left\{ - k \left(\frac{y - y_M}{L_o}\right)^2 \right\} \qquad (37)$$

and the resulting expression for $\frac{dL_o}{dx}$, after elimination of V_M as before, is:

$$\frac{dL_o}{dx} = \frac{1}{R_{T_o} \left\{ \frac{.321\ U_2}{U_1 - U_2} + .1455 \right\} + C} \qquad (38)$$

where C and R_{T_o} are again defined by equation (12). Using the appropriate values of R_{T_o} and C, as given in Table 1, the fol-

.../71

lowing equation can be derived:

$$\frac{\frac{dL_o}{dx}}{\left[\frac{dL_o}{dx}\right]_{U_2=0}} = \frac{\lambda}{\lambda + .356\ (1 - \lambda)} \qquad (39)$$

where $\lambda = \frac{U_1 - U_2}{U_1 + U_2}$ and $U_1 > U_2$.

The only experimental evidence available for comparison with equation (39) is that of ref. 39, which concluded that $\frac{dL_o}{dx} \Big/ \left[\frac{dL_o}{dx}\right]_{U_2=0}$ was approximately equal to λ. This conclusion is equivalent to the statement that $1/R_T$ is constant and independent of the velocity ratio $\frac{U_2}{U_1}$ and is in conflict with the conclusions of the present theory represented for this case by equation (39).

The experiments of ref. 39 were conducted in a water table, with a useful depth of water of 10 inches. Since in many cases the shear layers being investigated extended over a 6-inch mixing region, the effective aspect ratio of the experiments was of the order of unity, the smallest ratios of $\frac{U_2}{U_1}$ producing the largest mixing regions and therefore the smallest effective aspect ratios. Since no comparison between the data reported in ref. 39 and other references is yet possible (the case for $\frac{U_2}{U_1} = 0$ was not investigated in ref. 39) there is some doubt as to the validity of the experimental results. No definite conclusions can be made therefore concerning the applicability of equation (39).

The analysis for a mixing layer between two uniform streams can be readily extended to the non-zero pressure gradient

.../72

case. Without further experimental verification of the existing analysis however, it does not seem worthwhile to formulate this extension.

.../73

2.8 CONCLUDING SUMMARY FOR PART II

Measurements of intermittency have been made in several approximately self preserving wall jets (including the wall jet in still air), the free jet in still air and the mixing region between a uniform stream and fluid at rest. Further two-dimensional measurements are available for the smooth wall flat plate boundary layer, and for the small deficit wake. All of these measurements of intermittency have been used to examine the validity of the large eddy energy equilibrium hypothesis, which may be expressed by the following equation:

$$R_T = \frac{L_o U_o}{\nu_T} \propto \left(\frac{L_o}{L}\right)^2 \qquad (40)$$

L_o and U_o are mean velocity length and velocity scales, L is the length scale associated with the large eddies of the flow and ν_T is evaluated at a representative non-dimensional ordinate in the flow. By assuming that L is proportional to the standard deviation of the free turbulent boundary of the shear flow (σ), this equation can be experimentally verified for each flow in which mean velocity and intermittency measurements have been made. The results substantiate the equilibrium hypothesis, as may be seen from the summarizing plot of R_T vs. $\left(\frac{L_o}{\sigma}\right)^2$ presented in Figure 3.

Use is made of the energy equilibrium hypothesis in the analysis of shear flow development presented in Chapter I. The analysis has been applied in Chapter II, to five different types of shear flow: wall jets (in general adverse pressure gradients) free jets in uniform streaming flow, wakes in near-equilibrium pressure gradients, asymmetric free jets in uniform streaming flow

.../74

and the free mixing layer between fluid at rest and a uniform stream. The growth of L_o and decay of U_o predicted by the analysis have been compared with measured mean flow developments in every case.

The measured mean flow parameters of wall jets which were measured are predicted quite accurately by the method outlined in Chapt.I. Although no detailed measurements near separation are available, it is possible to make estimates, using the present analytical technique, of the point at which a given wall jet will separate in a specified pressure gradient.

Measured developments of free jets and wakes in streaming flow are predicted by the analysis with reasonable accuracy. Certain unexplained anomalies have arisen in comparing these cases with each other however. It was anticipated that the small increment jet in uniform streaming flow would approach an asymptotic condition of near self preservation exactly like that approached by the small deficit wake. From the data available, it would appear that the jet approaches a self-preserving condition unlike that of the wake, the jet flow having a non-dimensional shear stress of only about one-half of that in the corresponding wake flow at an equivalent non-dimensional ordinate. This incompatability is probably due to insufficient development lengths in the small increment and small deficit measurements reported so far.

Provided that an appropriate adjustment is made to one of the empirical constants used in the present analysis, reasonably accurate predictions can still be made in both free

.../75

jets and wakes however.

The asymmetric jet in uniform streaming flow formed by a free jet bounded on one side by a uniform stream and on the other by fluid at rest, can be divided into two adjacent layers, separated by the point of maximum velocity. The analysis in its present form takes into account the cross velocity at the point of maximum velocity but does not allow for a shear stress at this point or consider in other ways the effects of the development of the streaming velocity side which is apparently being strongly affected by the adjacent layer. However, the analysis does predict with good accuracy, the streamwise development of the still air side.

The mixing layer between a uniform stream and fluid at rest is a limiting case of the asymmetric jet. Only one layer, in the sense defined in the previous paragraph, is present in this flow and the analysis predicts its streamwise development with good accuracy.

One pair of constants has been used for the wake analysis, another for the free jet, asymmetric jet and mixing layer analyses, and a third for the wall jet predictions. These pairs of constants are all listed in Table I, together with the bases on which they were calculated. A recent survey by Newman (ref. 51) of the existing data for the free jet in still air and the small deficit wake indicates that more appropriate values of R_T for these two cases are 32.9 and 13.0 respectively so that corresponding values of R_{T_o} and C would become 13 and 9.13 respectively. Use of Newman's values does not significantly

.../76

change the results presented in this thesis and does not, of course, remove the apparent discrepancy between the values of R_T in the small increment jet and the small deficit wake.

In summary it appears that the present analytical method is capable of predicting the streamwise development of many two dimensional turbulent shear flows. It is not applicable to all cases however and cannot be used indiscriminately, since the constants found are apparently not universal.

.../77

CHAPTER III

AN APPLICATION OF THE WALL JET ANALYSIS: SEPARATION CONTROL ON AN AEROFOIL WITH TRAILING-EDGE FLAP

3.1 INTRODUCTION

The wall jet analysis of Chapter I, supplemented and substantiated by the measurements described in Chapter II, will be used in this Chapter to estimate the blowing requirements for the suppression of separation on a thin aerofoil with extended trailing edge flap. These calculations are intended to illustrate the type of prediction which can be made using the present method. Calculations of this sort have been one of the ultimate goals of this research however, and should be of almost immediate use in the development of devices for the control of separation by blowing.

No attempt has been made to consider a wide range of variables for the present computation. The flap chord has been fixed at 25% of the wing chord, the Reynolds number has been fixed at 5×10^6 (based on free stream velocity and total aerofoil chord) and the angle of incidence of the main chord has been maintained at zero degrees. Flap deflection angles from 30 to 90 degrees have been examined.

Two slot widths have been used in the calculations, the total chord to slot width ratios chosen as 2000 and 500. These two examples give some idea of the extent to which the usual blowing momentum coefficient, defined in section 3.4, provides a suitable parameter for collapsing results.

.../78

3.2 THE EXTERNAL PRESSURE DISTRIBUTION

Largely on the basis of its simplicity, the thin aerofoil theory for flapped flat plate aerofoils has been used to calculate the external pressure distribution over the aerofoil. This theory is known to overestimate the total lift for large flap angles (see ref. 40), and is therefore likely to provide results which overestimate the blowing requirements for a real flapped aerofoil at large flap angles and/or incidences.

From thin aerofoil theory one can obtain the following expression for the pressure distribution over the upper surface of an aerofoil located with its leading edge at x = 0 (ref. 41):

$$C_p = \frac{p - p_\infty}{\frac{1}{2}\rho U_\infty^2} = -2\left\{A_o \cot\left(\frac{\theta'}{2}\right) + \sum_{n=1}^{\infty} A_n \sin(n\theta')\right\} \qquad (41)$$

where θ' is related to the co-ordinate x and the chord c by the expression:

$$x = \frac{c}{2}(1 - \cos\theta') \qquad (42)$$

and the coefficients A_o and A_n are determined by the aerofoil shape:

$$A_o = \frac{1}{\pi}\int_o^{\pi} \frac{ds}{dx}\, d\theta'$$

$$A_n = \frac{2}{\pi}\int_o^{\pi} \frac{ds}{dx}\cos(n\theta')\, d\theta' \qquad (43)$$

where $\frac{ds}{dx}$ is the local inclination of the aerofoil surface.

Applying these equations to a 25% flap chord aerofoil at zero angle of attack and with flap angle η_1, the coefficients A_o and A_n become:

$$A_o = \frac{\eta_1}{3}$$

$$A_n = \frac{-2\eta_1(-1)^n \sin\left(\frac{n\pi}{3}\right)}{n\pi} \qquad (44)$$

.../79

Two singluarities occur in the equation (41), one at the leading edge ($\theta' = 0$), and the other at the flap knee ($\theta' = \frac{2\pi}{3}$). The latter has been avoided by placing the slot slightly downstream of the flap knee; the leading edge singularity will be considered later in connection with leading-edge boundary-layer calculations.

The pressure coefficient for unit flap deflection and zero incidence, $\frac{c_p}{\eta_1}$, was calculated at 26 stations along the flap chord and at 69 stations along the aerofoil chord ahead of the flap knee. At least 1000 terms of the series in equation (41) were summed at each station and the results are accurate to within 1%. At the flap knee the series does not converge as it reduces to:

$$\frac{c_p}{\eta_1} = -\frac{2}{3\sqrt{3}} - \frac{2}{\pi} \sum_{n=1}^{\infty} \left(\frac{1}{n}\right)$$

The ratio $\frac{c_p}{\eta_1}$ is plotted in Figure 29 for the aerofoil upstream of the flap knee and in Figure 30 for the flap chord.

.../80

3.3 THE INITIAL CONDITIONS FOR THE CALCULATION

Because preliminary calculations showed that the upstream boundary layer was of great importance, a method of incorporating its effect into the computation of the initial conditions had to be found. One must be able to predict the wall jet characteristics at some downstream point when given the properties of the boundary layers inside and outside the slot, the central slot ejection velocity and the pressure distribution. The method must be suitable for strong adverse pressure gradients since blowing is seldom used in any other situation.

Because the slot is very much smaller than the wing chord, the length of the potential core (about 10 slot widths) is negligible in comparison with the overall length of wall jet development. It is therefore possible to approximate the change in the flow which occurs from the slot to the end of the potential core by an instantaneous conversion at the slot: upstream boundary layer plus square jet velocity distribution equals fully developed wall jet. This assumption implies that the momentum surplus from the slot is greater than the momentum deficit from the boundary layer and that a fully developed wall jet profile i.e. one like that sketched in Figure 1, is formed a short distance downstream of the slot.

It is interesting to note that the effect of a strong adverse pressure gradient on an uneven velocity profile is an exaggeration of the original velocity variation. As an example of this effect, consider a wake in an adverse pressure gradient: let the external velocity be U_1 at station 1, and U_2 at station

.../81

2 while the minimum velocities are U_{M_1} and U_{M_2}. To assess the effect of the pressure gradient alone, neglect the energy loses along a mean stream line and apply Bernouilli's equation. If the pressure is constant across the flow at each station,

$$\frac{U_{M_2}^2}{U_2^2} - \frac{U_{M_1}^2}{U_1^2} = \left(1 - \frac{U_1^2}{U_2^2}\right)\left(1 - \frac{U_{M_1}^2}{U_1^2}\right) \qquad (45)$$

so that:

$$\frac{U_{M_2}^2}{U_2^2} < \frac{U_{M_1}^2}{U_1^2} \quad \text{if} \quad \frac{U_1}{U_2} > 1 \text{ and } \frac{U_{M_1}}{U_1} < 1$$

From this admittedly crude example it can be seen that if the boundary layer upstream of a wall jet is not small, its effect on the downstream velocity profile may be exaggerated by an adverse pressure gradient. In extreme cases, a region of very low or negative velocity may form above the wall jet even though the wall jet itself does not separate from the solid surface. The formation of a backflow region above the flap, with consequent loss of lift, might be avoided by blowing at an angle to the flap so that the wall jet separates from the solid surface near the slot and then reattaches at some subsequent downstream position. The relative thickness of the slot lip might be significant in the flow near the slot since its wake contributes to the momentum deficit which must be removed by the jet momentum. The effect of slot lip thickness on a wall jet in still air is discussed in ref. 8.

An example of flow reversal resulting from the exaggeration of an initial total head variation by an adverse pres-

.../82

sure gradient is reported by Moon (ref. 50). In the wide angle diffuser which Moon investigated, a wake from a centre body upstream of the diffuser created a central region of backflow even though the primary flow remained attached at the diffuser walls due to the action of distributed suction.

Returning now to the instantaneous conversion of the velocity profile at the slot, there are two alternative ways in which the conversion has been assumed to take place:

(a) The maximum velocity of the fully developed profile is equated to the slot velocity U_j and the total momentum thickness of the flow is assumed to remain constant.

(b) The total momentum flux and the total mass flux in the original profile is equated to the corresponding quantities of the fully developed profile. This assumption requires a consistent definition of the "outer edge" of the profile and the following relationship is assumed for this purpose:

$$\left[\frac{U}{U_1} - 1\right]_{edge} = .01$$

The further assumption for y_M, the thickness of the inner layer in the fully developed profile, has also been made:

$$\frac{y_M}{b} = \frac{1}{3} \quad \text{at } x = 0. \tag{46}$$

This value is somewhat arbitrary although it reflects known values of $y_{M/b}$ at the end of the potential core in zero pressure gradient cases (see, for example, Figure 6 of ref.9).

.../83

Representing the original mean velocity profiles at the slot by

$$\frac{U}{U_1} = \left(\frac{y - b}{y_s}\right)^{1/7} \qquad \text{for } y > b$$

and

$$\frac{U}{U_j} = 1 \qquad \text{for } 0 < y < b \tag{47}$$

and in the fully developed profile by:

$$\frac{U}{U_M} = \left(\frac{y}{y_M}\right)^n \quad \text{for } y \ll y_M$$

$$U - U_1 = (U_M - U_1) \exp\left\{-k \left(\frac{y - y_M}{y_{M/2} - y_M}\right)^2\right\} \text{ for } y \gg y_M \tag{48}$$

the total momentum flux in the original (subscript 1) and fully developed (subscript 2) profiles are:

$$\left[\text{momentum flux}\right]_1 = U_j^2 b + \frac{7}{9} U_1^2 y_s \tag{49}$$

$$\left[\text{momentum flux}\right]_2 \approx U_1^2 (y_1 - y_M) + 2U_1 (U_M - U_1) \frac{1}{2} \cdot \sqrt{\frac{\pi}{k}} \cdot (y_{M/2} - y_M) + \frac{(U_M - U_1)^2}{\sqrt{2}} \cdot \frac{1}{2}\sqrt{\frac{\pi}{k}} \cdot (y_{M/2} - y_M) + \frac{U_M^2 y_M}{2n + 1}$$

where y_1 is the value of y at which $\frac{U}{U_1} - 1 = .01$.

Similarly:

$$\left[\text{mass flux}\right]_1 = U_j b + \frac{7}{8} U_1 y_s \tag{50}$$

$$\left[\text{mass flux}\right]_2 \approx (y_{M/2} - y_M) U_1 \left\{\frac{y_1 - y_M}{y_{M/2} - y_M}\right\} + \frac{U_M - U_1}{2} \cdot (y_{M/2} - y_M) \sqrt{\frac{\pi}{k}}$$

The total momentum thicknesses for the two profiles are:

$$\theta_1 = \frac{7}{72} y_s - b \frac{U_j}{U_1} \left(\frac{U_j}{U_1} - 1\right) \tag{51}$$

.../84

$$\theta_2 = -(y_{M/2} - y_M)\left(\frac{U_M - U_1}{U_1}\right)\left(1 + \frac{(U_M - U_1)}{\sqrt{2}\,U_1}\right)\frac{1}{2}\sqrt{\frac{\pi}{k}}$$

$$+ y_M \frac{U_M}{U_1}\left\{\frac{1}{1+n} - \frac{U_M}{U_1}\frac{1}{1+2n}\right\}$$

The values of $\frac{U_M}{U_j}$ and $\frac{y_{M/2}}{b}$ can be found by methods (a) or (b) once $\frac{U_1}{U_j}$, y_s/b, n and y_M/b are known. The latter is obtained from equation (46).

Some results of the calculations are shown in Figure 31 for the particular case $U_1/U_j = 0.5$, $n = 1/7$. For very small values of y_s/b, method (b) predicts values of U_M/U_j which exceed unity. This is not possible since no velocity ever exceeds U_j in a wall jet in adverse pressure gradient. At high values of y_s/b, the values of $\frac{y_{M/2} - y_M}{b}$ predicted by method (a) become negative. This is again a physically unacceptable result.

Both types of calculation were finally used, method (b) where it provided values of U_M/U_j less than unity and method (a) for all other values of y_s/b.

For large y_s/b, the curve of $\left(\frac{U_M}{U_j}\right)_{(b)}$ in Figure 31 asymptotically approaches the value of $\frac{U_M}{U_j} = 0.5$ which is the value of U_1/U_j in this case. A conflict arises in the definition of mass flux when U_M is no longer greater than 1.01 U_1. This difficulty has been resolved by fixing U_M at 1.01 U_1 in cases where $U_1 < U_M < 1.01\ U_1$.

Very large y_s/b produce negative values of the total momentum excess at the slot (i.e. positive values of θ_1 in equation (51)). In this case a fully developed wall jet profile is no longer possible and the flow from the slot has been con-

.../85

verted to a boundary layer profile with momentum thickness equal to θ_1 and a velocity profile given by a 1/7th power law. Subsequent calculations then proceed as outlined in Appendix III.

Since the values of θ_2 found in the methods (a) and (b) are identical and since the downstream calculation is quite insensitive to slight changes in the initial shape of the fully developed wall jet, the matching method does not critically affect the final result. However the mixing of a wall jet with a large upstream boundary layer could usefully be studied in greater detail.

The value of y_s/c which has been presumed known in the preceding discussion, will be discussed in the next section. Since there are no published measurements from which typical values of this ratio could be determined, its value must be estimated theoretically. Some sample calculations, described in the next section, are presented to assess the importance of y_s/c.

The slot is presumed to be located at x/c = .7542, just downstream of the flap knee at x/c = .75. For leading edge calculations, which are very briefly discussed, a slot is presumed to be located at x/c = .0042. Boundary layer calculations described in the next section are also initiated from this station.

.../86

3.4 RESULTS AND DISCUSSION

For investigations of separation control by blowing the parameter usually used to correlate results is C_μ, the momentum coefficient, defined as:

$$C_\mu = \frac{\rho_j U_j^2 b}{\frac{1}{2} \rho_\infty U_\infty^2 c} \qquad (52)$$

where b is the slot width and c the total chord of the aerofoil. It is generally conceded (ref. 42, 43) that the coefficient C_μ collapses experimental results to a single curve only for large values of $\frac{U_j}{U_\infty}$, and the usefulness of C_μ in this regard will be examined using the present calculation method.

Consideration will be given at first to the effect of a slot located very close to the leading edge. Its role is to eliminate separation over the main aerofoil chord, and since the pressure gradient is favourable in the region $.40 < x/c < .75$, separation is possible only between the leading edge and the point of maximum pressure near $x/c = .40$ (see Figure 29). The momentum coefficient which describes the momentum flux from a leading edge slot will be designated as C_{μ_n} to distinguish it from the more usual flap knee blowing to be discussed in a later paragraph. Although leading edge blowing is primarily useful for high angles of attack, this investigation has been restricted to zero incidence, since the calculations are intended to illustrate the type of prediction which can be made rather than make predictions for a wide range of variables.

The boundary layer upstream of a leading edge blowing slot is probably very small and preliminary calculations for a

.../87

slot located at x/c = .0042 were carried out with $y_s/c = 0$. (y_s is defined in the previous section and denotes the nominal thickness of the upstream boundary layer). A slot width to chord ratio b/c of 1/2000 was chosen, and the angle of attack of the main chord was maintained at 0°. For the calculations, the initial conditions were found by the method outlined in section 3.4 and the numerical computations were carried out using a programme very like that of Appendix V. Separation was assumed at the point where the inner layer exponent, n, as defined by equation (13), reached the value 1/2.

For values of the flap angle η_1, between 30° and 90°, very small values of C_{μ_n} were sufficient to prevent separation of the boundary layer over the main chord of the aerofoil ($0 < x/c < .75$). The development of a turbulent boundary layer without blowing was also calculated, using the method outlined in Appendix III. A sample result is presented in Figure 32 and shows the shape factor H (which is related to the exponent n by the expression $H = 1 + 2n$) for a flap angle of $\eta_1 = 60°$. The usual criterion for separation, H = 2.0, shows that separation does take place at $x/c \approx .06$ but the distribution of H suggests that a slight relief in the magnitude or extent of the adverse pressure gradient would eliminate the separation. This qualitatively confirms that very little blowing from a leading edge slot would be required for the suppression of separation for $\eta_1 = 60°$. Results similar to those in Figure 32 showed that the boundary layer without blowing did not separate for $\eta_1 \leqslant 50°$.

Although very little blowing is required to prevent

.../88

separation on the main chord of the aerofoil, the values of C_{μ_n} do not approach zero. As has been pointed by Williams and Butler (ref. 44), the value of U_j must always exceed the local value of U_1 at the slot for blowing to be advantageous. A minimum value of C_μ can therefore be calculated, based on the equation $U_j = \left[U_1\right]_s$ (the subscript s denotes values at the slot) and, for the present case, the result can be expressed as:

$$C_{\mu_{min}} = 2\left\{\frac{U_1^2}{U_\infty^2}\right\}_s \cdot \frac{b}{c} \approx \frac{10.35\eta_1 + 1}{1000} \text{ for } \frac{b}{c} = 2000 \qquad (53)$$

Incompressible flow is assumed throughout this thesis so that

$$\rho_\infty = \rho_j = \rho = \text{constant}.$$

Since compressibility effects do not impair the usefulness of the co-efficient C_μ as a basis for correlating experimental data (ref. 42) the present calculations, which assume incompressible flow, should display trends representative of high pressure blowing situations in which $\rho_j \neq \rho_\infty$.

Thus $C_{\mu_{min}}$ is about .006 at $\eta_1 = 30°$ and rises to 0.016 at $\eta_1 = 90°$. The experimental values of C_{μ_n} mentioned in the sparse literature on the subject are "of the order of 0.02" (ref.44) and their close proximity to the calculated values of $C_{\mu_{min}}$ substantiates the conclusion that very little blowing is required to supress separation upstream of the flap knee. The values of $C_{\mu_{min}}$ quoted above are, of course, dependent on the ratio c/b and on the exact location of the slot, the latter determining $\left\{\frac{U_1}{U_\infty}\right\}_s$. Some upstream boundary layer must be present in practice and this effect could modify the small values of C_{μ_n} required to prevent separation.

.../89

Turning now to the problem of flow separation from the trailing edge flap, calculations havebeen performed for various η_1 with a blowing slot located at x/c = .7542 (i.e. just downstream of the flap knee located at x/c = .75). In order to examine the effect on the calculated results of an upstream boundary layer, results have been obtained both for $y_s/c = 0$ and for $y_s/c = .02$. The latter value is thought to be typical of the boundary layer occurring in practice just upstream of the flap knee on an aerofoil at zero incidence; rather surprisingly, no measurements of this upstream boundary layer for significant flap angle but without separation from the flap, have been reported. Further results have been obtained using the main-chord boundary-layer calculations just described to find y_s/c and assuming that the suction peak at the flap knee terminates at the value reached at the slot (i.e. $\frac{C_p}{\eta_1} = -3.669$). Since separation of the boundary layer upstream of the flap knee is predicted for $\eta_1 \geqslant 60°$, values of $\frac{y_s}{c}$ could be calculated only for angles less than 60°. The results of these calculations will be discussed later in connection with empirical data collected from various sources. For all these cases the ratio c/b was taken to be 2000 and the Reynolds number $\frac{U_\infty c}{\nu}$ was assumed to be 5×10^6.

Calculations were performed with various $\left\{\frac{U_1}{U_j}\right\}_s$ and for various flap angles; flow separation was assumed when the value of H for the inner layer exceeded 2.0 (i.e. $n > 1/2$). In this way a critical value of C_μ could be found for which separation was just avoided. Calculated values of $C_{\mu_{crit}}$ are shown in Figure 33.

.../90

Boundary layer calculations (no blowing) have been carried out for the trailing edge flap. An example of the results is shown in Figure 34, where the development of the shape factor H, is given for $\eta_1 = 60°$, starting from the position x/c = .7542 and with no upstream boundary layer. Results using the method of Spence (see, ref. 42), Head (ref. 45) and Appendix III are compared in this figure. Agreement between the three calculations is only good insofar as all three methods predict flow separation for this flap deflection. However the method of Head, which is probably the most reliable in this adverse pressure gradient (see ref. 24), and the method of Appendix III concur fairly well in predicting a separation near the trailing edge of the flap, as indicated by values of H greater than 2.0. This example suggests that a small momentum increase in the boundary layer, such as that provided by small values of C_μ from a slot at the flap knee, would be sufficient to preserve attached flow over the flap, in qualitative agreement with the results for $y_s/c = 0$ of Figure 33.

When $y_s/c = 0.02$ however, the values of $C_{\mu_{crit}}$ rise considerably and the magnitude of the increase, as shown in Figure 33, emphasizes the importance of the upstream boundary layer in the control of separation by blowing. A practical corollary to this observation is that the value of C_μ necessary to avoid separation from the flap would be significantly reduced if other flow control devices could be used to eliminate or minimize the boundary layer upstream of the blowing slot.

.../91

Ref. 46 reports large increases in lift when leading edge blowing was added to the more usual flap knee blowing. This result is not surprising in the light of the present calculations, since the nose blowing probably eliminated flow separation upstream of the flap knee and thereby reduced the boundary layer approaching the rear blowing slot.

There has been some question as to the usefulness of the coefficient C_μ in correlating experimental results, particularly for values of $\left[\frac{U_1}{U_j}\right]_s$ which are not small in comparison with unity. The parameter C_μ is the non-dimensional momentum flux from the slot and Kelly (ref. 43) has shown that a more significant parameter would be:

$$C_\mu' = C_\mu - 2 C_Q \left[\frac{U_1}{U_\infty}\right]_s$$

where $C_Q = \frac{U_j b}{U_\infty c}$ for incompressible flow. The parameter C_μ' represents the flux of excess momentum available at the slot in the absence of an upstream boundary layer. It approaches C_μ as $\left[\frac{U_1}{U_j}\right]_s$ approaches zero.

Since theoretical results for various c/b may be obtained using the present numerical technique, the usefulness of the parameter C_μ can be evaluated by examining its ability to correlate the various results in a single curve of $C_{\mu_{crit}}$ vs. η_1. Figure 35 shows values of $C_{\mu_{crit}}$ calculated for two ratios of c/b, 2000 and 500. Lines of constant $\left\{\left(\frac{U_1}{U_j}\right)_s^2 \cdot \frac{c}{b}\right\}$ are also drawn on Figure 35.

As shown by Kelly (ref. 43), the parameter $C_{\mu_{crit}}$

.../92

does not accurately correlate the results for different c/b. As has been found experimentally (see, for example Fig. 18, ref. 48) the smaller slot width is associated with the lower values of $C_{\mu_{crit}}$.

Another comparison of the calculated results is plotted in Figure 36 on the basis of the modified momentum coefficient C_μ'. The degree of correlation is fairly good using this modified parameter, as anticipated from the momentum analysis of ref. 43. For smaller values of $\left[\frac{U_1}{U_j}\right]_s$ correlation on the basis of C_μ would improve; the present values of $\left[\frac{U_1}{U_j}\right]_s$ which are about 0.5 for the smaller value of c/b shown in Figure 35, are larger than those which are usual in practice.

A final comparison is given in Figure 37 between various experimental values of $C_{\mu_{crit}}$ and the present calculated values for $y_s/c = 0.02$. No distinction has been made in this figure between the published values of C_μ required to prevent separation from the flap and those required to provide the potential lift predicted by theoretical means. The latter value of C_μ is slightly larger than the former.

The calculated values of $C_{\mu_{crit}}$ for which $y_s/c = .02$ do not adequately represent any of the widely scattered experimental curves. This is not surprising since the invariance of the parameter y_s/c in the present calculations is quite unrealistic. In practice, the upstream boundary layer would certainly be a function of the flap angle η_1 and would depend to some extent on the exact wing geometry and the Reynolds number. In particular, y_s/c, would tend to increase with increasing η_1, so

.../93

that the present value of 0.02 possibly overestimates the actual value of y_s/c for small flap angles and almost certainly underestimates y_s/c for large flap angles where upstream separation and reattachment would occur. The present values of $C_{\mu_{crit}}$ are therefore too large for small η_1 and too small for large η_1, a trend which is clearly shown in Figure 37. Appropriate modifications to y_s/c would therefore provide a more aggreeable comparison between calculated and measured values of $C_{\mu_{crit}}$.

Also plotted in figure 37 is the curve of $C_{\mu_{crit}}$ found from values of y_s/c calculated with the boundary layer technique of Appendix III. As already mentioned, separation of the boundary layer upstream of the flap knee for $\eta_1 > 50°$ precludes calculations of $\frac{y_s}{c}$ for flap angles larger than 50°. The curve of $C_{\mu_{crit}}$ for which the calculated upstream boundary layer was used is similar to that representing the French results in figure 37. Only when boundary layer calculations can be performed which include separation, development of the separated shear layer and the prediction of reattachment can the present curve of $C_{\mu_{crit}}$ be extended to larger flap angles. The calculated results shown in figure 37 suggest however that when a more accurate knowledge of the boundary layer upstream of the slot is obtained, the calculations can predict the measured variations of critical momentum co-efficient.

.../94

3.5 SUMMARY AND CONCLUSIONS

This thesis is concerned with the streamwise growth of those two dimensional shear flows in which the mean velocity can be represented by a single non-dimensional profile. The theoretical analysis of Chapter I contains two major postulates: that the shear stress in the flow may be related to the scale of the largest eddies by the energy equilibrium hypothesis and that the scale of the largest eddies may be determined by considering the effect of the two largest mean rates of strain on the vorticity in a typical large eddy. The additional assumptions required in order to obtain a practical relationship between shear stress and the mean rates of strain are reviewed and discussed in section 1.2.3.

In the use of blowing to prevent boundary layer separation, the wall jet is of great practical interest; yet because of the presence of the wall, it has a more complicated velocity profile than most free turbulent shear flows. The analysis just described can be applied directly in predicting the outer layer development of a wall jet, and in section 1.3 an empirical relation between the turbulent stresses in the inner and outer layers is presented by/the overall development which of the flow in a general pressure gradient can be predicted.

Chapter II describes two groups of measurements. The first of these provides a verification of the energy equilibrium hypothesis by assuming that/scale of the largest eddies the in the flow is directly proportional to the standard deviation of the position of the viscous "superlayer" which bounds the

.../95

vortical turbulent flow. This mean wrinkle amplitude of the superlayer may be related to the intermittency factor distribution, which has been measured directly. Intermittencies have been measured in four self-preserving wall jets, a free jet and a mixing layer, and further measurements in a wake and a boundary layer are available. All these results substantiate the large eddy energy equilibrium hypothesis.

The second group of measurements presented in Chapter II were made in wall jets, free jets, wakes, asymmetric free jets and mixing layers, for comparison with predictions obtained from the analysis of Chapter I. The results are summarized in section 2.8 and show that:

i. free jet and wake developments are predicted by the analysis with reasonable accuracy provided that appropriate empirical constants are used in each case.

ii. a wall jet development in any reasonable adverse pressure gradient is well predicted by the analysis.

iii. the small increment jet appears to be unlike the small deficit wake insofar as its non-dimensionalized shear stress is approximately one-half that in the corresponding wake.

iv. the development of the still-air side of an asymmetric jet in uniform streaming flow can be predicted with good accuracy, while that of the other or streaming flow side cannot be predicted by the analysis in its present form.

v. the growth of the mixing layer between fluid at rest and a uniform stream is predicted satisfactorily since this

.../96

flow is a limiting case of the asymmetric jet.

The wall jet appears in aeronautical applications when blowing is used to prevent separation, being formed in most cases on a deflected flap over which blowing is applied. Chapter III of this thesis presents a theoretical investigation of the momentum flux which must be emitted from a blowing slot in order to prevent boundary layer separation from an aerofoil at zero incidence. A flat plate with a 25% trailing-edge flap is assumed to represent the aerofoil and the blowing requirements are estimated for slots located either near the leading edge or near the flap wing junction.

Very little blowing is required from the leading edge slot for suppression of separation upstream of the flap hinge and quantitative results depend markedly on the size of the slot, its exact location and the aerofoil geometry near the leading edge.

Similarly very little blowing is required from the flap knee slot for the suppression of separation over the extended flap, even at large flap angles, provided no boundary layer is present upstream of the blowing slot. Blowing requirements increase to much larger values when a realistic upstream boundary layer is included in the calculation, and this result emphasizes that the major role of flap knee blowing is to re-energize the boundary layer which has formed over the forward part of the aerofoil.

The present results, calculated for various slot sizes, cannot be well correlated by means of the usual momentum

.../97

coefficient $C\mu$. The modified momentum coefficient, representing the flux of excess momentum at the slot, is shown to be a more appropriate paramenter for this purpose. The present analytical technique provides results in qualitative agreement with available experimental data. It should be readily applicable to particular aerofoils when the boundary layer parameters upstream of the blowing slot are either known or have been calculated analytically.

.../98

TABLE I

SUMMARY OF VALUES USED IN EQUATION (12) FOR THE CALCULATION OF TURBULENT SHEAR STRESS

No.	Flow	R_{T_o}	C
1	Wall Jets	29.4	11.12
2	Wakes	12.1	8.91
3	Free Jets	12.1	10.15
4	Free Jet (with modified constants)	20.5	6.29

The basis for calculation of values:

No.

1. a) Wall jet in still air (ref. 9)
   b) Wall jet in uniform streaming flow, $U_1/U_j = 0.487$ (ref. 9)
2. a) Townsend's small deficit wake (ref. 11)
   b) Reichardt's jet in still air (ref. 34)
3. a) Townsend's small deficit wake (ref. 11)
   b) Forthmann's jet in still air (ref. 35)
4. a) Bradbury's small increment jet (ref. 14)
   b) Forthmann's jet in still air (ref. 35).

Notes

Reichardt's free jet growth is 14% larger than Forthmann's. The first calculations, those for the wakes, were made on the basis of Reichardt's measurements, but since Forthmann's free jet

.../99

values provide better agreement with Bradbury's measurements, the later calculations of constants for the free jets were based on Forthmann's results.

The pair of constants listed above as number 4 was also used for analyses of the asymmetric free jet and of the mixing layer between a uniform stream and fluid at rest.

Newman (ref. 51) has concluded from a recent survey of measurements in the jet in still air and the small deficit wake, that the most accurate values of R_{T_o} and C based on these two flows are 13.0 and 9.13 respectively.

.../100

TABLE II

DETAILS OF THE FULLY OR APPROXIMATELY SELF-PRESERVING FLOWS IN WHICH INTERMITTENCY WAS MEASURED

No.	Flow	$\frac{U_1}{U_o}$	m	$\frac{dL_o}{dx}$	$\frac{U_j b}{\nu}$	$\frac{x_o}{b}$
1	Wall Jet	0	-	.059	19,200	-
2	Wall Jet	.52	- .413	.038	15,700	13.5
3	Wall Jet	1.10	- .386	.028	12,400	- 4
4	Wall Jet	3.04	- .356	.014	10,200	-27
5	Free Jet	0	-	.115	23,100	-

The numbers in this table refer to those in Figures 2 and 3 and in Table III.

.../101

TABLE III

DETAILS OF INTERMITTENCY MEASUREMENTS

No.	Flow	$\frac{x}{b}$	$\left[\frac{U_o L_o}{\nu_T}\right]_{@ L_o}$	$\frac{\sigma}{L_o}$	k_1	k_2	$\frac{y_M}{L_o}$
1	Wall Jet	68.5	55	.310	2.28	2.09	.161
2	Wall Jet	126	49	.336	2.10	1.72	.285
3	Wall Jet	145	36	.403	1.75	1.59	.374
4	Wall Jet	126	34	.471	1.50	1.40	.960
5	Free Jet	100	31	.400	1.77	1.81	0

The numbers in this table refer to those in Figures 2 and 3 and in Table II.

.../102

REFERENCES

1. Kuchemann, D. and Weber, J. — Aerodynamics of Propulsion. McGraw Hill Publications in Aeronautical Science, p.237 (1953).

2. Abramovich, G.N. — The Turbulent Jet in a Moving Fluid. R.A.E. Library translation No. 778 (1958).

2A. Abramovich, G.N. — The Theory of Turbulent Jets; M.I.T. Press (1963).

3. Ribner, H.S. — Field of Flow about a Jet and Effect of Jets on Stability of Jet Propelled Airplanes; NACA Wartime report, L-213 (1946).

4. Kruka, V. and Eskinazi, S. — The Wall Jet in a Moving Stream. Syracuse Univ. Mech.Eng. Dept., Rep. No.ME-937-6309 F (1963).

5. Squire, H.B. and Trouncer — Round Jets in a General Stream. A.R.C., R. & M. No. 1974 (1944).

6. Forstall, W. and Shapiro, A.H. — Momentum and Mass Transfer in Co-axial Gas Jets; Journ.App.Mech. 17, 339-408 (1950).

7. Townsend, A.A. — The Structure of Turbulent Shear Flow; Cambridge Univ. Press (1956).

8. Gartshore, I.S. and Hawaleshka, O. — The Design of a Two-Dimensional Blowing Slot and Its Application to a Turbulent Wall Jet in Still Air; M.E.R.L. Tech.Note 64-5 (1964) McGill U.

9. Gartshore, I.S. — Jets and Wall Jets in Uniform Streaming Flow; M.E.R.L. Report 64-4 (1964), McGill U.

.../103

10. Gartshore, I.S. — The Streamwise Development of Certain Two Dimensional Turbulent Shear Flows; M.E.R.L. Report 65-3 (1965), McGill U.

11. Townsend, A.A. — The Fully Developed Turbulent Wake of a Circular Cylinder; Australian Journal of Sci.Res., Vol. 2, p. 451 (1949).

12. Klebanoff, P.S. — Characteristics of Turbulence in a Boundary Layer with Zero Pressure Gradient; NACA Report 1247 (1955).

13. Reynolds, A.J. — Observations on Distorted Turbulent Wakes; Journ. of Fluid Mechanics, Vol. 13, p.333 (1962).

14. Bradbury, L.J.S. — An Investigation into the Structure of a Turbulent Plane Jet; Ph.D. Thesis, Univ. of London (1963).

15. Grant, H.L. — The Large Eddies of Turbulent Motion; Journ. of Fluid Mechanics, Vol. 4 (1958).

16. Patel, R.P. and Newman, B.G. — Self-Preserving, Two-Dimensional Turbulent Jets and Wall Jets in a Moving Stream; M.E.R.L. Report Ae.5. McGill University (1961).

17. Clauser, F.M. — The Turbulent Boundary Layer; Advances in Applied Mechanics, Vol. 4 (1956).

18. Patel, R.P. — Self-Preserving, Two-Dimensional Turbulent Jets and Wall Jets in a Moving Stream; M.Eng. Thesis, Dept. of Mech.Engineering. (1962), McGill U.

19. Patel, R.P. — Private communication of unpublished measurements.

.../104

20. Bradshaw, P. — The Effect of Wind Tunnel Screens on "Two Dimensional" Boundary Layers; NPL Aero Report 1805, ARC 25 402 (1963)

21. Patel, R.P. — The Effects of Wind Tunnel Screens and Honeycombs on the Spanwise Variation of Skin Friction in "Two Dimensional" Turbulent Boundary Layers; M.E.R.L., TN 64-7 (1964).

22. Bradshaw, P. and Gee, M.T. — Turbulent Wall Jets With and Without an External Stream, A.R.C. R. and M. No. 3252 (1962).

23. Rotta, J.C. — Fundamentals of Turbulent Boundary Layer Theory; Progress in Aeronautical Sciences, Vol. 2, Pergamon Press (1962).

24. Thompson, B.G.J. — A Critical Review of Existing Methods of Calculating the Turbulent Boundary Layer; A.R.C., F.M. 3492 (1964).

25. Newman, B.G. — Some Contributions to the Study of the Turbulent Boundary Layer Near Separation; Australian Depart. of Supply Report ACA-53 (1951).

26. Bradshaw, P. — N.P.L. Turbulent Boundary Layer Measurements; Private Communication to Dr.B.G. Newman, Jan. 1965.

27. Coles, D. — The Law of the Wake in the Turbulent Boundary Layer; Journ. of Fluid Mechanics, Vol. 1, pp. 191-226 (1956).

.../105

28. Wygnanski, I. and Gartshore, I.S. — General Description and Calibration of the McGill 17 in. x 30 in. Blower Cascade Wind Tunnel; M.E.R.L. Tech. Note 63-7 (1963).

29. Patel, R.P. — Measurement of the Reynolds Stresses in a Circular Pipe as a Means of Testing a DISA Constant Temperature Hot Wire Anemometer; M.E.R.L. TN 63-6 (1963).

30. Laufer, J. — The Structure of Turbulence in Fully Developed Pipe Flow; NACA TN 2954 (1953).

31. Corrsin, S. and Kistler, A.L. — Free Stream Boundaries of Turbulent Flows; NACA Report 1244 (1955).

32. Heskestad, G. — Two Turbulent Shear Flows; Johns Hopkins University, Department of Mechanics, AFOSR Contract AF (638)-248, June 1963.

33. Moller, P.S. — An Investigation of a Radial Diffuser Using Incompressible Flow Without Swirl; M.E.R.L. Report 63-9 (1963).

34. Schlichting, H. — Boundary Layer Theory, Pergamon Press Ltd. (1955).

35. Förthmann, E. — Turbulent Jet Expansion; NACA TM No. 789.

36. Kuethe, AM. — Investigations of the Turbulent Mixing Regions Formed by Jets; Journal of Applied Mechanics, Transactions of the A.S.M.E. Vol. 57 (1935) A 87.

37. Liepmann, H.W. and Laufer, J. — Investigation of Free Turbulent Mixing; NACA TN 1257 (1947).

.../106

38. Bradshaw, P. — The Effect of Initial Conditions on the Development of a Free Shear Layer; NPL Aero Report 1117, ARC 26202, F.M. 3509, N.311 (1964).

39. Sabin, C.M. — An Analytical and Experimental Study of the Plane Incompressible Turbulent Free Shear Layer with Arbitrary Velocity Ratio and Pressure Gradient; AFOSR TN 5443, Dept. of Mech. Engineering, Stanford Univ. Report MD-9 (1963).

40. Hay, J.A. and Eggington, W.J. — An Exact Theory of Thin Airfoil with Large Flap Deflection; Journ.Roy.Aero.Soc. 60 (1956).

41. Glauert, H. — The Elements of Aerofoil and Airscrew Theory; Cambridge University Press, Second Edition, (1948).

42. Lachmann, G.V. — Boundary Layer and Flow Control, Vol. I, Pergamon Press (1961).

43. Kelly, M.W. — Analysis of Some Parameters Used in Correlating Blowing Type Boundary Layer Control Data; NACA RM A56F12 (1956).

44. Williams, J. and Butler, S.F.J. — Aerodynamic Aspects of Boundary Layer Control for High Lift at Low Speeds; AGARO Report 414 (1963).

45. Head, M.R. — Entrainment in the Turbulent Boundary Layer; R. & M. No. 3152 (1960).

46. Löhr, R. — Erhöhung des Maximalauftriebes eines Rechteckflügels in Bodennähe durch kombiniertes Ausblasen an der Flügelnase und an der Hinterkantenklappe; Deutche Luft-und Raumfahrt,

.../107

DLR, FB 64-02 (1964).

47. Thomas, F. — Unterschungen über die Erhöhung des Auftriebes von Tragflugeln mittels Grenzschichbeinflussung durch Ausblasen; Z. Flugwiss. 10 (1962).

48. Streit, G. and Thomas, F. — Experimentelle und Theoretische Untersuchungen an Ausblaseflügeln und Ihre Anwendung beim Flugzugentwerf; DFL Bericht Nr. 220 (1963).

49. Weinstein, A.S. Osterle, J.F. and Forstall, W. — Momentum Diffusion from a Slot Jet into a Moving Secondary; Journ. of Applied Mechanics, Vol. 23, p. 437 (1956).

50. Moon, I Man — Distributed Suction Boundary Layer Control on Conical Diffusers; Research Report No. 17, Aerophysics Department of Mississippi State University (1958).

51. Newman, B.G. — Unpublished work at McGill University.

.../Appendix 1.

APPENDIX I

A MODEL FLOW WITH SIMPLE VELOCITY DISTRIBUTION

The following model is designed to illustrate the mechanism whereby a small plane rate of strain ($\frac{\partial U}{\partial x}$) can be of importance even though a much larger shear rate of strain ($\frac{\partial U}{\partial y}$) is present.

The mean velocity field is postulated as:

$$\frac{\partial U}{\partial y} = A$$

$$\frac{\partial U}{\partial x} = B \qquad \text{where A and B are constants and } B/A \ll 1 \qquad \text{(A-1-1)}$$

$$\frac{\partial V}{\partial x} = 0$$

$$W = 0$$

A stream function satisfying the above relationships is:

$$\psi = \frac{Ay^2}{2} + Bxy \qquad \text{(A-1-2)}$$

The streamline $\psi = 0$ passing through the origin has a location given by:

$$y = 0 \quad \text{or} \quad y/x = -\frac{2B}{A} \qquad \text{(A-1-3)}$$

The mean streamlines are sketched in Figure A1, for positive A and B. Similar patterns can be sketched easily for negative A or B.

A small vorticity perturbation vector is now introduced at the origin; the components of this vorticity vector in the x and y directions are assumed to be of approximately equal magnitude.

Consider an infinitesimally short line of fluid particles to be marked in the x, y plane such that x = y = 0 is included in the line. This marked fluid may be considered as a projection on the x-y plane of the perturbation vortex line passing through the origin. For simplicity, the diffusion of vorticity from the perturbation will be neglected as in the main analysis so that the vortex line moves with the fluid.

The line is being strained along its length at a rate given by:

$$e_{ss} = \tfrac{1}{2}(A \sin 2\theta + 2B \cos 2\theta) \qquad \text{(A-1-4)}$$

where θ is the angle between the line and the x axis.

For $\theta > \pi/4$, the plane rate of strain B decreases the total rate of strain parallel to the line e_{ss}. However the time spent by the line in the region $\pi/2 > \theta > \pi/4$ is relatively small, since its angular velocity is:

$$\Omega = A/2\ (1 - \cos 2\theta) + B \sin 2\theta \qquad \text{(A-1-5)}$$

where $A/B \gg 1$.

For $\theta < \pi/4$, the magnitude of e_{ss} is increased by B (which is assumed positive), and it is for values of θ for which $A/2B \tan(2\theta) \lesssim 1$ that this effect dominates e_{ss}. For small θ, the angular velocity of the line is small, so that a significant length of time may be spent by the line in an orientation for which the effect of B is not small.

The effect of the rates of strain on the vortex line may be summarized by the following two quantities (for a given value

of A): the direction of the larger principal mean rate of strain, typifying the strain pattern, and the asymptotic orientation of the line for very large time, typifying the rotation of the vortex line. The magnitude of the larger principal mean rate of strain is very nearly equal to A, as can be shown by calculating the maximum value of e_{ss} from equation (A-1-4).

Since the effect of the mean rates of strain on the vortex line should be independent of the co-ordinate system from which it is viewed, the angle between the larger principal mean rate of strain and the asymptotic orientation should be the dominant parameter in assessing the effect of the mean flow on the perturbation vortex line. Let this angle by θ_1.

For positive A and B, θ_1 is given by:

$$\left[\theta_1\right]_{B>0} = \tan^{-1}\left\{\frac{-2B}{A} + \left(\frac{4B^2}{A^2} + 1\right)^{\frac{1}{2}}\right\} \qquad \text{(A-1-6)}$$

which is the direction of the larger principal mean rate of strain from equation A-1-4). The asymptotic inclination of a vortex line will be the x-axis, as may be seen by reference to Figure A1.

Since $\frac{B^2}{A^2} << 1$,

$$\tan\theta_1 \approx \left\{1 - \frac{2B}{A}\right\} \quad \text{or,}$$

$$\left[\theta_1\right]_{B>0} \approx \left\{\frac{\pi}{4} - \frac{B}{A}\right\} \qquad \text{(A-1-7)}$$

A convenient orientation for the axis system from which to study the flow would probably place the x-axis along the

asymptotic inclination of the vortex line. In this way, different flows could be compared from a consistent viewpoint. Alternatively, of course, an axis system could be chosen in which the larger principal mean rate of strain is parallel to the x axis; this is not likely to be as convenient since this direction is at roughly 45° to the largest velocity components far from the origin and hence at 45° to the usual axis system for shear flows for which the boundary-layer approximation is valid.

The only change which a small rotation of co-ordinates makes in the final equations is to change the rate of strain ratio $\frac{\partial U/\partial x}{\partial U/\partial y}$ from $\frac{B}{A}$ to $(\frac{B}{A} + \epsilon)$ where $B = \frac{\partial U}{\partial x}$ and $A = \frac{\partial U}{\partial y}$ in the original co-ordinate system, and ϵ is the angle of rotation. (It has been assumed that ϵ is small so that $\cos\epsilon \approx 1$, $\sin\epsilon \approx \tan\epsilon \approx \epsilon$) The angle of rotation ϵ is given by $\tan^{-1}(-\frac{2B}{A}) \approx -\frac{2B}{A}$. The rate of strain ratio in the new co-ordinates is therefore $\frac{B}{A} - \frac{2B}{A} = -\frac{B}{A}$. Since rotation is required only when $\frac{B}{A}$ is negative, the effect of consistently orienting the co-ordinate system as described in previous paragraphs is to maintain positive values of the rate of strain ratio. This can be accomplished very simply in any convenient co-ordinate frame by putting $\frac{B}{A}$ equal to $+\left|\frac{B}{A}\right|$, provided that $\left|\frac{B}{A}\right|$ is not too large (say $\left|\frac{B}{A}\right| < 0.2$).

For $B < 0$, $A > 0$, the asymptotic inclination is $\tan^{-1}(-\frac{2B}{A})$ to the x axis, as a sketch of the mean streamlines for this case quickly shows. Then:

$$[\theta_1]_{B<0} = \tan^{-1}\left\{-\frac{2B}{A} + \left(\frac{4B^2}{A^2} + 1\right)^{\frac{1}{2}}\right\} - \tan^{-1}\left(-\frac{2B}{A}\right)$$

$$\approx \tan^{-1}\left(1 - 2\frac{B}{A}\right) - \tan^{-1}\left(-\frac{2B}{A}\right)$$

$$\approx \frac{\pi}{4} + \frac{B}{A} \qquad \text{(A-1-8)}$$

again assuming that $\frac{B}{A} << 1$.

A comparison of equations (A-1-7) and (A-1-8), with their restrictions on the sign of B, shows that θ_1 is unchanged by altering the sign of B. This result is reflected in the expression derived for the total vorticity of the perturbation (equation 8 of Section 1.2.3) which is also unaffected by a change in the sign of B, and by the fact, already noted, that a negative value of $\frac{B}{A}$ suggests a re-orientation of co-ordinates which simply changes the sign of $\frac{B}{A}$ and nothing more.

APPENDIX 2

AN EXTENSION OF THE MODEL FLOW IN APPENDIX I TO INCLUDE $\frac{\partial V}{\partial x}$

Proceeding as in Appendix I, the mean velocity field is postulated as:

$$\begin{aligned} \frac{\partial U}{\partial y} &= A \\ \frac{\partial U}{\partial x} &= B \\ \frac{\partial V}{\partial x} &= C \\ W &= 0 \end{aligned} \qquad \text{(A-2-1)}$$

where A, B, and C are constants and $\frac{A}{B} \gg 1$, $\frac{B}{C} \gg 1$.

A stream function satisfying these relationships is:

$$\psi = \frac{Ay^2}{2} + Bxy - \frac{Cx^2}{2} \qquad \text{(A-2-2)}$$

The streamline passing through the origin ($\psi = 0$) has a location given by:

$$\frac{y}{x} = \frac{B}{A}[-D - 1] \quad \text{OR} \quad \frac{y}{x} = \frac{B}{A}[D - 1] \qquad \text{(A-2-3)}$$

where

$$D = \left(1 + \frac{CA}{B^2}\right)^{\frac{1}{2}}$$

Provided that D is real, the x-axis of the co-ordinate system can be oriented along the line $y/x = \frac{B}{A}[-1 \pm D]$, the sign depending on the asymptotic inclination of a line of fluid particles placed through the origin (see the analogous disucssion in Appendix 1).

For real values of D, there is no essential change resulting from the addition of the rate of strain $\frac{\partial V}{\partial x}$, beyond the slight rotation of co-ordinates necessary to align the abscissae of the system with the asymptotic inclination of the vortex line.

Negative values of $\frac{CA}{B^2}$ may occur, and since this ratio is of order unity, the values of D may be imaginary. In this case the streamlines of the model mean flow form closed curves about the origin and there is no longer an asymptotic inclination of the vortex line. The angular velocity of the perturbation vortex line passing through the origin becomes:

$$\sim = \tfrac{1}{2} \left\{ (A - C) - (A + C) \cos 2\theta + 2B \sin 2\theta \right\} \qquad \text{(A-2-4)}$$

which cannot be approximated by neglecting C with respect to A.

The minimum angular velocity occurs when the rate of strain along the length of the line is zero, at an angle $\theta \approx \tan^{-1}(-\frac{B}{A})$. This inclination appears to be significant for cases in which values of D are imaginary, and may replace the asymptotic inclination of the previous analysis as a criterion for orientation of the co-ordinate system. Problems arise in an analysis of the vortex strength in this case however and it does not appear useful to incorporate the effects of $\frac{\partial V}{\partial x}$ at this stage.

In conclusion, it seems worthwhile to indicate the values of $\frac{CA}{B^2}$ in a few real self preserving flows, the values of A, B, and C being evaluated at $y = L_o$ as is usual in this thesis.

Values of D in three self preserving flows:

a) Small deficit wake

$$U_o \propto x^{-\frac{1}{2}}, \quad L_o = \beta x^{\frac{1}{2}}$$

where β is a dimensional constant.

Putting $U = U_1 - U_o e^{-k\eta^2}$ where $\eta = y/L_o$

$$\frac{C}{A} = \left\{ \frac{\partial V}{\partial x} / \frac{\partial U}{\partial y} \right\}_{y=L_o} = \frac{\beta^2}{x} \frac{1}{4k} \left[\frac{3}{2} - k \right]$$

$$\left\{ \frac{B}{A} \right\}^2 = \left\{ \frac{\partial U}{\partial x} / \frac{\partial U}{\partial y} \right\}^2 = \frac{9}{16} \frac{\beta^2}{k^2} \frac{1}{x}$$

Therefore

$$\frac{CA}{B^2} = \frac{4}{9} k \left(\frac{3}{2} - k \right) = 0.248 \qquad \text{since } k = \log 2.$$

b) Mixing layer

$$U_o = \text{constant}, \quad L_o = \beta x$$

Putting $U = U_o e^{-k\eta^2}$ where $\eta = y/L_o$ as before:

$$\frac{CA}{B^2} = -1$$

In terms of parameter $D = \left(1 + \frac{CA}{B^2}\right)^{\frac{1}{2}}$, the mixing layer is a critical case.

c) Jet in still air

$$U_o \propto x^{-\frac{1}{2}}, \quad L_o = \beta x$$

Putting $U = U_o e^{-k\eta^2}$

$$\frac{CA}{B^2} = -1.40$$

Thus these three cases represent real, zero and imaginary values of D, respectively, and indicate the wide range of possibilities which exist when $\frac{\partial V}{\partial x}$ is considered.

APPENDIX 3

THE DOUBLE INTEGRAL APPROACH TO THE CALCULATION OF A PLANE TURBULENT BOUNDARY LAYER

Two recent reviews dealing solely with the plane incompressible turbulent boundary layer (refs. 23 and 24) indicate the effort which is continuing to be expended on this important flow problem and the multiplicity of approaches which have been proposed for its solution. The simple, semi-empirical technique described in this appendix was constructed as a basis for calculating the development of the inner layer of a wall jet. Its application to two boundary layer flows, as described hereafter, indicates that the technique may be worthwhile for the calculation of the plane boundary layer, and improvements to the technique are suggested at the conclusion of this appendix which might provide a more accurate alternative to the many treatments described in ref. 24.

The double integral technique, as applied to the plane turbulent boundary layer, consists in writing two integrals of the equations of motion (modified by the usual boundary layer assumptions, including the neglect of normal turbulent stress terms) with limits $y = 0$, $y = \delta$ for the first equation and $y = 0$, $y = \frac{\delta}{2}$ for the second equation, where δ is the nominal thickness of the layer. From these two equations, the thickness δ and a shape parameter can be found. The central problem in the analysis is the calculation of the shear stress, which must be known at the limits of the integrals. A novel semi-empirical basis is used in this appendix, as described below.

The velocity profile of the boundary layer is represented by a simple power law of the form:

$$\frac{U}{U_1} = \left(\frac{y}{\delta}\right)^n \qquad \text{(A-3-1)}$$

where U_1 is the external velocity and δ is the nominal thickness of the layer. The exponent n, which describes the shape of the profile, is allowed to vary in the streamwise direction.

The shear stress at the wall, τ_o, is formulated on a Ludweig-Tillman basis, as that:

$$C_f = \frac{\tau_o}{\frac{1}{2}\rho U_1^2} = 2\left(\frac{\gamma}{c}\right)^{2/m+1} R_\theta^{-2m/m+1} \qquad \text{(A-3-2)}$$

where $\frac{U}{U_\tau} = C\left(\frac{yU_\tau}{\nu}\right)^m$ is the form of the law of the wall for $y \ll \theta$, θ is the usual momentum thickness of the layer, γ is the value of $\frac{U}{U_1}$ at $y = \theta$ and R_θ is $\left(\frac{\theta U_1}{\nu}\right)$. This relation for C_f will be forced to conform with the wall shear stress beneath a flat plate boundary layer, where $C_f = .0256\, R_\theta^{-\frac{1}{4}}$, $n = 7$, and $\gamma = 0.717$, by measurement. Thus, in general:

$$C_f = .045\, \gamma^{7/4} R_\theta^{-\frac{1}{4}} \qquad \text{(A-3-3)}$$

Using equation (A-3-1)

$$\gamma = \left\{\frac{n}{(2n+1)(n+1)}\right\}^n$$

so that

$$C_f = .045 \left\{ \frac{n}{(n+1)(2n+1)} \right\}^{(7n-1)/4} \left\{ \frac{U_1 \delta}{\nu} \right\}^{-\frac{1}{4}} \qquad \text{(A-3-4)}$$

The shear stress at $y = \frac{\delta}{2}$ may be represented by:

$$\frac{1}{R_T^*} = \left\{ \frac{\nu_T}{U_1 \delta^*} \right\}_{y=\frac{\delta}{2}} \qquad \text{(A-3-5)}$$

where δ^* is the usual displacement thickness, $\nu_T = -\frac{\overline{uv}}{\partial U/\partial y}$. For boundary layers in equilibrium pressure gradients, Clauser (ref. 17) has shown that a parameter equivalent to R_T^* is approximately constant. The simplest assumption for R_T^* in non self preserving cases, is that R_T^* is again constant. Using this simple hypothesis a value of R_T^* has been found by comparison with the experimental data of Newman (ref. 25). A further trial of the technique is made by comparing with measured values of $\frac{dn}{dx}$ in a non-equilibrium zero pressure gradient case recently examined experimentally by Bradshaw (ref. 26). These latter measurements were made in a boundary layer in transition from an equilibrium case (for which $U_1 \propto x^{-0.255}$) to the zero pressure gradient case, the transition itself occurring in a stream of nearly constant velocity.

Figure A2 shows a comparison between the measured values of $H = \frac{\delta^*}{\theta}$ from ref. 23 (Series II) and corresponding curves are shown, each for a different value of R_T^*. For each curve, the measured values of θ and $\frac{\delta^*}{\theta}$ at $x = 2$ ft. were used as initial values in the calculations. The measured external velocity was approximated by a polynomial for the calculations.

The results of two other calculation techniques are also shown on Figure A2, the methods being those due to Spence and

Head, as indicated. (These results were obtained from the review of Thompson, ref. 24). The technique due to Head was formulated in large measure on the basis of this data, and so agrees quite well with the measured values. From Figure A2 it appears that a value of $R_T^* = 50$ provides reasonable agreement between measured and calculated values of $\frac{\delta^*}{\theta}$ up to the region of separation itself. It must be emphasized that no corrections have been made in the present calculations for three dimensionality of the flow. The measured values do not quite obey the two dimensional boundary layer equations of motion (even when normal stress terms are included) which indicates that some spanwise flow was present (see ref. 24).

Figure A3 shows a comparison between measured and calculated values of $-\theta \frac{dH}{dx}$ (where $H = \frac{\delta^*}{\theta}$ which in turn is equal to $(2n + 1)$ by equation (A-3-1)) for the N.P.L. measurements of Bradshaw (ref. 26). The effects of possible cross flow velocity components are minimized in this presentation by basing the calculations on measured values of H and θ at each streamwise station. Although the predictions based on $R_T^* = 50$ do not agree particularly well with the measured values, it is encouraging to find that a better representation is obtained with this curve than with any other calculation method, the best of which is that of Head whose prediction for this case is also shown in Figure A3. (The calculations of $-\theta \frac{dH}{dx}$ from the measured values and for the prediction based on Head's method, were carried out by Bradshaw).

It has been concluded from the results shown in Figures A2 and A3 that the value for R_T^* of 50 provides a reasonable basis for the calculation of the turbulent boundary layer in an adverse

pressure gradient. Certain refinements to this technique, as applied to the plane boundary layer, immediately suggest themselves. In particular the assumption of a more representative velocity profile should provide greater accuracy, and Coles' two parameter family of profiles appears to be particularly attractive in this regard (see ref. 27). For present purposes however, the simple power law profile of equation (A-3-1) will be assumed.

APPENDIX 4

FINAL EQUATIONS USED IN THE ANALYSIS OF A WALL JET

Eqn. 1 Momentum integral equation with limits $y = y_M$ and $y = \infty$ (neglecting the normal Reynolds stresses)

$$\int_o^\infty \frac{\partial}{\partial x}\left[U(U - U_1)\right]d\eta + \frac{dU_1}{dx} \int_o^\infty (U - U_1)d\eta - \frac{U_o V_M}{L_o} = 0$$

where

$$\eta = \frac{y - y_M}{y_{M/2} - y_M}, \quad L_o = (y_{M/2} - y_M), \quad V_M = \text{velocity at } y = y_M$$

and

$$U_o = U_M - U_1$$

Let $U = U_1 + U_o\, f(\eta)$ for $y \geqslant y_M$

$U = U_M(y/y_M)^n$ for $y \leqslant y_M$

This equation becomes:

$$U_1' \left\{U_o(2K_{T_1} - 2K_{T_2}) - U_1 K_{T_1}\right\}$$

$$+ U_M' \left\{U_1 K_{T_1} + 2U_o K_{T_2} + \frac{U_o y_M}{L_o} \frac{1}{n+1}\right\}$$

$$+ L_o' \left\{\frac{U_1 U_o}{L_o} K_{T_1} + \frac{U_o^2}{L_o} K_{T_2}\right\}$$

$$+ y_M' \left\{\frac{U_o U_M}{L_o} \frac{1}{n+1}\right\}$$

$$+ n' \left\{-\frac{U_M U_o}{(n+1)^2} \frac{y_M}{L_o}\right\} = 0$$

where

$$K_1 = \int_0^1 f\,d\eta = .8101$$

$$K_2 = \int_0^1 f^2\,d\eta = .6805$$

$$K_{T_1} = \int_0^\infty f\,d\eta = 1.0645$$

$$K_{T_2} = \int_0^\infty f^2\,d\eta = .7526 \text{ , if } f = \exp(-k\eta^2) \text{ and,}$$

$$k = \text{Log}_e 2.$$

Primes indicate differentiation w.r.t.x.

Eqn. 2 Momentum integral equation with limits $y = y_M$, $y = y_{M/2}$.

$$\frac{dU_1}{dx}\int_0^1 (U - U_1)\,d\eta + \int_0^1 \frac{\partial}{\partial x}\left[U(U - U_1)\right]d\eta - \frac{U_o}{2}\int_0^1 \frac{\partial U}{\partial x}\,d\eta - \frac{V_M U_o}{2L_o} - \frac{\tau_{y_{M/2}}}{\rho \cdot L_o} = 0$$

This equation becomes:

$$U_1'\left\{U_o\left(\frac{5K_1}{2} - 2K_2 - \frac{1}{2}\right) - K_1U_1\right\}$$

$$+ U_M'\left\{K_1U_1 + U_o\left(2K_2 - \frac{K_1}{2}\right) + \frac{1}{2(n+1)}\,\frac{y_M U_o}{L_o}\right\}$$

$$+ L_o'\left\{\frac{U_o^2}{L_o}\left(K_2 - \frac{K_1}{2}\right) + \frac{U_1U_o}{L_o}\left(K_1 - \frac{1}{2}\right)\right\}$$

$$+ y_M'\left\{\frac{U_o^2}{L_o}\left(\frac{1}{2} - \frac{n}{2(n+1)}\right) + \frac{U_1U_o}{L_o}\left(\frac{1}{2} - \frac{n}{2(n+1)}\right)\right\}$$

$$+ n'\left\{-\frac{U_M}{(n+1)^2}\,\frac{U_o}{2L_o}\,y_M\right\}$$

$$+ \frac{U_o^2 k}{R_T L_o} = 0$$

with

$$\frac{1}{R_T} = \left[\frac{\nu_T}{U_o L_o}\right]_{@\ y_{M/2}}$$

Eqn. 3 Momentum integral equation with limits y = 0, y = y_M.

$$\int_o^1 \frac{\partial}{\partial x}\ (U^2)\ d\left(\frac{y}{y_M}\right) - U_M \int_o^1 \frac{\partial U}{\partial x}\ d\left(\frac{y}{y_M}\right) - U_1 \frac{dU_1}{dx} + \frac{\tau_o}{\rho\, y_M} = 0$$

This equation becomes:

$$U_1' \left\{ - U_1 y_M \right\}$$

$$+\ U_M' \left\{ \frac{U_M y_M}{(2n+1)(n+1)} \right\}$$

$$+\ y_M' \left\{ \frac{-\ U_M^{\,2}\ n}{(2n+1)(n+1)} \right\}$$

$$+\ n' \left\{ y_M U_M^{\,2} \left(\frac{1}{(n+1)^2} - \frac{2}{(2n+1)^2} \right) \right\}$$

$$+\ \frac{\tau_o}{\rho} = 0$$

Eqn. 4 Momentum integral equation with limits y = 0, y = $\frac{y_M}{2}$

$$\int_o^{1/2} \frac{\partial (U^2)}{\partial x}\ d\left(\frac{y}{y_M}\right) - \frac{U_M}{2^n} \int_o^{1/2} \frac{\partial U}{\partial x}\ d\left(\frac{y}{y_M}\right) - \frac{U_1}{2} \frac{dU_1}{dx} - \frac{1}{\rho\, y_M} \left(\tau_{\frac{y_M}{2}} - \tau_o\right) = 0$$

This equation becomes:

$$U_1' \left\{ - \frac{U_1}{2} \quad y_M \right\}$$

$$+ \; U_M' \left\{ \frac{y_M U_M}{(2n+1)(n+1)} \left(\frac{1}{2} \right)^{2n+1} \right\}$$

$$+ \; y_M' \left\{ - \frac{U_M{}^2 n}{(2n+1)(n+1)} \left(\frac{1}{2} \right)^{2n+1} \right\}$$

$$+ n' \left\{ \frac{2U_M{}^2 y_M}{(2n+1)} \left(\frac{1}{2} \right)^{2n+1} \left(\text{Log} \left(\frac{1}{2} \right) - \frac{1}{2n+1} \right) \right.$$

$$\left. - \frac{U_M{}^2 y_M}{(n+1)} \left(\frac{1}{2} \right)^{2n+1} \left(\text{Log} \left(\frac{1}{2} \right) - \frac{1}{n+1} \right) \right\}$$

$$- \frac{1}{R_T^*} \frac{n}{(2n+1)(n+1)} U_M{}^2 \left(\frac{1}{2} \right)^{n-1} + \frac{\tau_o}{\rho} = 0$$

with

$$\frac{1}{R_T^*} = \left[\frac{\nu_T}{U_M \delta_M^*} \right]_{y = \frac{y_M}{2}}$$

given by equations (14) and (16).

Eqn. 5 Free stream velocity equation:

$$U_1' = f(x)$$

where f(x) is known.

Once R_T, R_T^*, $\frac{\tau_o}{\rho}$ are known, the five equations may be solved for the five unknowns U_1, U_M, $y_{M/2}$, y_M and n.

APPENDIX 5

THE COMPUTER PROGRAMME USED FOR THE NUMERICAL SOLUTION OF THE WALL JET EQUATIONS

A reproduction of the programme used for all the wall jet calculations discussed in this report, is included in this appendix. The total execute time for this programme, when run on the McGill University 7040 computer, was approximately 1½ minutes.

The main symbols are:

COMPUTER SYMBOL	SYMBOL USED IN TEXT OR MEANING
H	step width in numerical solution
X	x/b
XMAX	maximum value of x/b
Y(1)	U_1/U_j
Y(2)	U_M/U_j
Y(3)	$(y_{M/2} - y_M)/b$
Y(4)	$(y_M)/b$
Y(5)	n (equation 13)
R	$U_j b/\nu$
Z(N)	$dY(N)/dx$
BETA	C/R_{T_o} (equation 12)
RS	B/A
VS	Φ (equation 16).

The following notes refer to the statements in the accompanying programme which are designated as note 1, note 2, etc.

NOTE 1 The initial conditions are read in, including the virtual origin and appropriate exponent for the external velocity variation.

NOTE 2 These statements ensure that the sign of the rate of strain ratio does not affect the calculation, as discussed in Appendix I.

NOTE 3 The statements indicated prevent the rate of strain ratio (RS) from exceeding 0.09 and thereby limit the variable $\nu_T/U_o L_o$ to values greater than or equal to zero.

NOTE 4 The external velocity variation is calculated. The cases N = 2 and N = 3 describe non-self-preserving cases in which the external velocity variation has been approximated by a polynomial.

NOTE 5 For the first 30 slot widths, the exponent of the inner layer is held constant at its initial value. This procedure was found necessary to avoid numerical instabilities resulting from the prescribed initial conditions.

Statement 124 was replaced, for all results presented in this thesis, by the statement:

```
RTD = .033* (1.+ .67* VS - .039* VS* VS) - .013* EXP(-VS)
```

```
C      WALL JET ANALYSIS   EXPERIMENTAL STARTING CONDITIONS
C      VARIABLE EDDY VISCOSITY IN INNER LAYER
    2 FORMAT(1H1,19X,2HU1,11X,2HUM,11X,3HDEL,10X,2HYM,11X,5HEXP N,8X,
     13HYM2,11X,1HR,13X,2HVS,9X,5H1/RT*)
    3 FORMAT (4HJ X=,F8.3,9F13.5)
    4 FORMAT (1HO,5X,15HLIMITS EXCEEDED)
    6 FORMAT (8F7.0)
      DIMENSION YI(5),YE(5),Y(5),Z(5),A(5)
      DIMENSION P(10),T(10),S(10),XI(10),PI(10),Q(10),V(10),XCO(10)
      H=5.
      NEQNS=5
      DO 7 N=1,10
    7 READ 6, P(N),T(N),S(N),XI(N),PI(N),Q(N),V(N),XCO(N)
      DO 200 N=1,10                                              Note 1
      YI(1)=P(N)
      YI(2)=PI(N)
      YI(3)=S(N)
      YI(4)=T(N)
      YI(5)=.0909
      R=Q(N)
      XO=XI(N)
      PRINT 2
      XMAX=XI(N)+200.
  101 A(1)=H/2.
      A(2)=H/2.
      A(3)=H
      A(4)=H
      A(5)=H/2.
      X=XC
      VX=XO
      YM2=YI(3)+YI(4)
      PRINT 3,X,(YI(I),I=1,NEQNS),YM2,R
  102 X=VX
      DO 103 K=1,NEQNS
      Z(K)=0.
      YE(K)=YI(K)
  103 Y(K)=YI(K)
      IF((Y(5).LE.0.065).OR.(Y(5).GE.0.5))GO TO 109
  303 DO 104 J=1,4
      U=Y(2)-Y(1)
      W=(1.-.5**(2.*Y(5)+1.))/((2.*Y(5)+1.)*(Y(5)+1.))
      BETA=0.3793911
      RS=(Z(1)+Z(2))*Y(3)*.7215/U+Z(3)+Z(4)
      IF(RS.GE.0.) GO TO 304
      RS=-RS                                                     Note 2
      BETA=-BETA
  304 A4=-Y(1)*Y(4)
      B4=2.*Y(2)*Y(4)/(2.*Y(5)+1.)-Y(2)*Y(4)/(Y(5)+1.)
      C4=0.
      D4=-2.*Y(2)*Y(2)*Y(5)/(2.*Y(5)+1.)+Y(2)*Y(2)*Y(5)/(Y(5)+1.)
      E4=-2.*Y(2)*Y(2)/((2.*Y(5)+1.)*(2.*Y(5)+1.))*Y(4)+Y(2)*Y(2)*Y(4)/
     1((Y(5)+1.)*(Y(5)+1.))
      F4=Y(2)*Y(2)*.01285* (Y(5)/((Y(5)+1.)*(2.*Y(5)+1.)))**((11.
     1*Y(5)-1.)/6.)*(R*Y(2)*Y(4))**(-.1667)
  307 A3=-Y(1)*Y(4)/(2.*Y(2)*Y(2))
      B3=Y(4)*W/Y(2)
      C3=0.
      D3=-Y(5)*W
  100 E3=Y(4)*((2.*Y(5)*Y(5)-1.)/((Y(5)+1.)*(2.*Y(5)+1.))*W+
     10.6931*.5**(2.*Y(5)+1.)/((2.*Y(5)+1.)*(Y(5)+1.)))
```

```
101         F1=U*U*.6931/Y(3)*.034
102         IF(RS.LE.0.09) GO TO 305
105         BETA=0.                                   } Note 3
106         F1=0.
107         RS=.09
110     305 A1=.1642*U-.8101*Y(1)-BETA/2.*U
111         B1=.8101*Y(1)+U*.9560+Y(4)*U/(Y(3)*2.*(Y(5)+1.))-BETA/2.*U
112         C1=U*U*.2755/Y(3)+Y(1)*U*.3101/Y(3)-.6931*BETA*U*U/Y(3)
113         D1=U*Y(2)/Y(3)*(.5-Y(5)/(2.*(Y(5)+1.)))-.6931*BETA*U*U/Y(3)
114         E1=-Y(2)*U*Y(4)/(2.*Y(3)*(Y(5)+1.)*(Y(5)+1.))
115         A2=.6238*U-1.0645*Y(1)
116         B2=1.0645*Y(1)+1.5052*U+U*Y(4)/(Y(3)*(Y(5)+1.))
117         C2=1.0645*Y(1)*U/Y(3)+U*U*.7526/Y(3)
120         D2=Y(1)*U/Y(3)*(1.-Y(5)/(Y(5)+1.))+U*U/Y(3)*(1.-Y(5)/(Y(5)+1.))
121         E2=-(Y(1)+U)*U*Y(4)/(Y(3)*(Y(5)+1.)*(Y(5)+1.))
122         F2=0.
123         VS=U*U*(.034-.379*RS)/F4
124         RTD=.033*(1.+.67*VS-.039*VS*VS)
125         F3=Y(5)*Y(5)*.5**(Y(5)-1.)*RTD/(Y(5)+1.)
126         Z(1)=P(N)/(XI(N)+XOO(N))*V(N)*((X+XCO(N))/(XI(N)+XOO(N)))**(V(N)-  } Note 4
           11.)                                                                 }
127         IF (N.EQ.3) Z(1)=(.1506*X*X*.0001-.003584*X-.0389)/100.
132         IF (N.EQ.2) Z(1)=-.000159*(1.+.0705*X)
135         AL=Z(1)
136         CB=C2*B1-B2*C1
137         G1=(D3*B1-B3*D1)*CB+(C3*B1-B3*C1)*(B2*D1-D2*B1)
140         G2=(E3*B1-B3*E1)*CB+(C3*B1-B3*C1)*(B2*E1-E2*B1)
141         G3=CB*(AL*(A3*B1-B3*A1)+(F3*B1)-B3*F1)
142         G4=(C3*B1-B3*C1)*(AL*(A1*B2-A2*B1)+(B2*F1)-(F2*B1))
143         H1=(D4*B1-B4*D1)*CB+(C4*B1-B4*C1)*(B2*D1-D2*B1)
144         H2=(E4*B1-B4*E1)*CB+(C4*B1-B4*C1)*(B2*E1-E2*B1)
145         H3=CB*(AL*(A4*B1-B4*A1)+F4*B1-B4*F1)
146         H4=(C4*B1-B4*C1)*(AL*(B2*A1-A2*B1)+B2*F1-F2*B1)
147         IF(X.GE.(XI(N)+30.)) GO TO 306
152         Z(5)=0.                                   } Note 5
153         Z(4)=-(H4+H3)/H1                          }
154         GO TO 308
155     306 Z(5)=(G3*H1-G1*H3+G4*H1-G1*H4)/(G1*H2-G2*H1)
156         Z(4)=-(G3+G4+Z(5)*G2)/G1
157     308 Z(3)=(Z(4)*(B2*D1-D2*B1)+Z(5)*(B2*E1-E2*B1)+B2*F1-F2*B1+Z(1)*(B2*
           1A1-A2*B1))/(C2*B1-B2*C1)
160     309 Z(2)=-(F1+Z(1)*A1+Z(3)*C1+Z(4)*D1+Z(5)*E1)/B1
161     310 X=VX+A(J)
162         DO 104 L=1,NEQNS
163         Y(L)=YI(L)+A(J)*Z(L)
164     104 YE(L)=YE(L)+A(J+1)*Z(L)/3.
167         DO 105 M=1,NEQNS
170     105 YI(M)=YE(M)
172         YM2=YE(3)+YE(4)
173         PRINT 3,X,(YI(I),I=1,NEQNS),YM2,RS,VS,RTD
200     106 VX=VX+H
201     108 IF(XMAX.GE.VX) GO TO 102
204         GO TO 200
205     109 PRINT 4
206     200 CONTINUE
210         CALL EXIT
211         END
```

APPENDIX 6

AN INVESTIGATION OF THE TURBULENT SHEAR STRESS IN FULLY DEVELOPED PIPE FLOW

The experiments described in this appendix are identical to those of ref. 29, and were undertaken primarily to gain familiarity with hot wire measurement techniques.

A straight circular pipe 3 inches in diameter was connected via a symmetrical bleed valve to a supply of compressed air. The velocity in the pipe could be regulated by the bleed valve with no possibility of compressor surging.

The static pressures at various streamwise locations were measured by means of suitable static taps. The pitot pressure at the outlet was obtained by traversing a flattened pitot tube across the flow. The pitot tube had sharpened lips and was .014 in. (outside dimension) in height.

Slanting and normal hot wires were also traversed across the pipe in the plane of the outlet. The angle between the wire and its supports was measured by projecting a shadow of the wire and supports within a photographic enlarger.

For a wire inclined to the mean flow direction by an angle Ψ (which is not small):

$$\frac{V^2}{R} = \frac{V_o^2}{R} + B\,U^c \sin^c \Psi \qquad \text{(A-6-1)}$$

where V_o, the voltage at zero velocity, R the resistance of the wire

and ψ are easily measured constants, U is the velocity and B is a constant whose value is determined by calibration, if required.

As shown in ref. 29, equation (A-6-1) can be used to derive expressions for the double velocity correlations $\overline{uv}$ and $\overline{u^2}$ once values of the RMS voltages from normal and slanting wires have been measured. The results are summarized in the following equations:

$$-\frac{\overline{uv}}{U^2} = \frac{\tan\psi\,(\overline{e_1^2} - \overline{e_2^2})}{c^2 V_1^2 \left(1 - \frac{V_o^2}{V_1^2}\right)^2}$$

$$\frac{\overline{u^2}}{U^2} = \frac{\overline{e_3^2}}{c^2} \frac{4 V_3^2}{V_3^2 - V_{o_3}^2}$$

(A-6-2)

$$\frac{\overline{v^2}}{U^2} = \frac{\tan^2\psi}{c^2}\left\{\frac{2(\overline{e_1^2} + \overline{e_2^2})}{V_1^2\left(1 - \frac{V_{o_1}^2}{V_1^2}\right)^2} - \frac{4\,\overline{e_3^2}}{V_3^2\left(1 - \frac{V_{o_3}^2}{V_3^2}\right)^2}\right\}$$

where V is D.C. voltage

V_o is D.C. voltage with zero velocity

$\sqrt{\overline{e^2}}$ is R.M.S. voltage

subscripts 1, 2, and 3 refer to slanting wire (larger R.M.S. reading) at angle ψ to the mean flow direction, slanting wire at angle $(\pi - \psi)$ to mean flow direction (lower R.M.S. reading), and normal wire, respectively. It has been assumed that $V_1 = V_2$ and that $V_{o_1} = V_{o_2}$.

In order to confirm the value of c, which was reported to be equal to 0.45 in ref. 29, the normal wire which was used was calibrated in a uniform stream whose velocity was measured with a

standard pitot static probe. This calibration is shown in Figure A4, where $V_3^2 - V_{o_3}^2$ is plotted against U^{*45}. The resulting points are well described by a straight line passing through the origin, confirming the usefulness of the value for c reported in ref. 29. The conditions under which the calibration was made are listed in Figure A4. It was assumed that the value of c = 0.45 could also be applied to the slanting wires, for which no calibrations were made.

From the pitot traverses, the distribution of mean velocity in the pipe was obtained. This is plotted in Figure A5 in order to show the agreement between the measured data and the usual logarithmic velocity distribution, given by

$$\frac{U}{U_\tau} = A \log \left(\frac{y U_\tau}{\nu} \right) + B \qquad (A-6-3)$$

Complete agreement has not been reached concerning the values of A and B, but the present data supports the values given by Townsend (ref. 7) of 2.44 and 5.85 for A and B respectively. The line using these values of A and B is plotted in Figure A5. Deviations from the logarithmic law must be expected near the centre of the pipe and near the wall. The measurements near the wall have not been corrected in any way and are unlikely to be accurate for distances between the probe and the wall of less than the probe width (0.014 in.). The value of U_τ used in this plot (Figure A5) was obtained from the measured pressure gradient along the pipe. Figure A5 confirms that the flow in the pipe was fully developed.

The shear stress distribution calculated from the pressure gradient along the pipe and that from the hot wire readings and

equation (A-6-2) is plotted in Figure A6. Agreement is quite good over most of the pipe radius. Values of $\sqrt{\overline{u^2}}$ and $\sqrt{\overline{v^2}}$ are plotted in Figure A7 and are compared there with the measurements of Laufer (ref. 30). The measured values of $\sqrt{\overline{u^2}}$ are slightly lower than those of Laufer, an effect which is possibly due to dust accumulation on the wire used in the present experiment (the wire was found to be slightly dusty after completion of the experimental measurements). The slightly low values of $\overline{e_3^2}$, which produce this result tend to raise the values of $\overline{v^2}$. Thus the present values of $\overline{v^2}$ are larger than Laufer's values. Some difference exists in the Reynolds numbers of the two experiments, the present value being 2×10^5 whereas Laufer's Reynolds number was 5×10^5. However this difference is unlikely to create as significant a discrepancy in the turbulent intensity distributions as is seen in Figure A7.

APPENDIX 7

FLOW VISUALIZATION OF A PLANE WALL JET

As a preliminary investigation, in order to gain familiarity with wall jet flows, a series of flow visualization experiments were undertaken in the National Research Council water tunnel. The tunnel itself has a working section with dimensions 9.8 inches x 13.1 inches. The maximum working section velocity is approximately 13 ft./sec.

The apparatus used in this investigation is sketched in Figure A8. Water entered the head box through a radial diffuser (the design being taken from that developed by Moller, ref. 33) and the wall jet flowed from the slot, which was 3/16 inch wide, and along a specially constructed roof of the tunnel working section. A circular brass cylinder formed part of the entrance shape for the secondary flow contraction. A concentrated suspension of fine aluminum particles was injected into the jet on the centre-line. A narrow plane of light flashing 360 times a second was provided by a mercury arc lamp. With this illumination, photographs of the secondary flow appear brightly opaque in contrast with the relatively clear primary flow and the black tunnel wall.

Because of the intense turbulence generated in the wall jet flow, entrained fluid becomes very quickly contaminated with aluminum particles and so appears as part of the secondary flow. Although continued entrainment dilutes the concentration of particles, the jet could be visualized throughout the length of the working section. Since the primary flow became contaminated with suspended particles after a short period of injection, the running time was

necessarily short. The water in the tunnel was drained and replaced between each run.

By placing a flat plate at a moderate incidence in the tunnel working section, the effect on the wall jet of a small pressure gradient could be observed.

The appearance of the flow was photographed using a 35 mm Arriflex camera (supplied by kind permission of the Flight Test Section, N.R.C.) and several frames have been enlarged for display in this thesis. Since the aluminum particles in the free stream appear as short dots, because of the periodic illumination, the velocity of the free stream could be calculated. The jet velocity was found by assuming a uniform flow across the slot and by measuring the volume flow of water entering the head box. A flow meter in the secondary supply line provided the latter value directly.

A system of plane mirrors used to allow visualization of the flow along the roof of the working section, make the wall jet in the photographs appear to be flowing over two tapped holes and occasionally over air bubbles, and to be surrounded on both sides by streaming flow. These effects are optical illusions and should be disregarded.

Figure A9 shows a wall jet in nominally still surroundings. Due to the effect of the wall jet injection on the primary flow the velocity ratio $\frac{U_1}{U_J}$ was in fact about .066. The outline of the jet is fairly distinct and one can see evidence of an irregular series of mixing jets similar to those observed by Grant in a small deficit wake (ref. 15). Because of the large velocity difference between the wall

jet and its surroundings, these mixing jets become distorted and disappear quite quickly. From consecutive frames, it appears that these jets appear in groups and are apparent only part of the time. This observation was also made by Grant.

Figure A10^{A} shows a wall jet in uniform streaming flow, in which the velocity ratio $\frac{U_1}{U_J}$ is 0.497. No evidence of the mixing jets is now seen although the outline of the jet is less distinct, due to the larger velocities involved. (These pictures were all taken at 64 frames per second which was the maximum speed available with the camera. The calculated jet velocity was constant and equal to 43.4 inches per second). Considerable irregularity of the jet outline is still evident however.

Figures A10^{B} and A10^{C} show the wall jet in a positive and a negative pressure gradient respectively . An initially surprising feature of these two photographs is the appearance of greater irregularity of the jet outline in the favourable pressure gradient than in the adverse pressure gradient case. This qualitative relationship can be substantiated from the analysis of Section 1.2, however. The analysis relates the extent of intermittency to the non-dimensional shear stress R_T and hence to the rate of strain ratio $B/|A|$, defined by

$$\frac{B}{|A|} = \left\{ \frac{\partial U/\partial x}{|\partial U/\partial y|} \right\}_{@L_o} = \frac{\frac{dU_1}{dx} L_o}{k U_o} + \frac{\frac{dU_o}{dx} L_o}{2 k U_o} + \frac{d(L_o + y_M)}{dx}$$

The symbols are defined by equation (20) of Section 2.2.2.

An increasingly adverse pressure gradient increases $\frac{dL_o}{dx}$ and, although $\frac{dU_1}{dx}$ ~~and~~ $\frac{dU_o}{dx}$ ~~are~~ is decreased (i.e. made more

negative), this change in $\frac{dL_o}{dx}$ dominates the expression for $B/|A|$. An increase in $B/|A|$ is associated with an increase of R_T by equation (12), and an increase in R_T, in turn, is related to a decrease in the relative extent of intermittency (Figure 3). The overall effect of an increasingly adverse pressure gradient is therefore to decrease the relative extent of the intermittent region, as suggested by the photographs of Figures $A10^B$ and $A10^C$.

The self-preserving wall jets in which the intermittency was measured (Section 2.2) are good examples of the qualitative relationship described above. The least adverse pressure gradient was present in the self preserving wall jet for which $\frac{U_1}{U_M}$ was greatest; this case is designated in Table II and in Figure 3 by the number four. From the figure, it is clear that this case corresponds with the largest value of $\delta/(y_{m/2} - y_m)$ of all the wall jets in which intermittency was measured.

The intermittency factor $\gamma(y)$ defined by equation (18) of Section 2.2.1 can be measured directly from a series of photographs by investigating the statistical probability that a fixed point lies within or outside of the region contaiminated by the aluminum particles. The continuous sequence of photographs provided by the cine camera offers an ideal means of measuring the intermittency. Although values of $\gamma(y)$ were found in several of the cases which were photographed, no mean velocity measudrements in the jet itself were taken. Thus the width of the outer layer, and the extent of the inner layer were not determined. Since these quantities were not available for the wall jets photographed, no accurate comparison of the intermittency from case to case is possible and the results are not

included herein. This method of intermittency measurement has the great advantage of simplicity however, and presents a possibility for direct comparison with the usual hot wire or hot film techniques.

APPENDIX 8

A COMPARISON OF PRESENT MEASUREMENTS OF INTERMITTENCY WITH OTHER PUBLISHED RESULTS

So far as the present author is aware, measurements of intermittency have been reported for the following flows (excluding the present work):

i. The fully developed small deficit wake - ref. 11

ii. The partly developed small deficit wake - ref. 7

iii. The smooth wall boundary layer in zero pressure gradient - ref. 12

iv. The rough wall boundary layer in zero pressure gradient - ref. 31

v. The round jet in still air - see ref. 31

vi. The plane jet in uniform streaming flow (3 values of $\frac{U_1}{U_J}$ were studied) - ref. 14

vii. The plane jet in still air - ref. 32.

A comparison of the present results with those listed above is possible in three cases: the smooth wall boundary layer, the partly developed small deficit wake and the plane jet in still air (the smallest value of $\frac{U_1}{U_J}$ considered in ref. 14 was 0.07 and this case is probably comparable to the present results for which $\frac{U_1}{U_J} = 0$).

The smooth-wall boundary layer has been measured twice in the current work. After the first measurements, objections were raised concerning the upstream conditions of the flow, and the measurements were made again with improved results. The first

measurements were reported in ref. 9, and were obtained by the technique described in Section 2.2.1 as "the construction of a "δ" signal". This was the first distribution of intermittency which was obtained by any means. The re-measurement of intermittency in the smooth wall boundary layer was made after smoothing a step which was present in the floor upstream of the measurement station. The distribution of turbulent intensity remained quite similar to the previously measured values, both of which are plotted in Figure A11 together with the measurements of the same quantity from reference 12. (Note that the distribution of turbulent intensity plotted in Figure A3 of reference 9 does not represent the values of ref. 12 correctly. The correct curve is given in Figure A11 of the present thesis). The difference of about 10% between the results of ref. 12 and the present results might be attributed to the assumption of Collis' law for the present calculation and King's law for Klebanoff's calculation, the difference in exponent between the two laws providing a 10% difference in intensity in favour of the Collis' law results. However the scatter in the present data does not justify great dismay over the 10% discrepancy.

The second distribution of intermittency was significantly different from the first, which can be attributed either to the alterations to the floor or to alterations in the measuring technique. The second measurements were reduced by the method described in Section 2.2.1 as "visual observation of trace recordings". Both results are compared with those of ref. 12 in Figure A12; it is evident that the second measurements agree very closely with Klebanoff's whereas those of the first observations depart from them.

It is strongly suspected that improvements in the flow in the second measurements affected the results more than did the change in technique. Support is given to this view by the fact that the first results lie between the intermittency distribution for a smooth wall and that for a rough wall boundary layer as would be expected by a rough upstream condition. The change in the upstream conditions between the two measurements is most likely to affect the largest eddies (hence the intermittency) since these persist longest, yet is unlikely to affect the turbulence intensity as much since the large eddies contain only a small fraction of the turbulent energy.

A comparison of the results for a partly developed small deficit wake is shown in Figure A13. Although a slight shift occurs between the two results, the distributions are quite similar. It should be noted that the present measurements were made in the wake of a square rod of dimension d placed with one flat face normal to the oncoming stream, whereas Townsend's results (ref. 7) were obtained in the wake of a round circular cylinder of diameter d. Thus the relative degree of development in the two cases is not accurately known. The present results were obtained by visual observation of a trace recording made from the undifferentiated hot wire signal. Differentiation could not be used in this case because of the relatively high noise to signal ratio (see Section 2.2.1 for a description of this problem).

Finally, Figure A14 shows a comparison between the results of ref. 14 and the present results for a plane free jet in a relatively weak or zero velocity stream. Again, despite a shift in the intermittent region from one case to another (which is easily

explained in terms of the uncertainty in locating the point of maximum velocity) the distributions are very similar. The present results were obtained by the technique described as "construction of a "δ" signal".

From these comparisons, it has been concluded that the accuracy of measurement of the intermittency factor is probably not greater than $\pm$ .025 in any technique used, but that the present measurements methods are comparable in accuracy with those developed for previous investigations.

The measurement of intermittency reported in ref. 32 for the plane jet in still air differ from those shown in Figure A14. The difference is probably due to the use in ref. 32 of an arbitrarily fixed frequency to define the intermittency. This frequency discrimination level should be based on observations of the original and processed signals. Alternatively the particular frequency chosen must be justified by some means.

Fig. A1

Sketch of Streamlines for Model Flow
of Appendix I

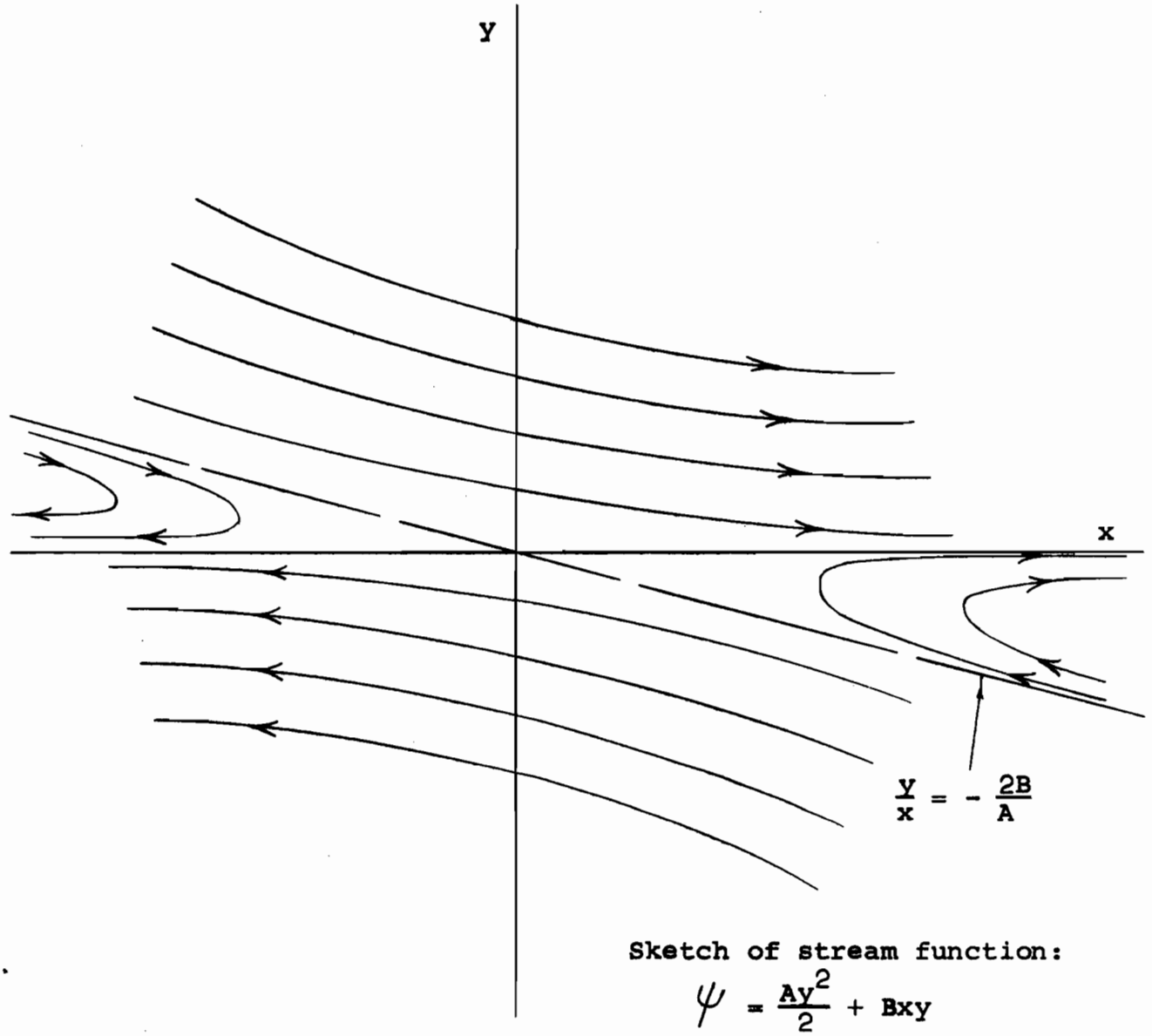

Sketch of stream function:

$$\psi = \frac{Ay^2}{2} + Bxy$$

The Form Parameter in a Plane Turbulent Boundary Layer of Newman (Series II)

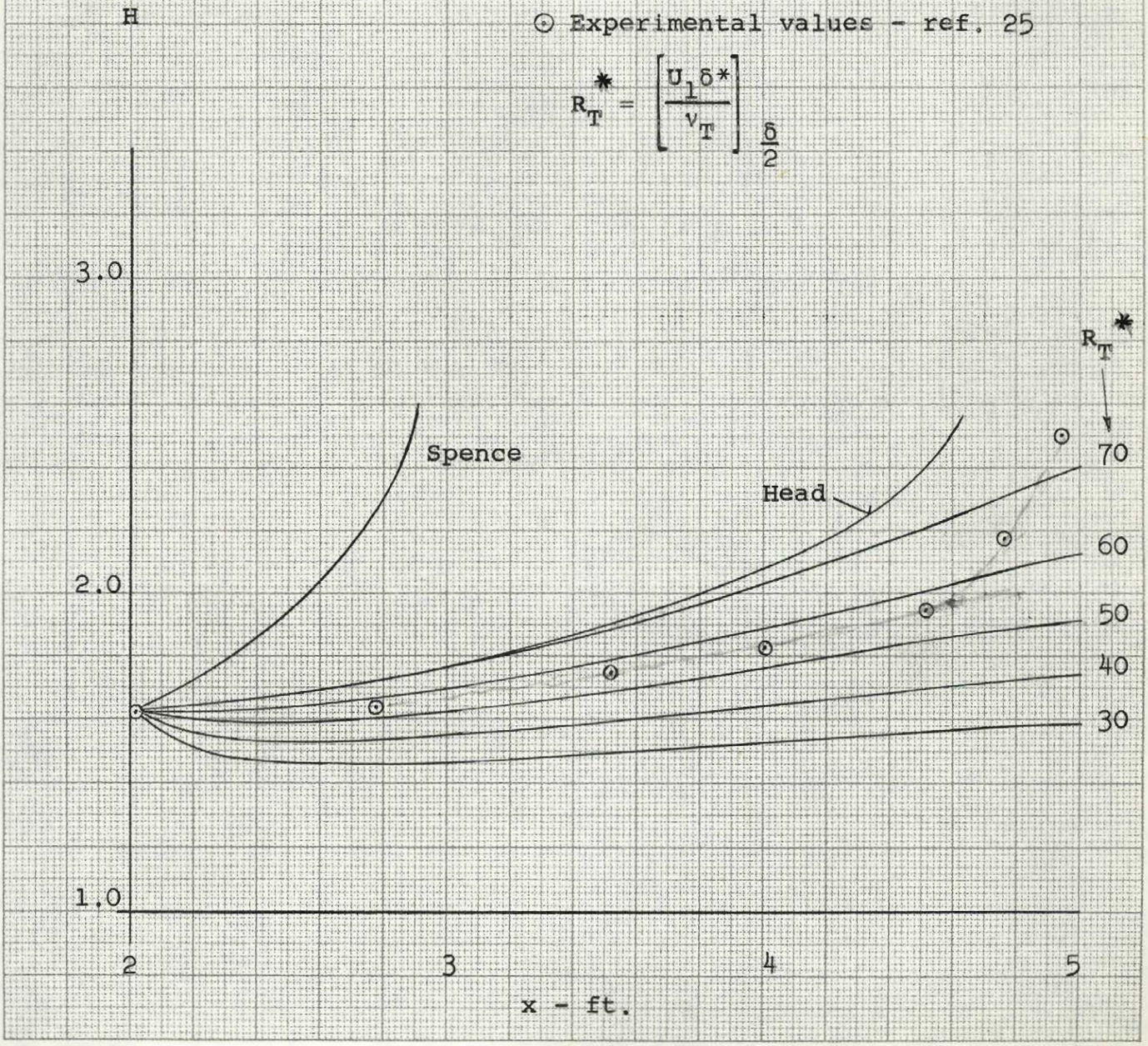

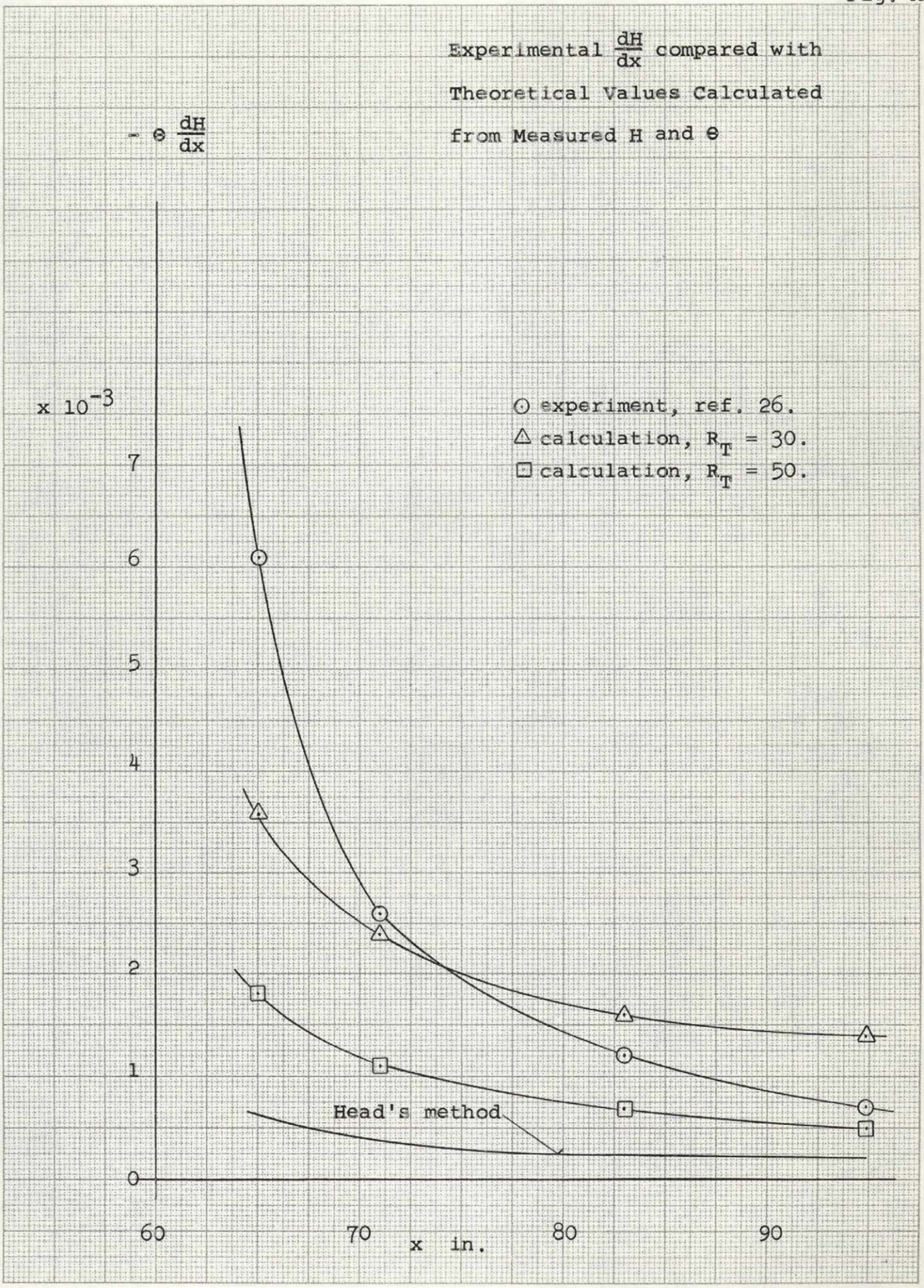
Experimental $\frac{dH}{dx}$ compared with
Theoretical Values Calculated
from Measured H and Θ
$-\Theta \frac{dH}{dx}$
x 10^{-3}
⊙ experiment, ref. 26.
△ calculation, R_T = 30.
□ calculation, R_T = 50.
Head's method
0
1
2
3
4
5
6
7
60
70
80
90
x in.

Fig.A 4

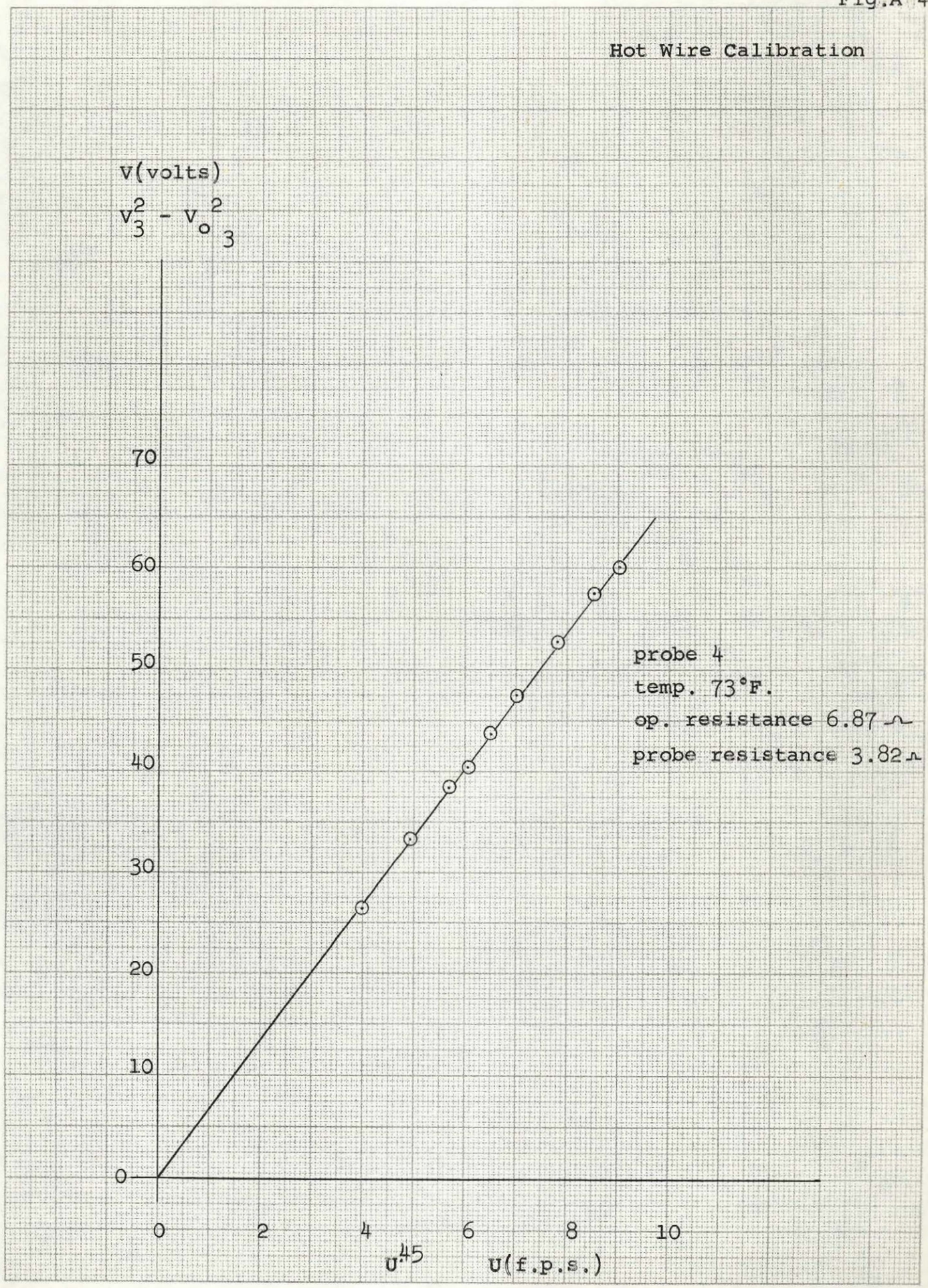
Hot Wire Calibration
V(volts)
$V_3^2 - V_{o\,3}^2$
70
60
50
40
30
20
10
0
0
2
4
6
8
10
U(f.p.s.)
probe 4
temp. 73°F.
op. resistance 6.87 Ω
probe resistance 3.82 Ω

Fig. A 5

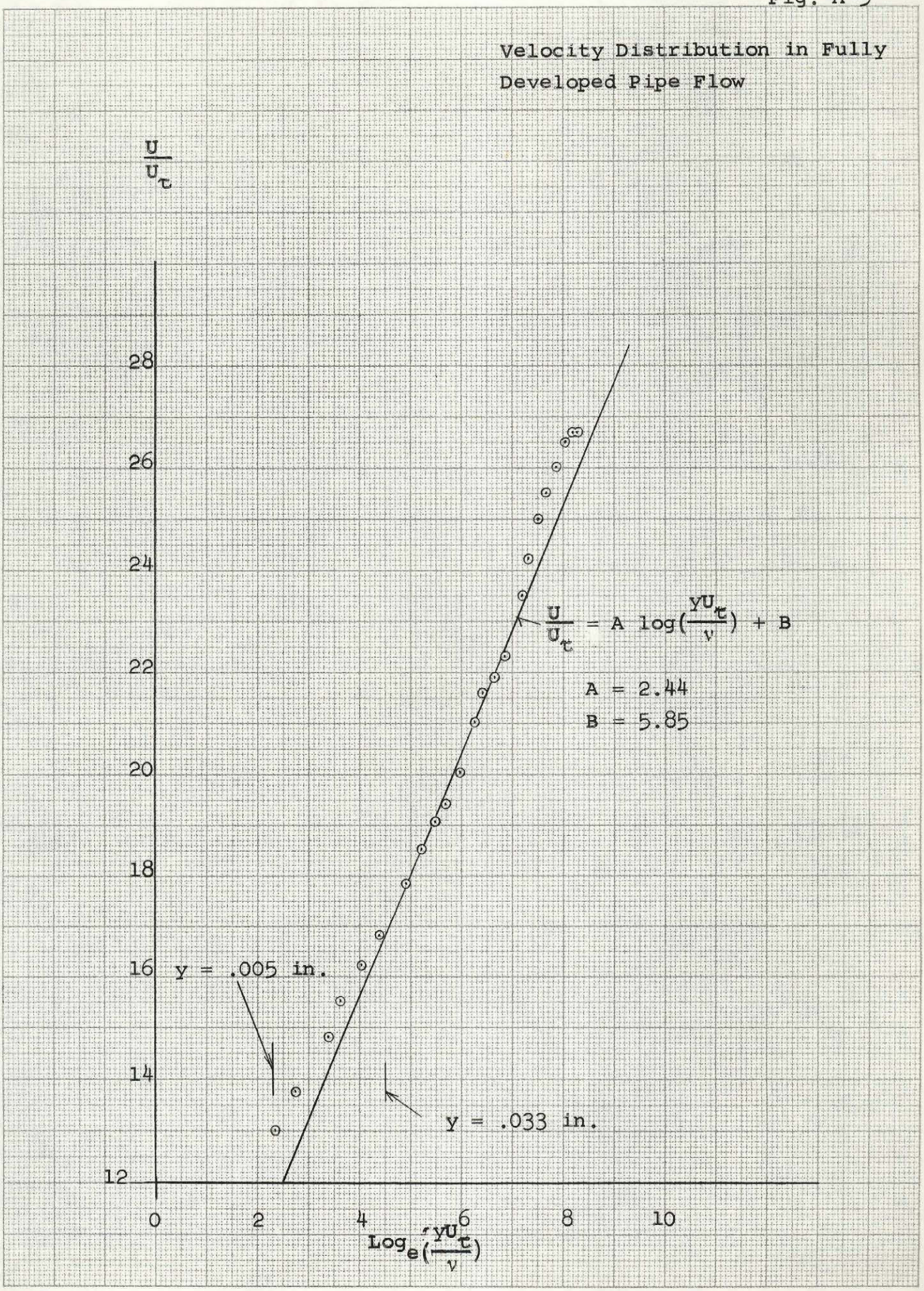
Velocity Distribution in Fully Developed Pipe Flow
U/U_τ
28
26
24
22
20
18
16
14
12
0
2
4
6
8
10
U/U_τ = A log(yU_τ/ν) + B
A = 2.44
B = 5.85
y = .005 in.
y = .033 in.
Log_e(yU_τ/ν)

Fig. A 6

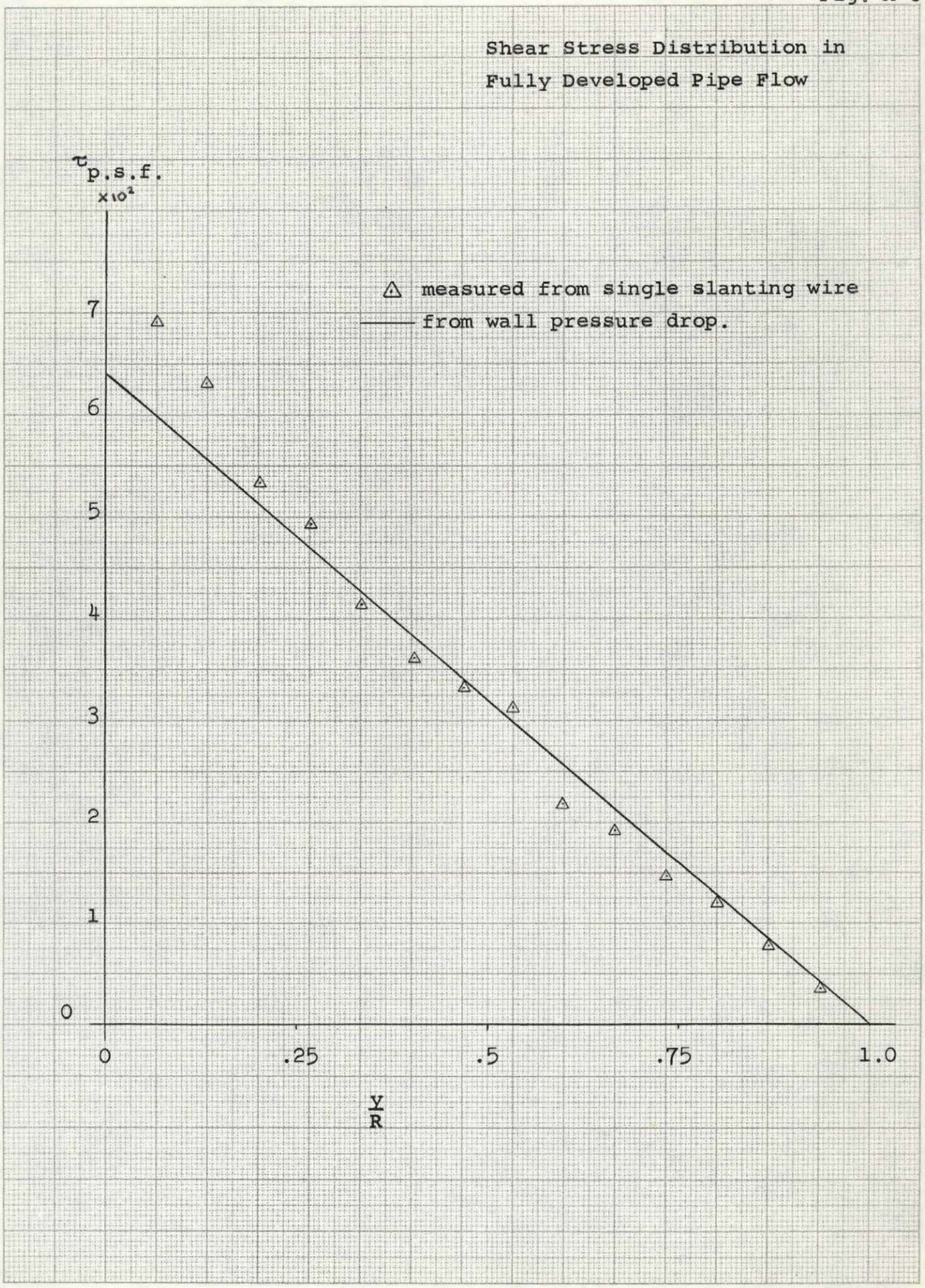
Shear Stress Distribution in
Fully Developed Pipe Flow
τ p.s.f.
x10²
△ measured from single slanting wire
—— from wall pressure drop.
7
6
5
4
3
2
1
0
0
.25
.5
.75
1.0
Y/R

Turbulence Intensities in Fully Developed Pipe Flow.

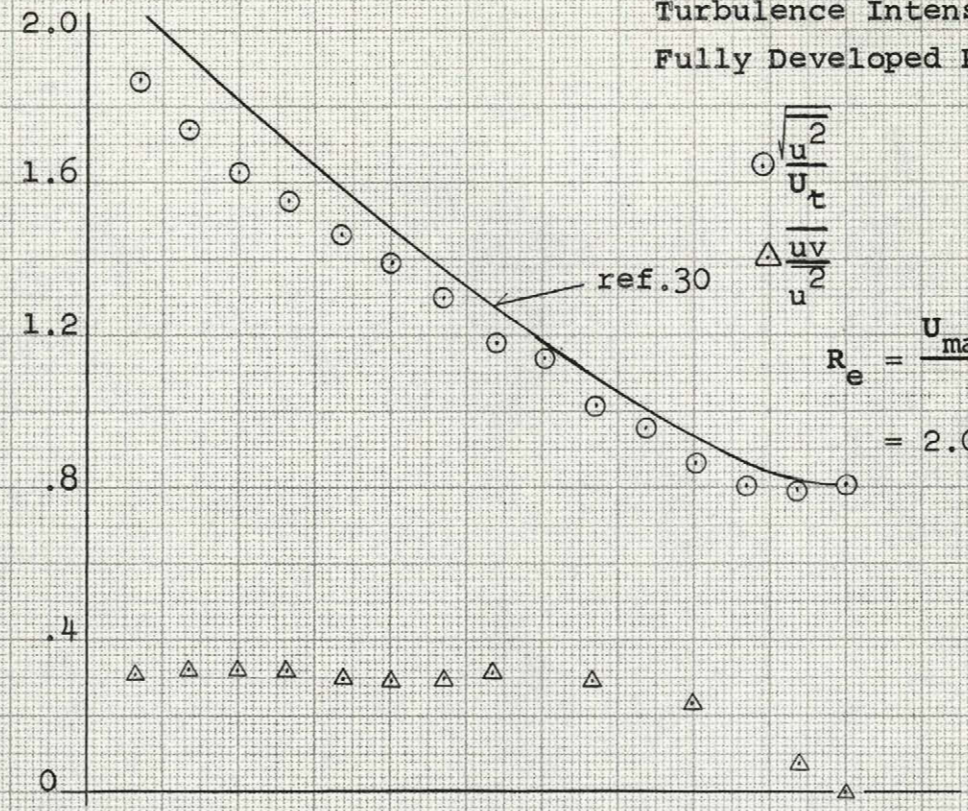

$$R_e = \frac{U_{max} \times 2R}{\nu} = 2.0 \times 10^5$$

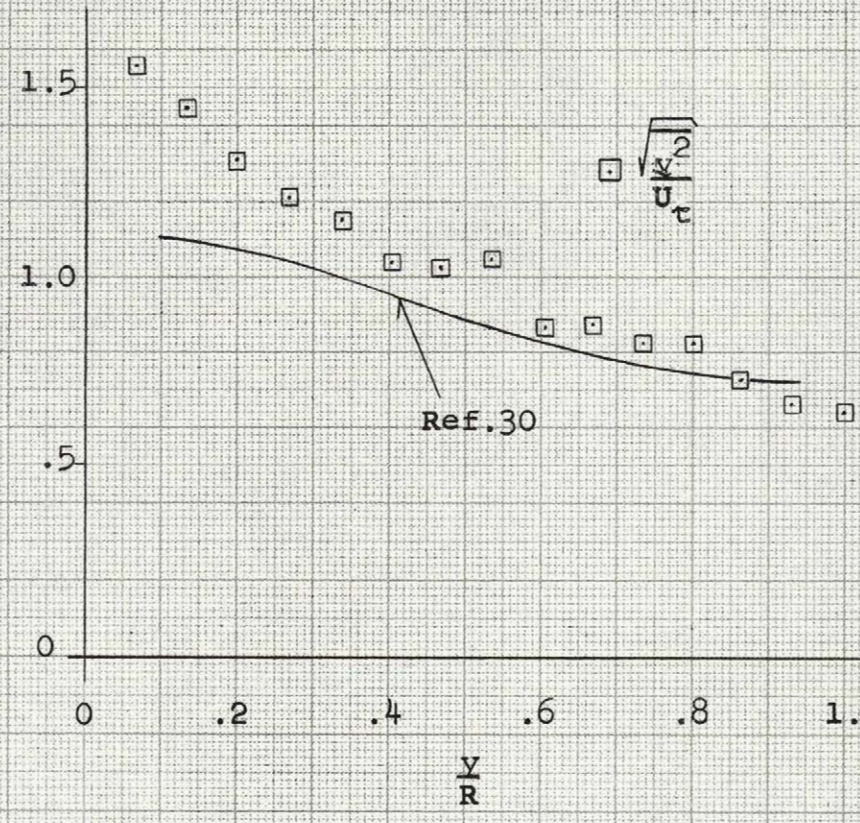

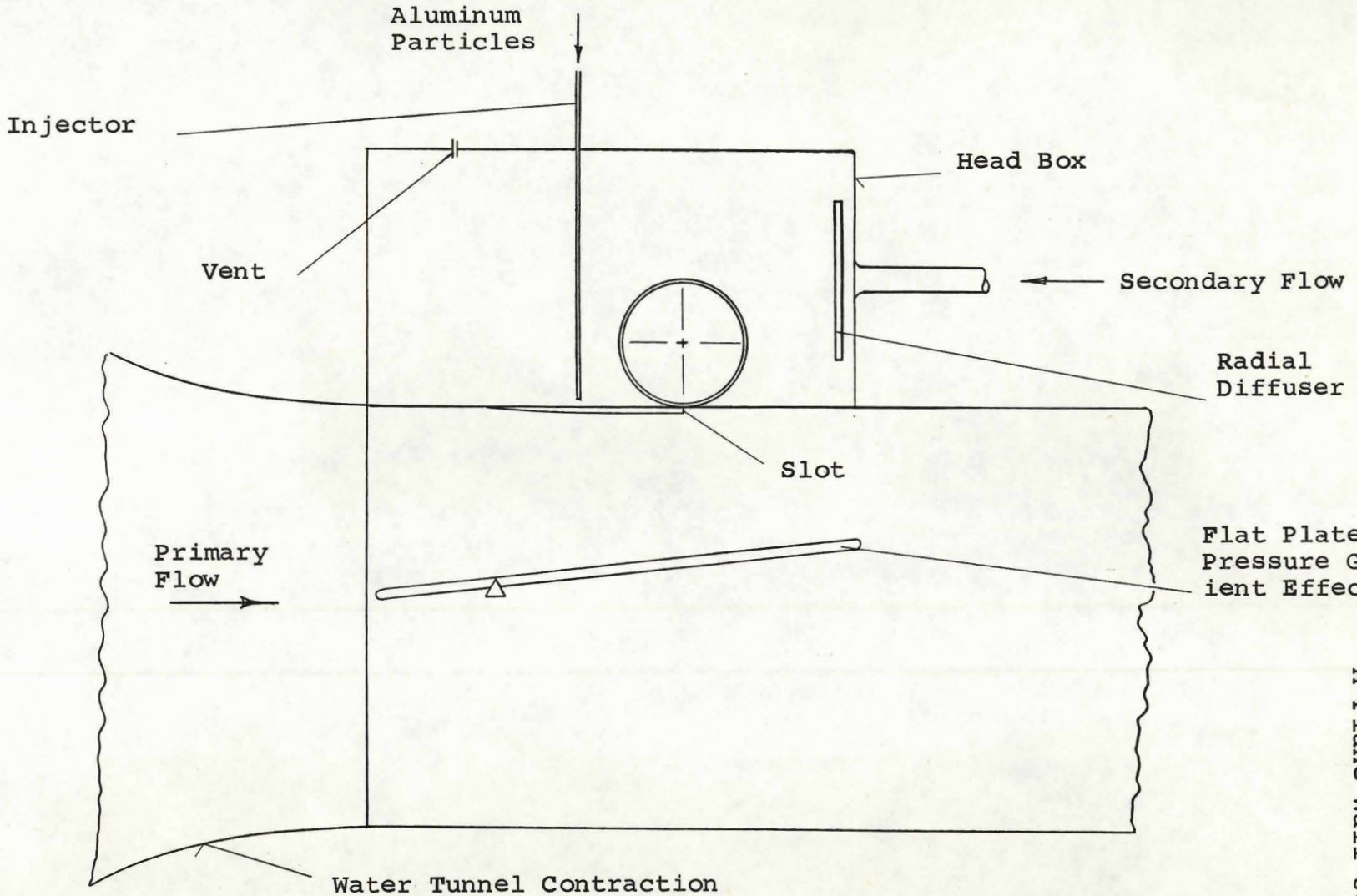

Fig. A 8
Experimental Arrangements
for Flow Visualization of
A Plane Wall Jet

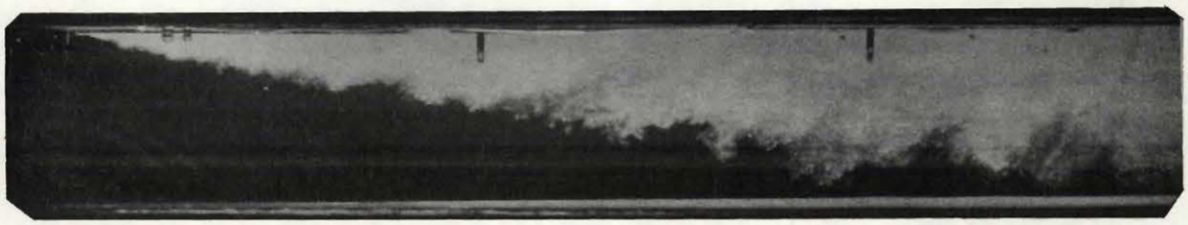

Flow Visualization: Wall Jet In Still Surroundings

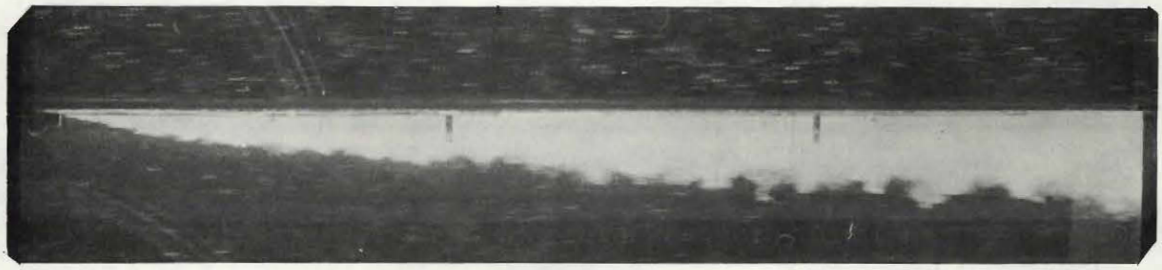

(A) Wall Jet In Uniform Streaming Flow $\frac{U_1}{U_j} = .50$

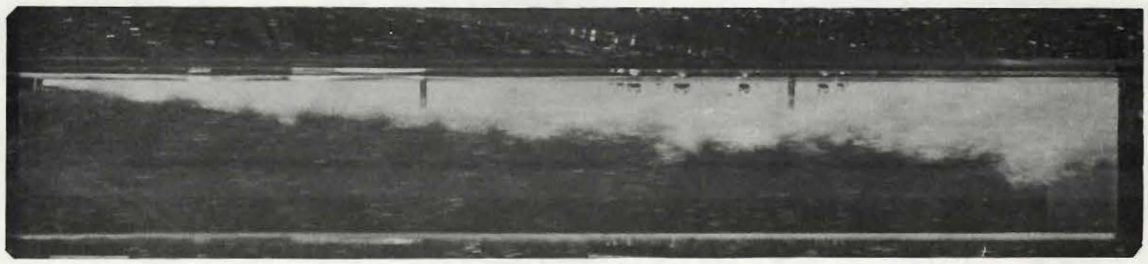

(B) Wall Jet In Adverse Pressure Gradient

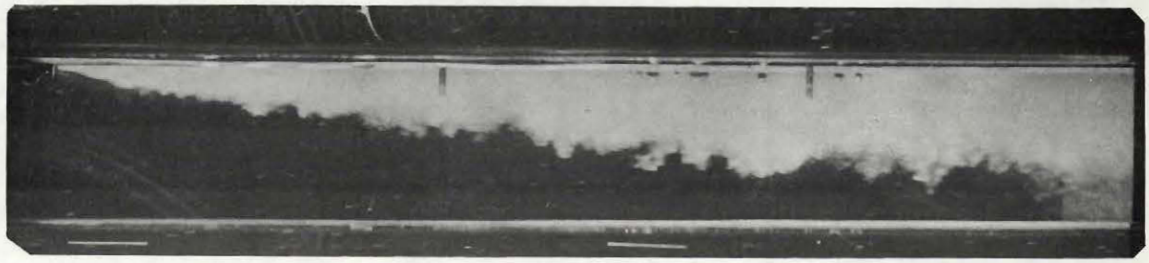

(C) Wall Jet In Favourable Pressure Gradient

Flow Visualization Photographs

Fig. A 11

Longitudinal Turbulence Intensity and Mean Velocity Distribution in B.L. on Tunnel Floor

$\delta_{.99}$ = 1.2 in.

original distribution

$\frac{U_1 \Theta}{\nu}$ = 4,550

Final distributions

$\frac{U_1 \Theta}{\nu}$ = 3,840

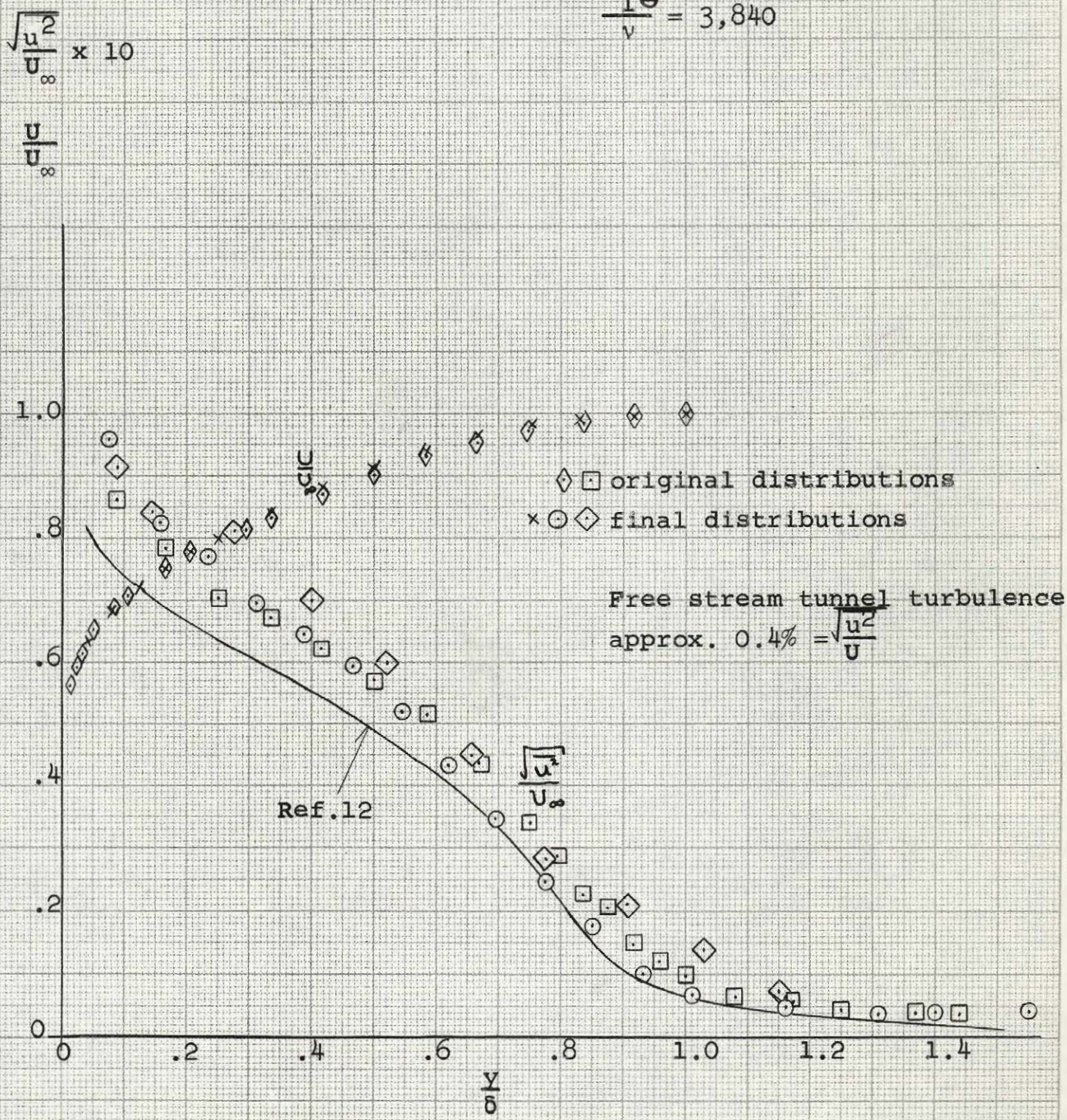

Fig. A 12

Intermittency Factor in a Flat Plate Boundary Layer

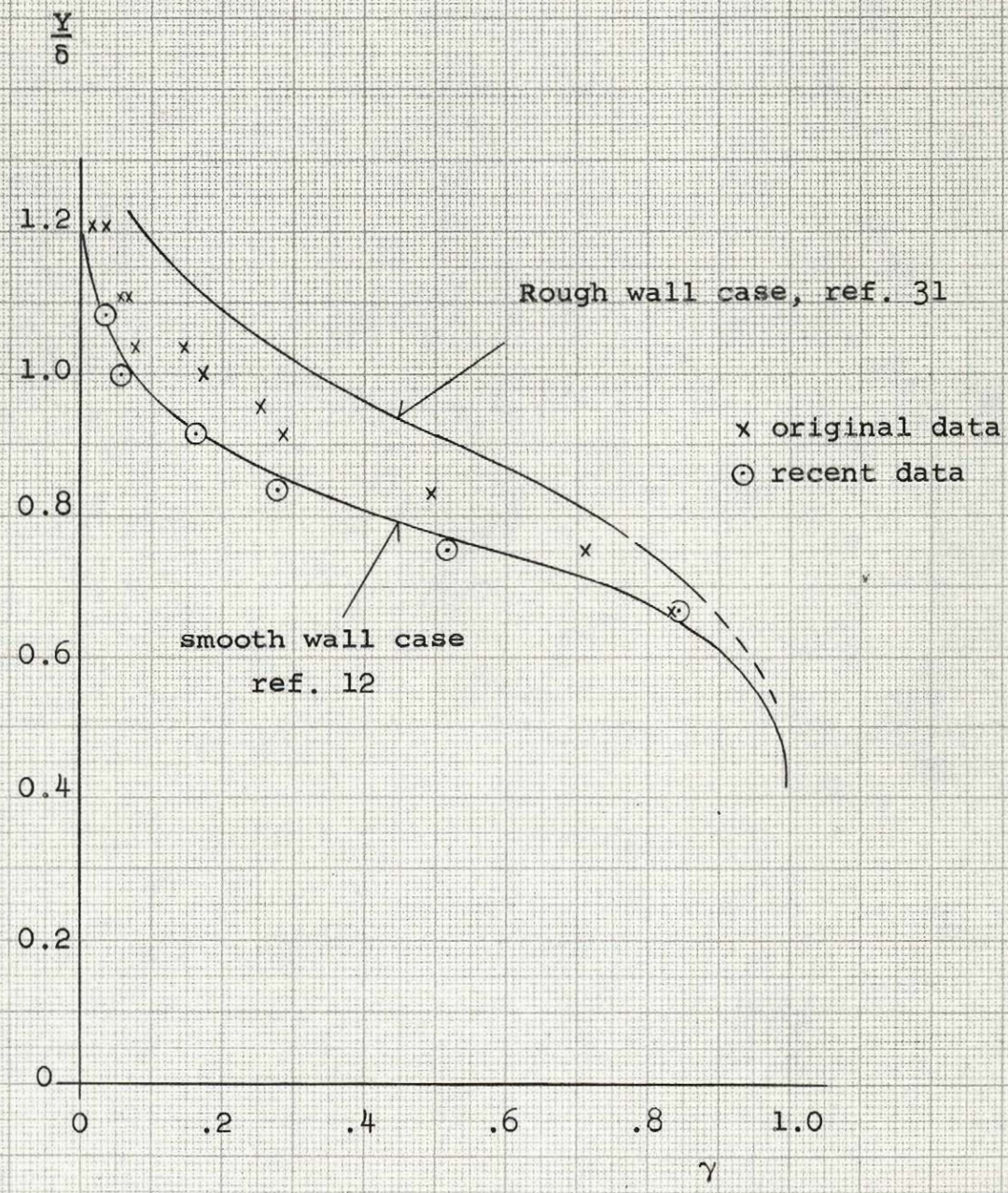

Fig. A 13

Intermittency Factor in a Partly Developed Small Deficit Wake

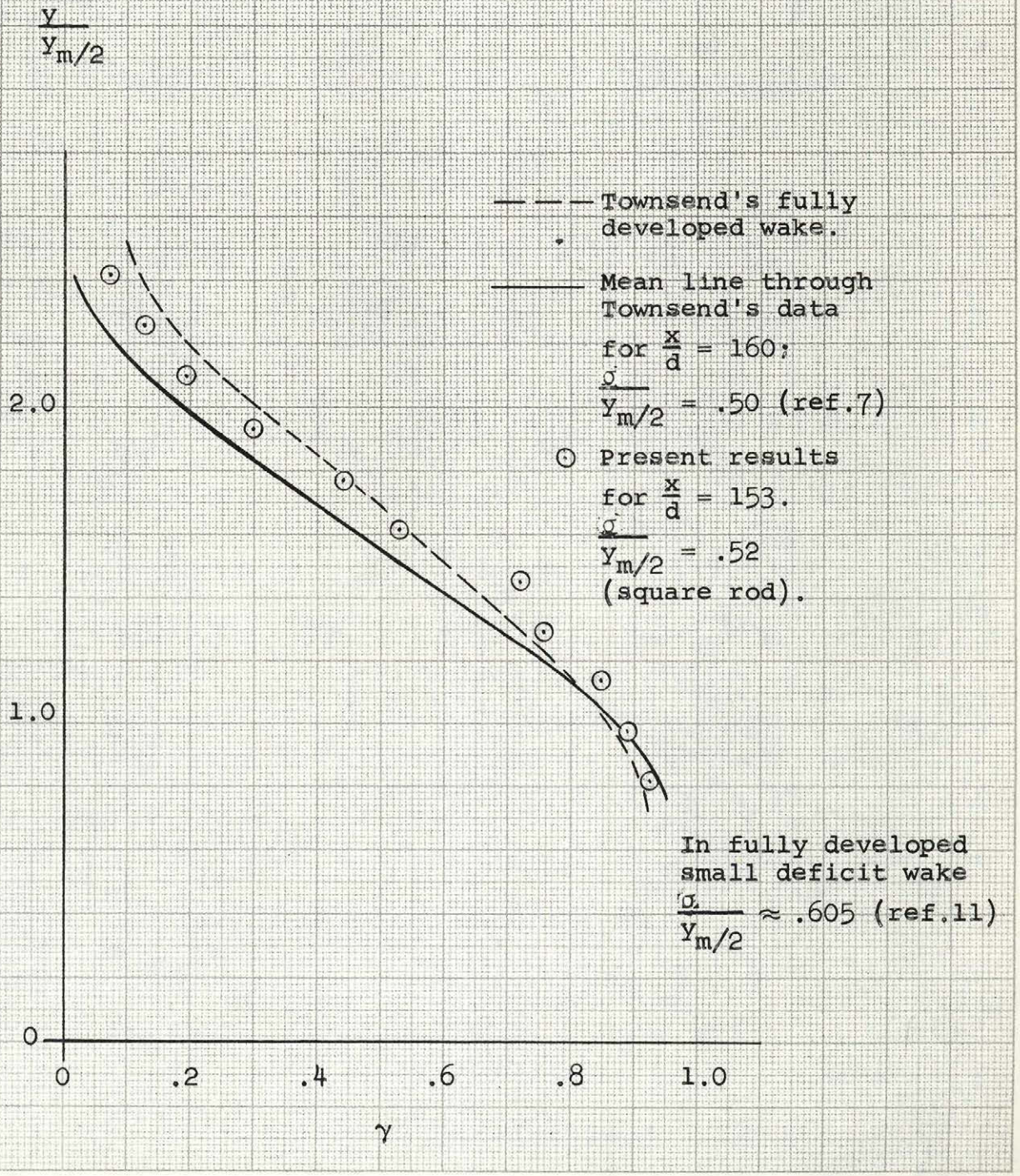

Fig. A 14

Intermittency Factor in a Plane Free Jet in Small or Zero Velocity Stream.

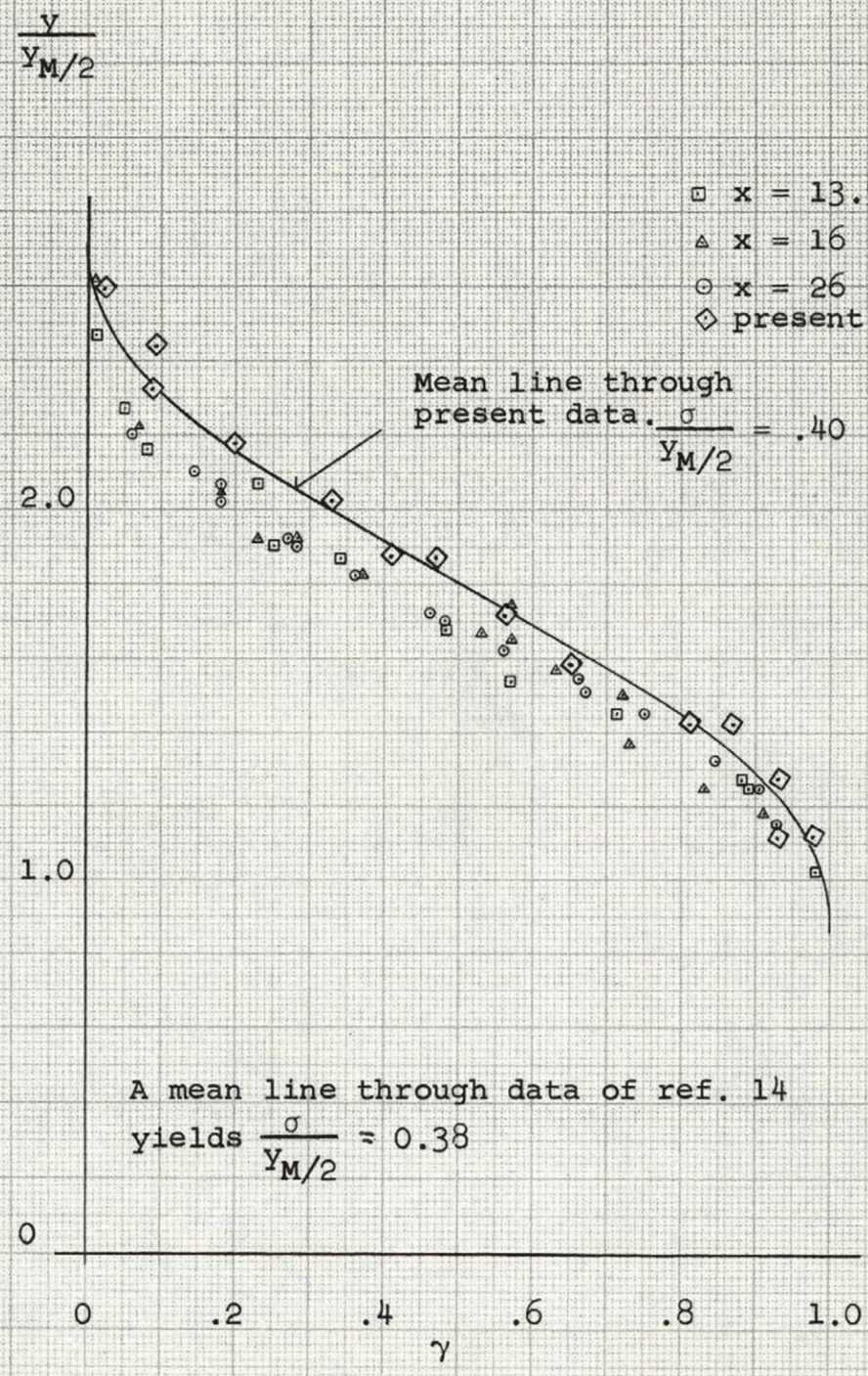

Velocity Profile Sketches to Illustrate Definition of Terms

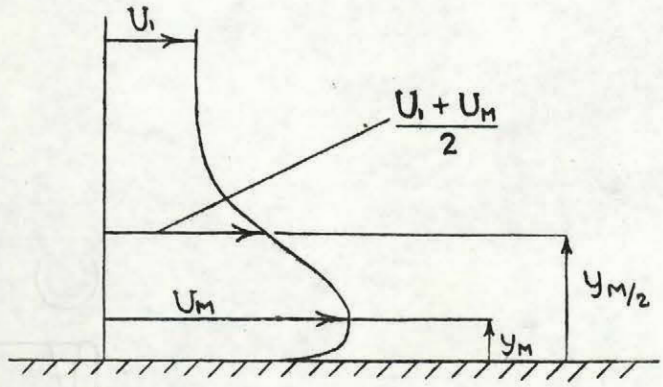

a) Wall jet

Length and velocity scales:

$L_o = y_{M/2} - y_M$

$U_o = U_M - U_1$

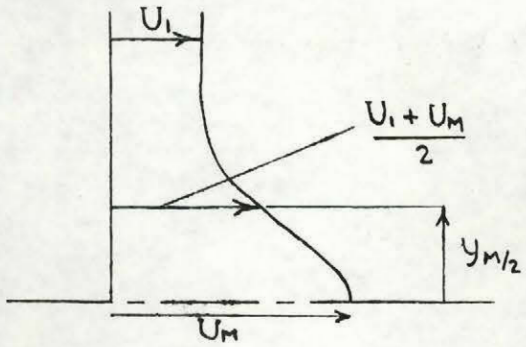

b) Jet

$L_o = y_{M/2}$

$U_o = U_M - U_1$

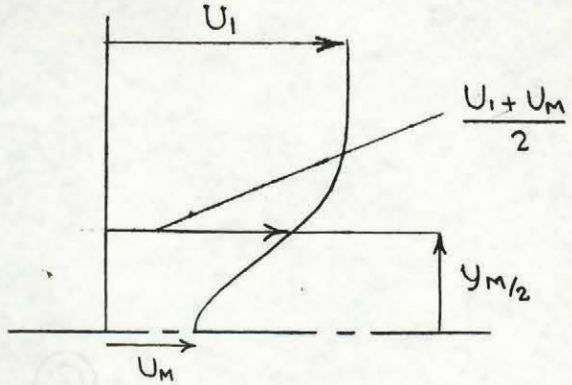

c) Wake

$L_o = y_{M/2}$

$U_o = U_1 - U_M$

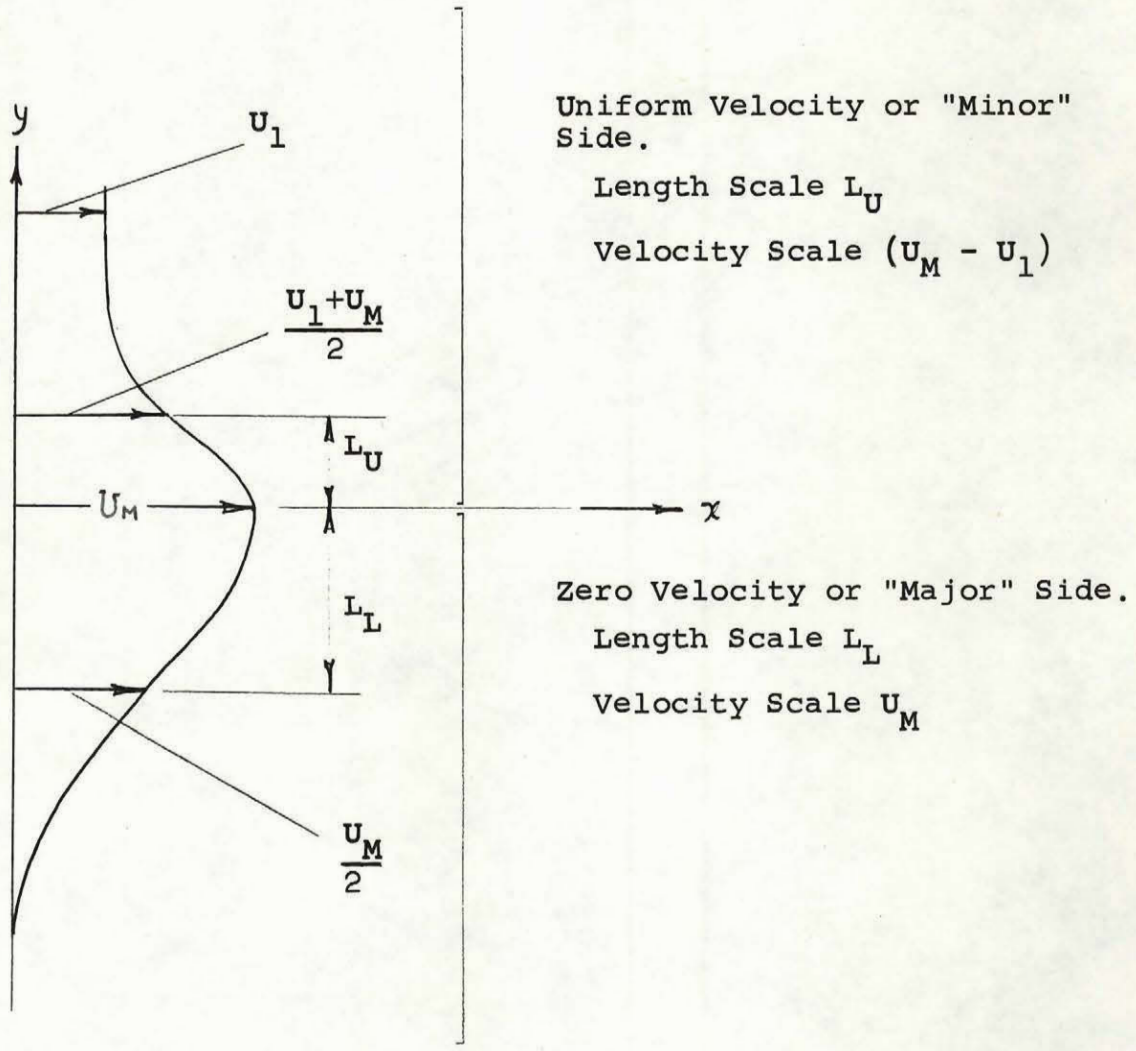

d) Asymmetric Jet in Uniform Streaming Flow.

Fig. 2

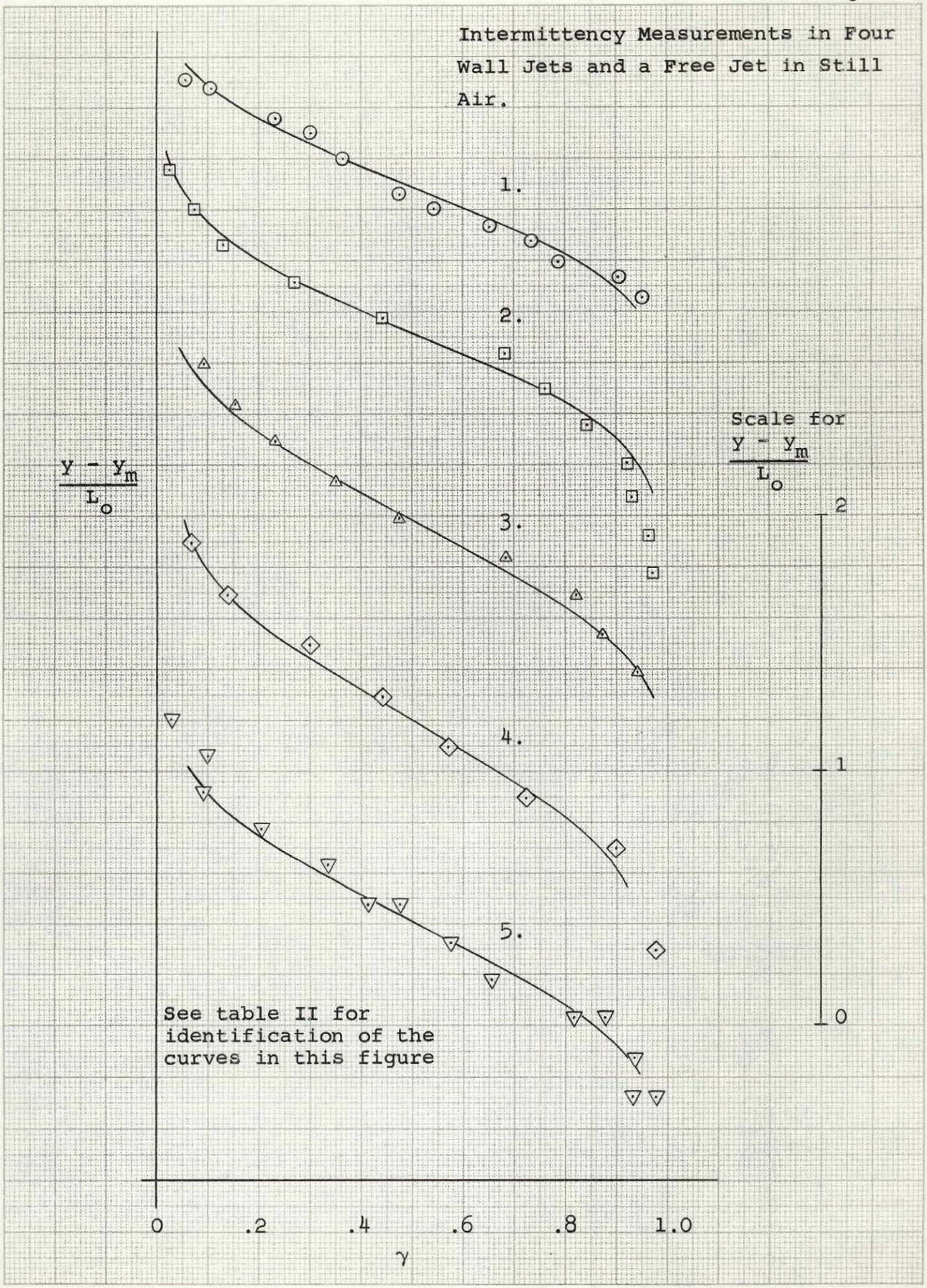
Intermittency Measurements in Four Wall Jets and a Free Jet in Still Air.
1.
2.
3.
4.
5.
$\frac{y - y_m}{L_o}$
Scale for $\frac{y - y_m}{L_o}$
2
1
0
See table II for identification of the curves in this figure
0
.2
.4
.6
.8
1.0
γ

Fig. 3

The Shear Stress Parameter R_T As A Function of Large Eddy Scale.

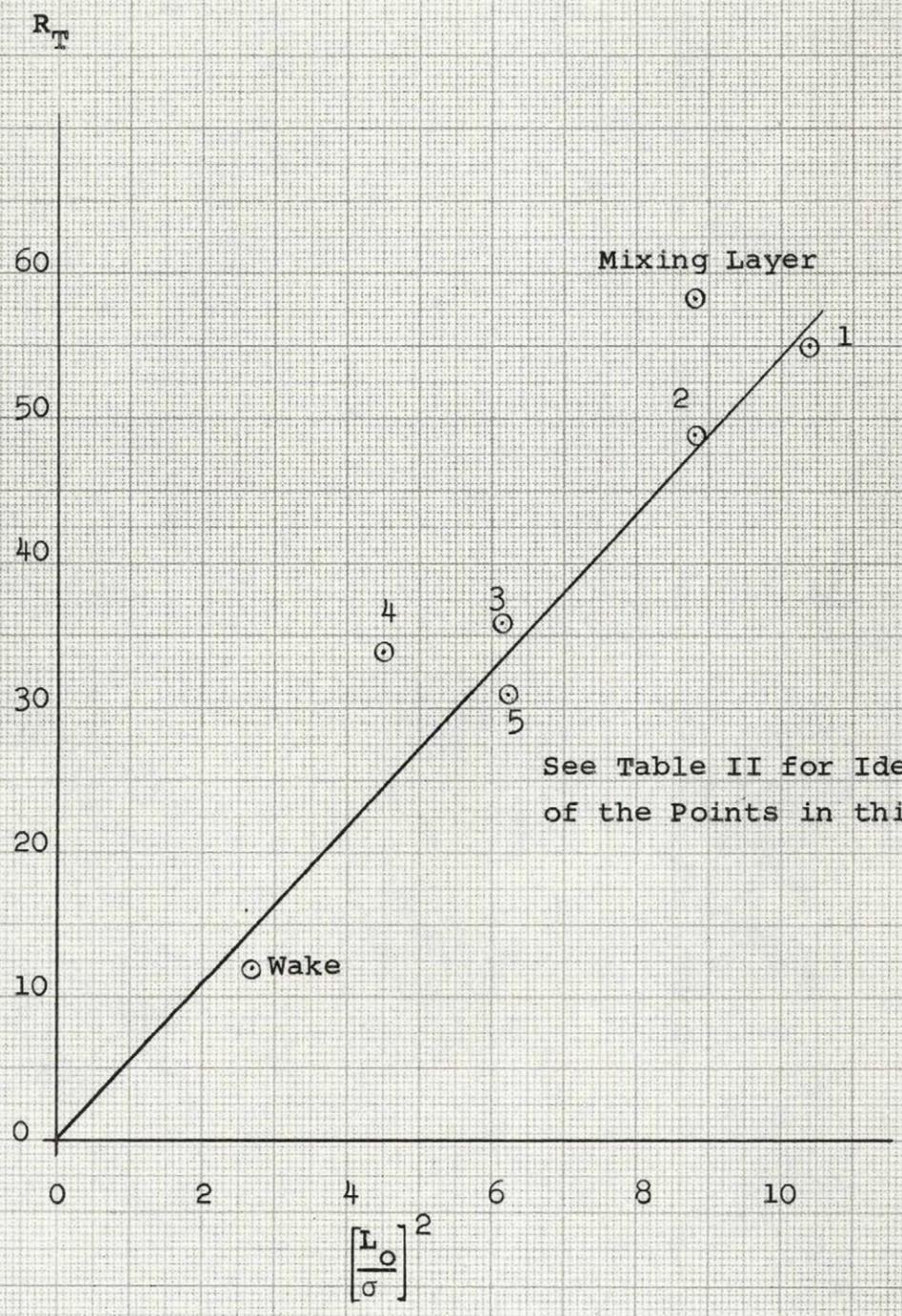

See Table II for Identification of the Points in this Figure.

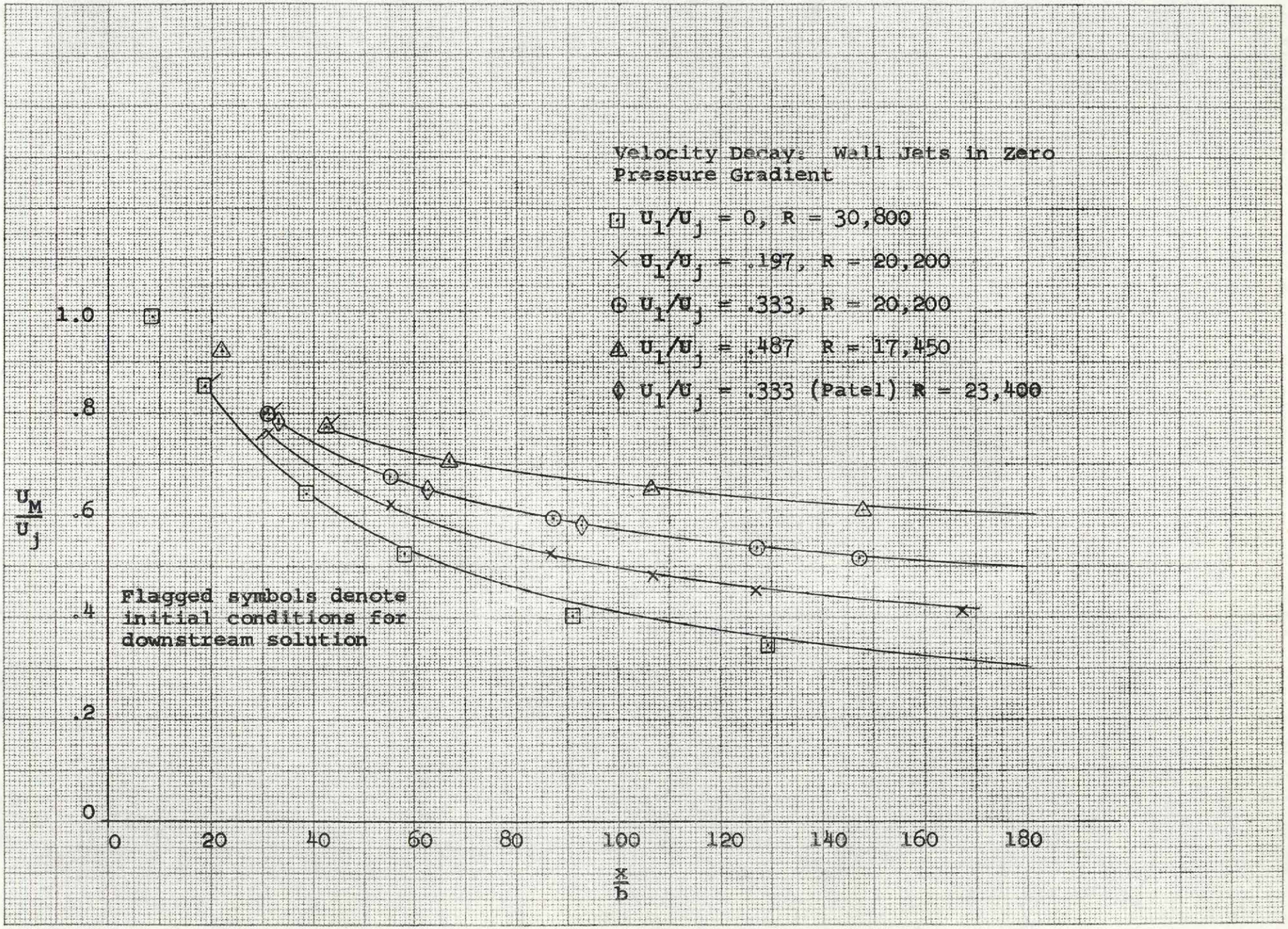
Velocity Decay: Wall Jets in Zero Pressure Gradient
U_1/U_j = 0, R = 30,800
U_1/U_j = .197, R = 20,200
U_1/U_j = .333, R = 20,200
U_1/U_j = .487 R = 17,450
U_1/U_j = .333 (Patel) R = 23,400
Flagged symbols denote initial conditions for downstream solution
$\frac{U_M}{U_j}$
1.0
.8
.6
.4
.2
0
0
20
40
60
80
100
120
140
160
180
$\frac{x}{b}$

Fig. 4.

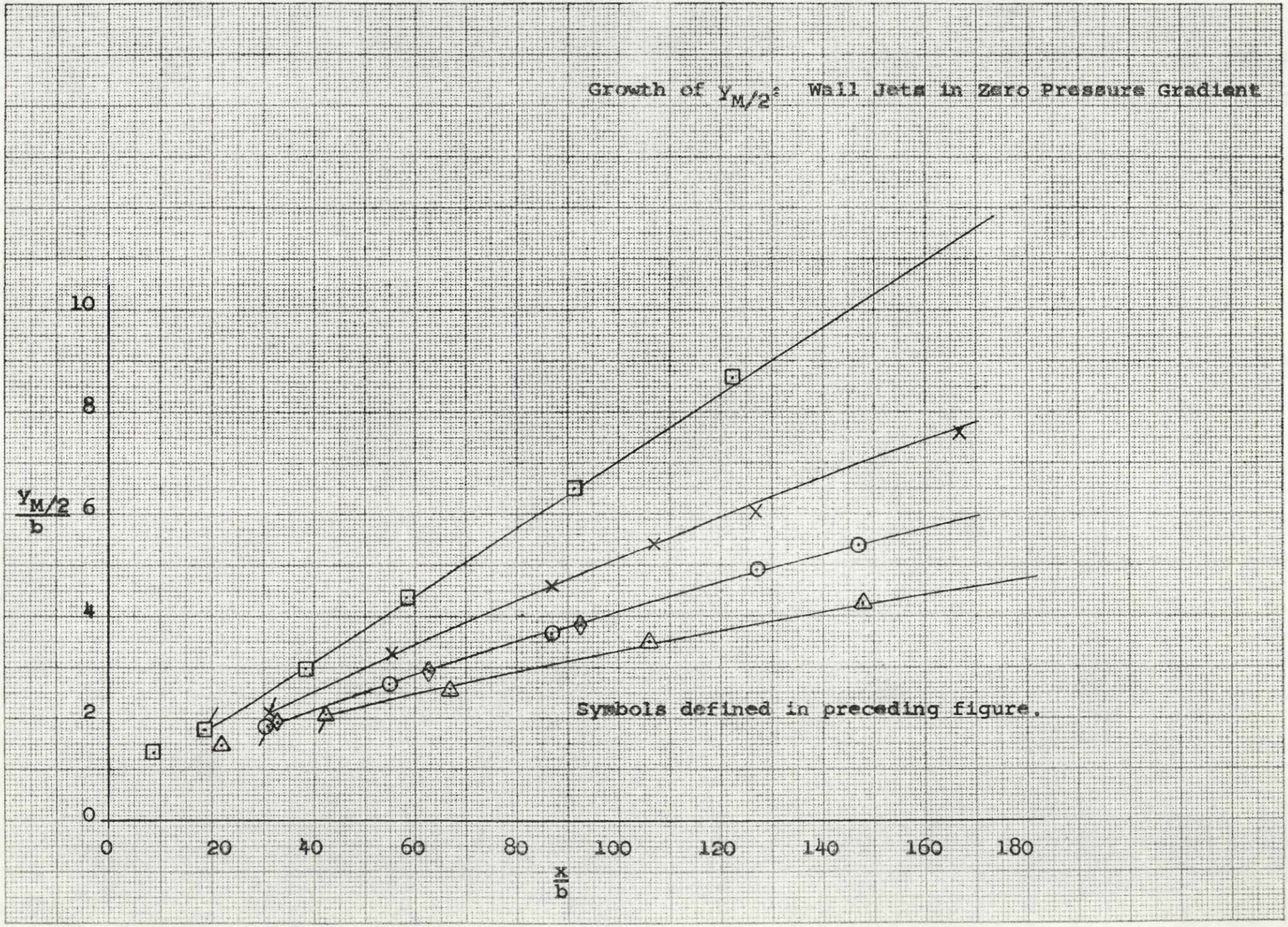
Growth of $y_{M/2}$: Wall Jets in Zero Pressure Gradient
$\frac{y_{M/2}}{b}$
10
8
6
4
2
0
0
20
40
60
80
100
120
140
160
180
$\frac{x}{b}$
Symbols defined in preceding figure.

Fig. 5

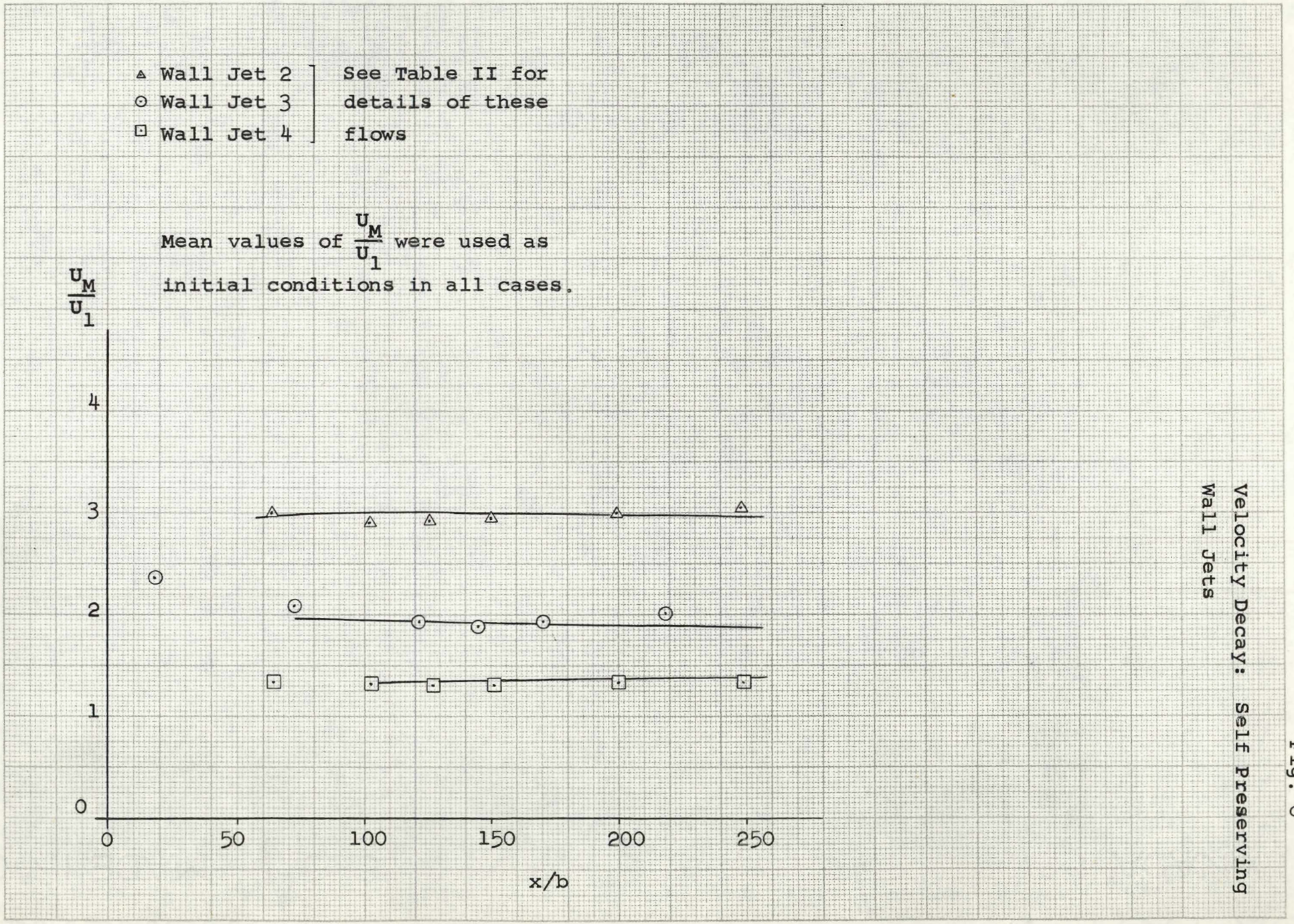

Velocity Decay: Self Preserving Wall Jets

Fig. 6

Fig. 7

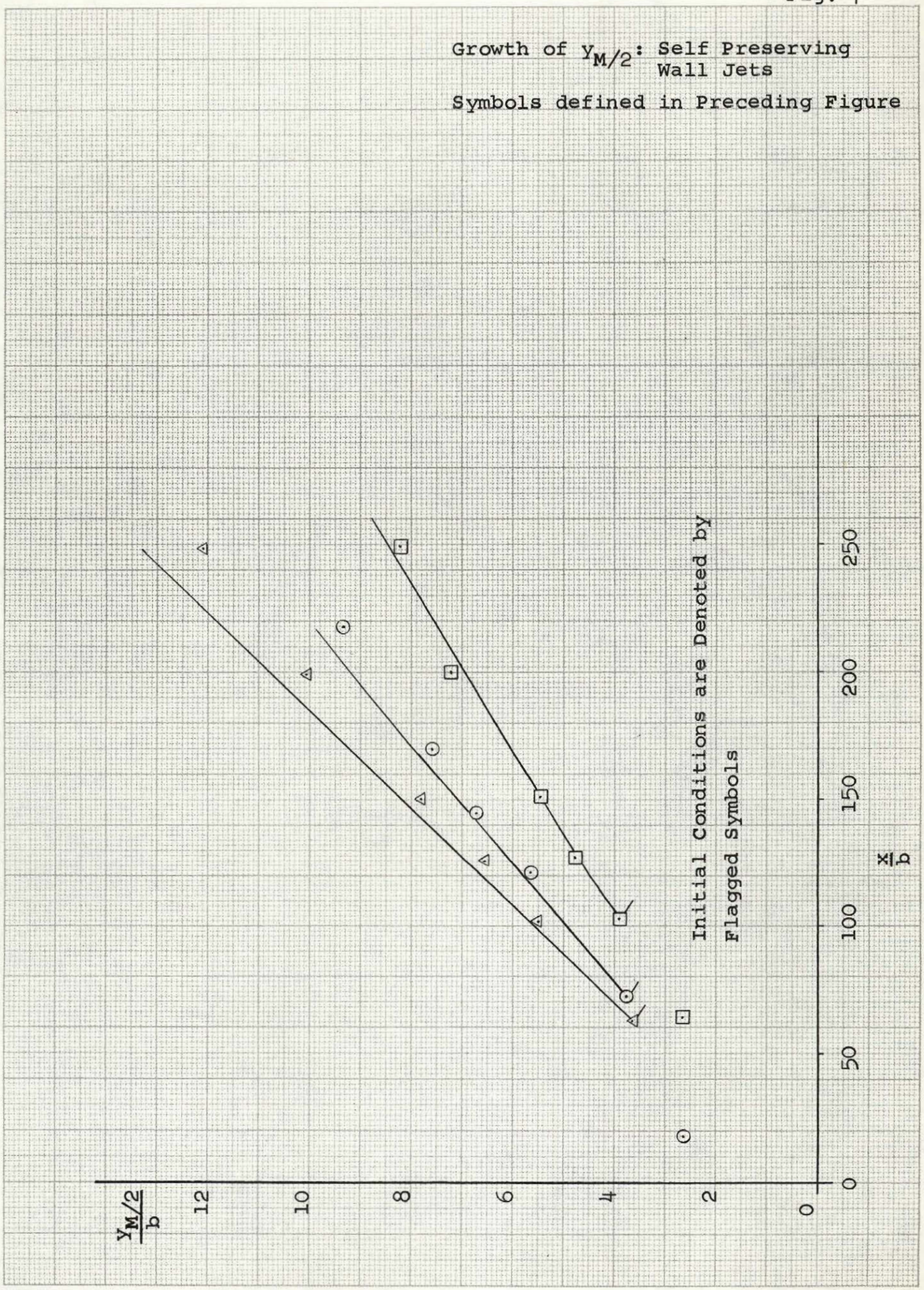
Growth of $y_{M/2}$: Self Preserving Wall Jets
Symbols defined in Preceding Figure
$\frac{y_{M/2}}{b}$
0
2
4
6
8
10
12
0
50
100
150
200
250
$\frac{x}{b}$
Initial Conditions are Denoted by Flagged Symbols

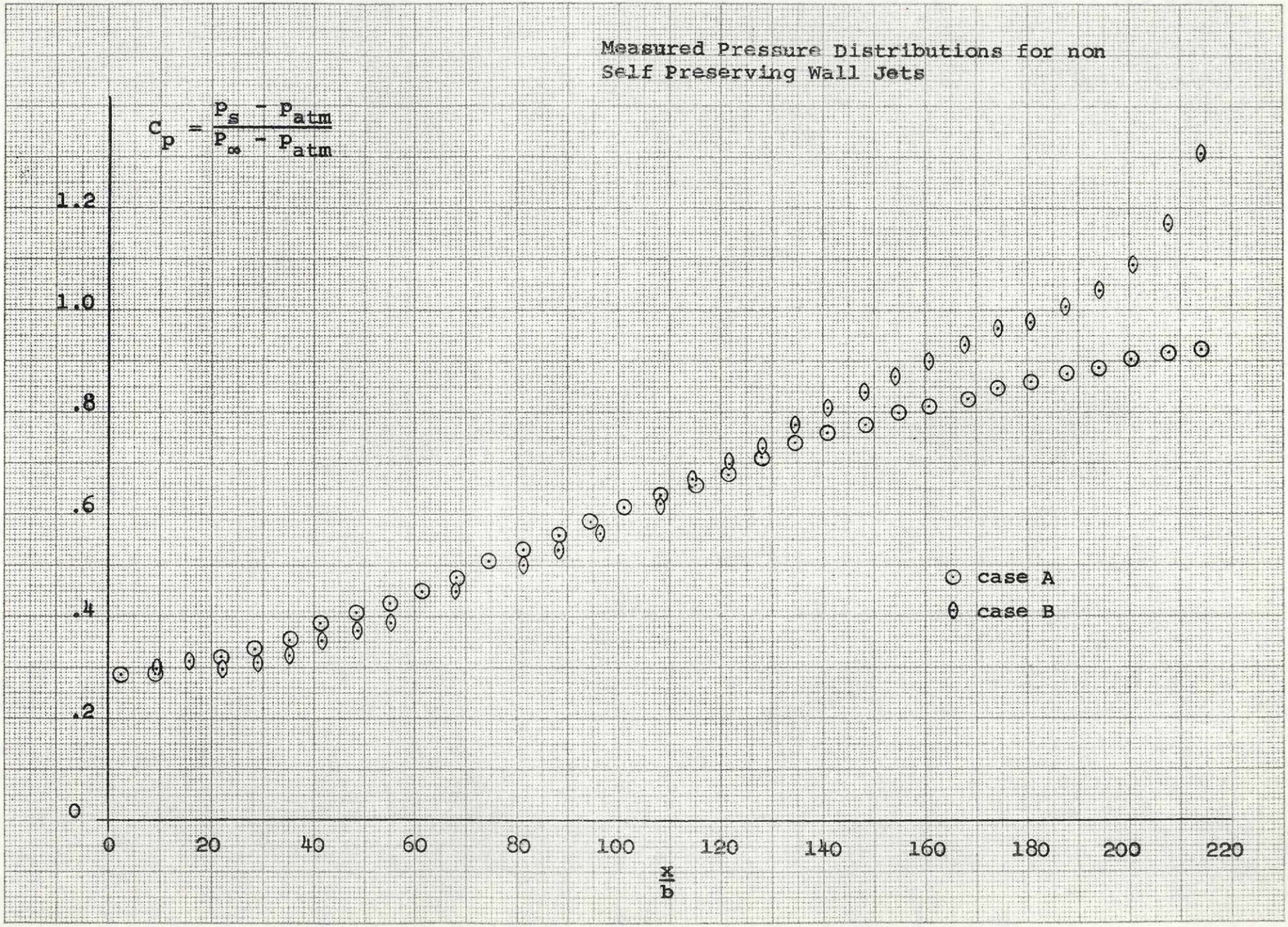
Measured Pressure Distributions for non Self Preserving Wall Jets
$C_p = \frac{P_s - P_{atm}}{P_\infty - P_{atm}}$
1.2
1.0
.8
.6
.4
.2
0
0
20
40
60
80
100
120
140
160
180
200
220
x/b
case A
case B

Fig. 8

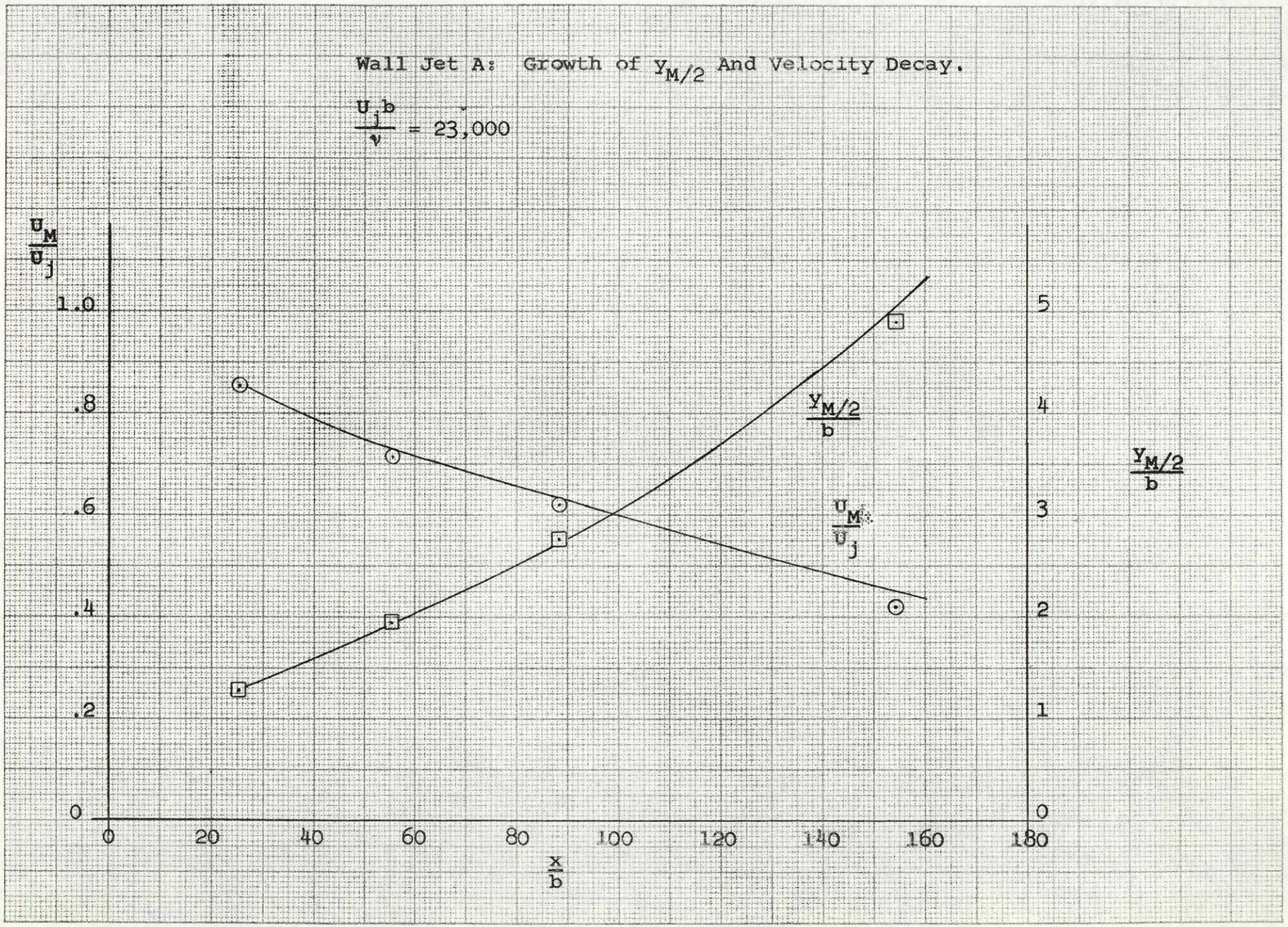
Wall Jet A: Growth of $y_{M/2}$ And Velocity Decay.
$\frac{U_j b}{\nu} = 23,000$
$\frac{U_M}{U_j}$
1.0
.8
.6
.4
.2
0
$\frac{y_{M/2}}{b}$
5
4
3
2
1
0
0
20
40
60
80
100
120
140
160
180
$\frac{x}{b}$

Fig. 9

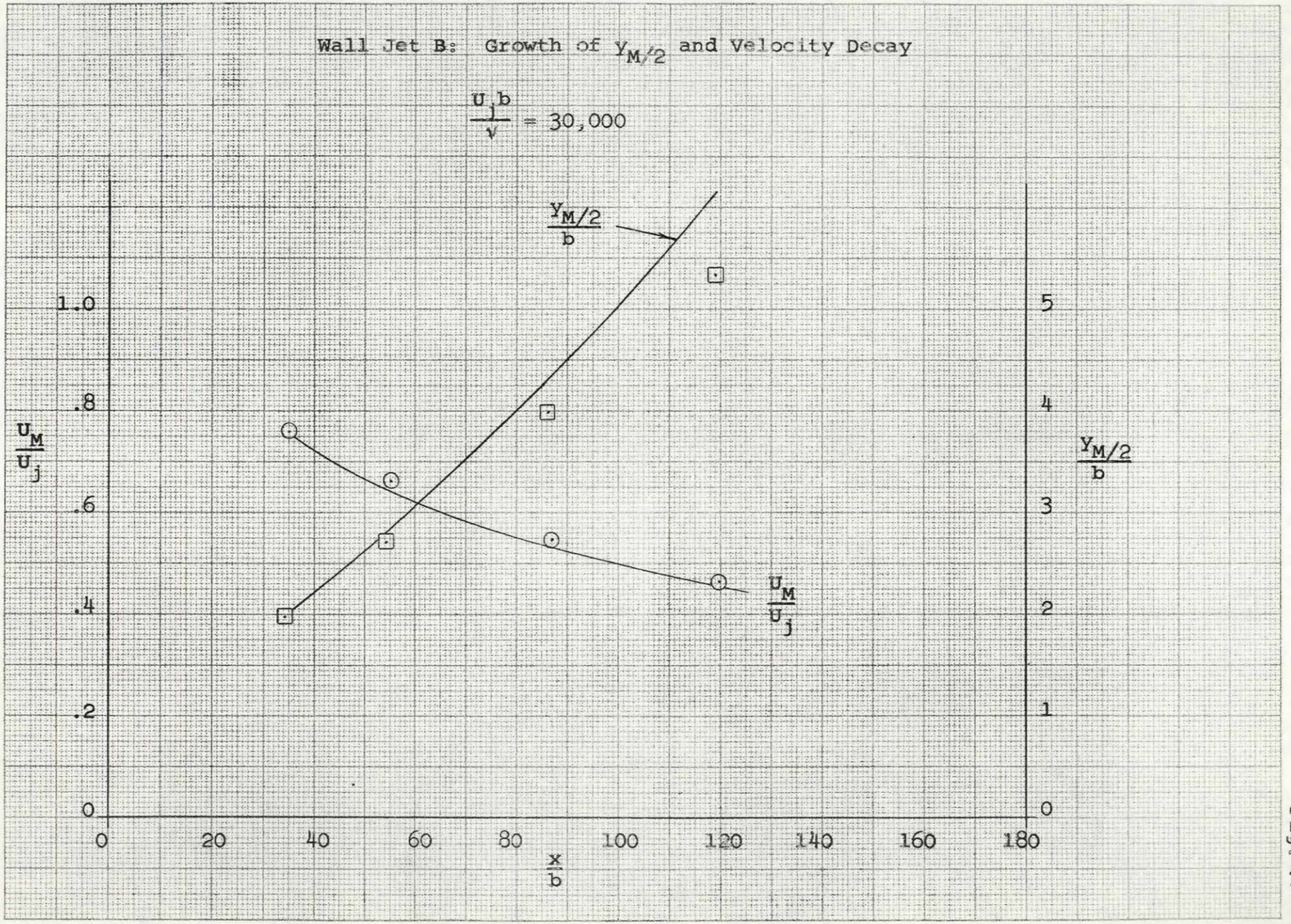
Wall Jet B: Growth of $y_{M/2}$ and Velocity Decay
$\frac{U_j b}{\nu} = 30,000$
$\frac{y_{M/2}}{b}$
$\frac{U_M}{U_j}$
1.0
.8
.6
.4
.2
0
5
4
3
2
1
0
0
20
40
60
80
100
120
140
160
180
$\frac{x}{b}$

Fig. 10.

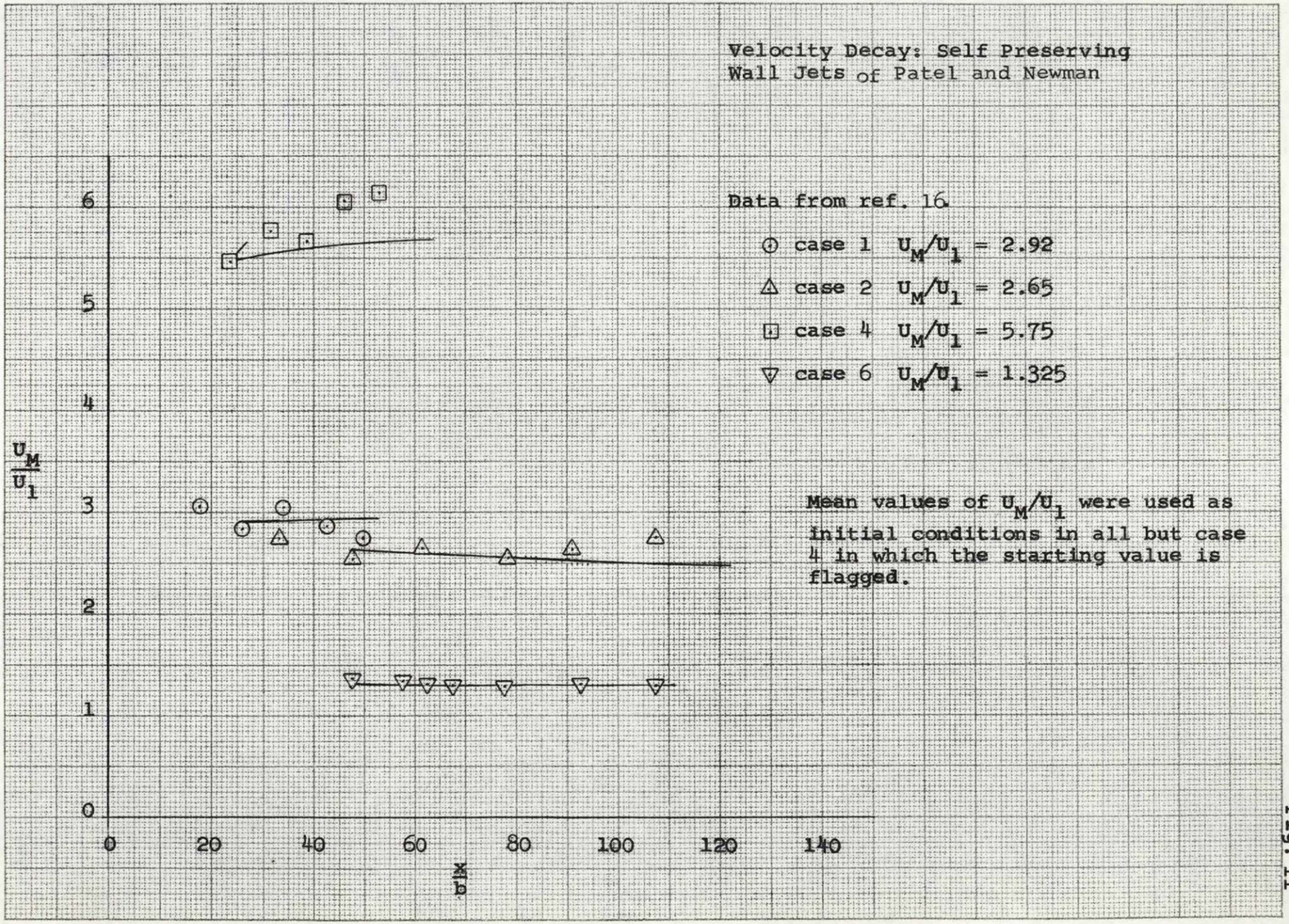
Velocity Decay: Self Preserving
Wall Jets of Patel and Newman
Data from ref. 16
⊙ case 1 U_M/U_1 = 2.92
△ case 2 U_M/U_1 = 2.65
⊡ case 4 U_M/U_1 = 5.75
▽ case 6 U_M/U_1 = 1.325
Mean values of U_M/U_1 were used as initial conditions in all but case 4 in which the starting value is flagged.
$\frac{U_M}{U_1}$
0
1
2
3
4
5
6
0
20
40
60
80
100
120
140
x/b

Fig. 11

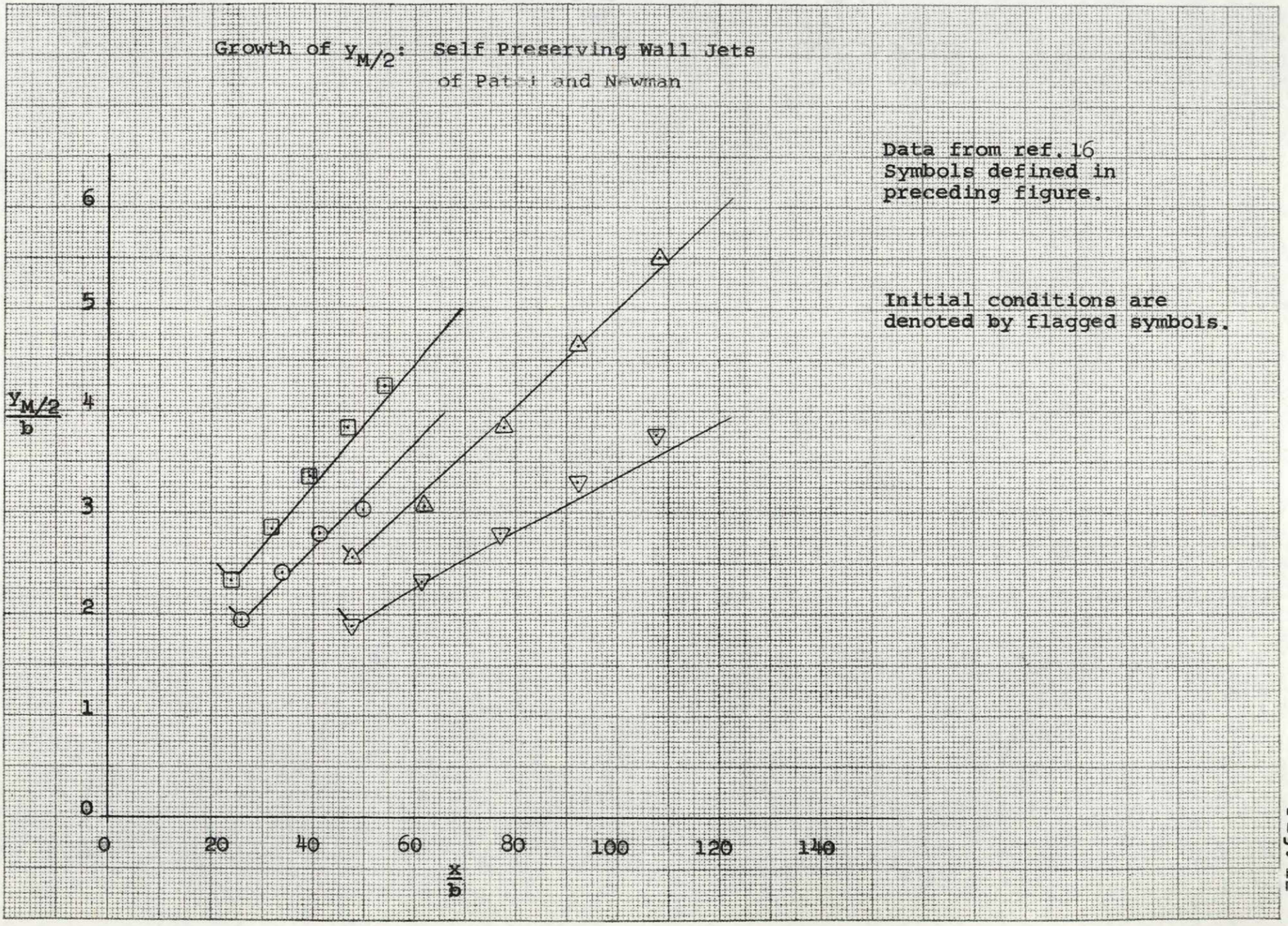
Growth of $y_{M/2}$: Self Preserving Wall Jets
of Patel and Newman
Data from ref. 16
Symbols defined in preceding figure.
Initial conditions are denoted by flagged symbols.
$\frac{y_{M/2}}{b}$
0
1
2
3
4
5
6
0
20
40
60
80
100
120
140
$\frac{x}{b}$

Fig. 12

Fig. 13

Rate of Growth $\frac{dy_{M/2}}{dx}$ for self preserving wall jets.

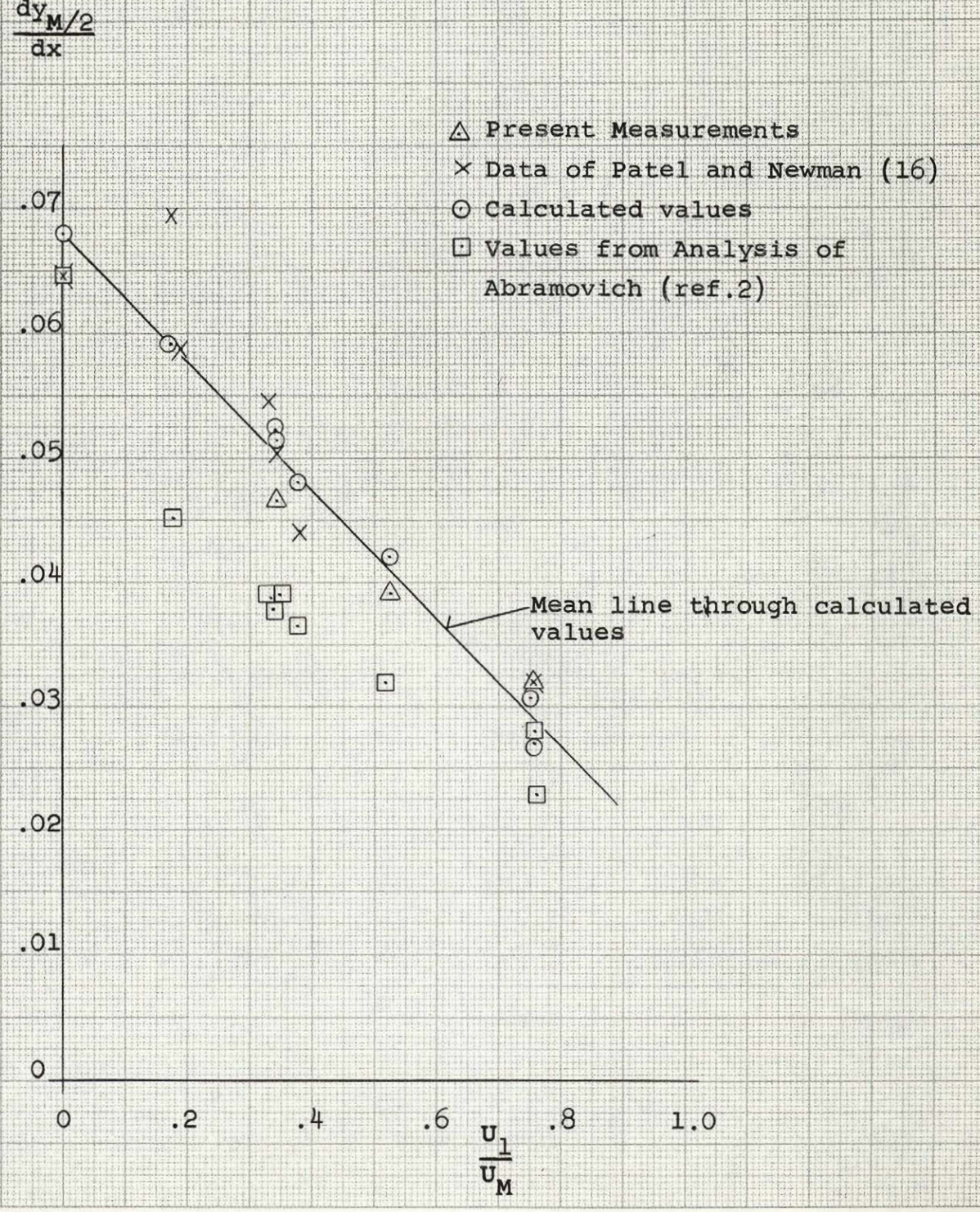

Fig. 14

Intermittency in a Plane Mixing Layer

$x = 34\frac{1}{2}$ inches.

$\frac{U_1 x}{\nu} = 1.15 \times 10^6$

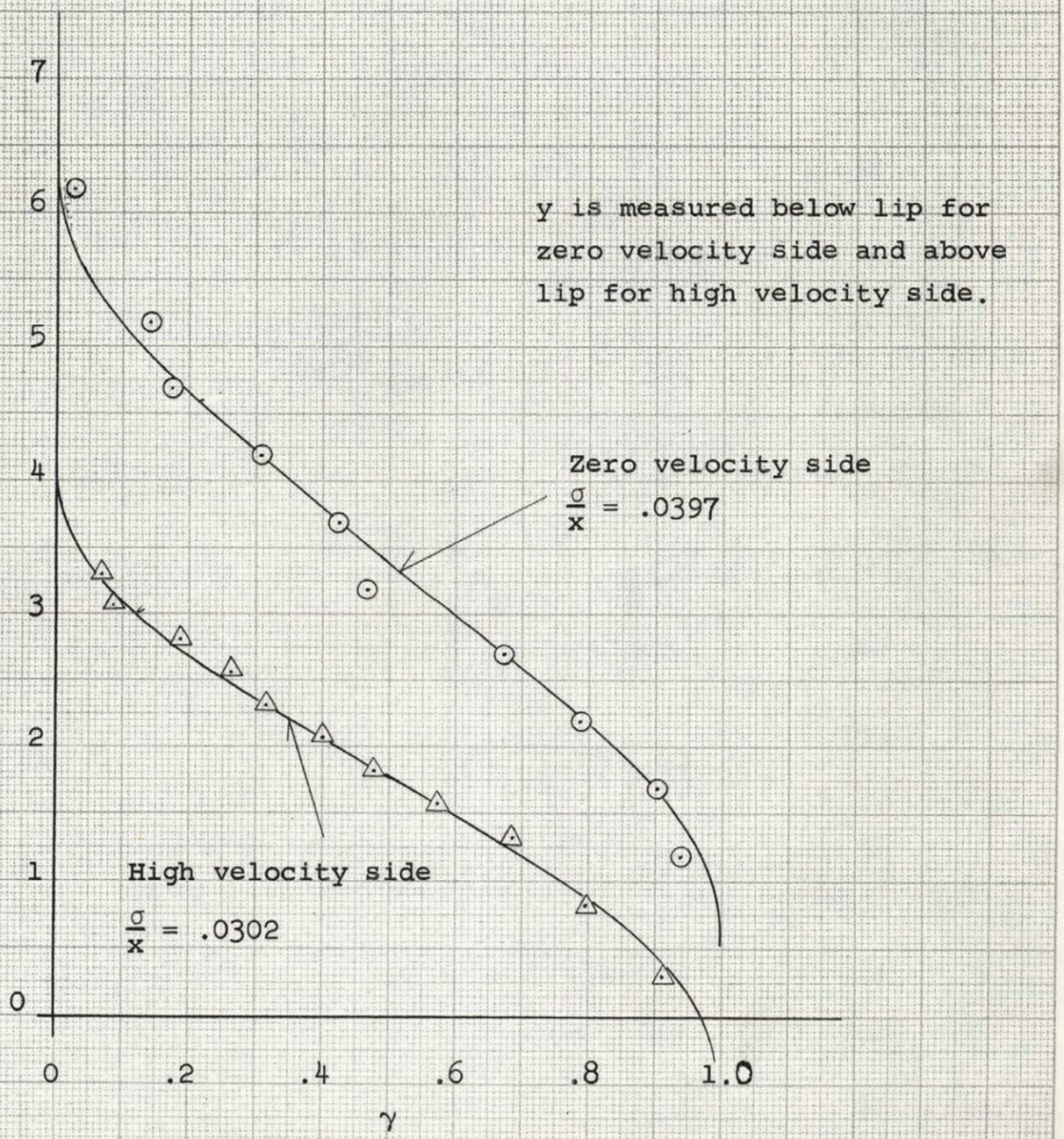

Fig. 15.

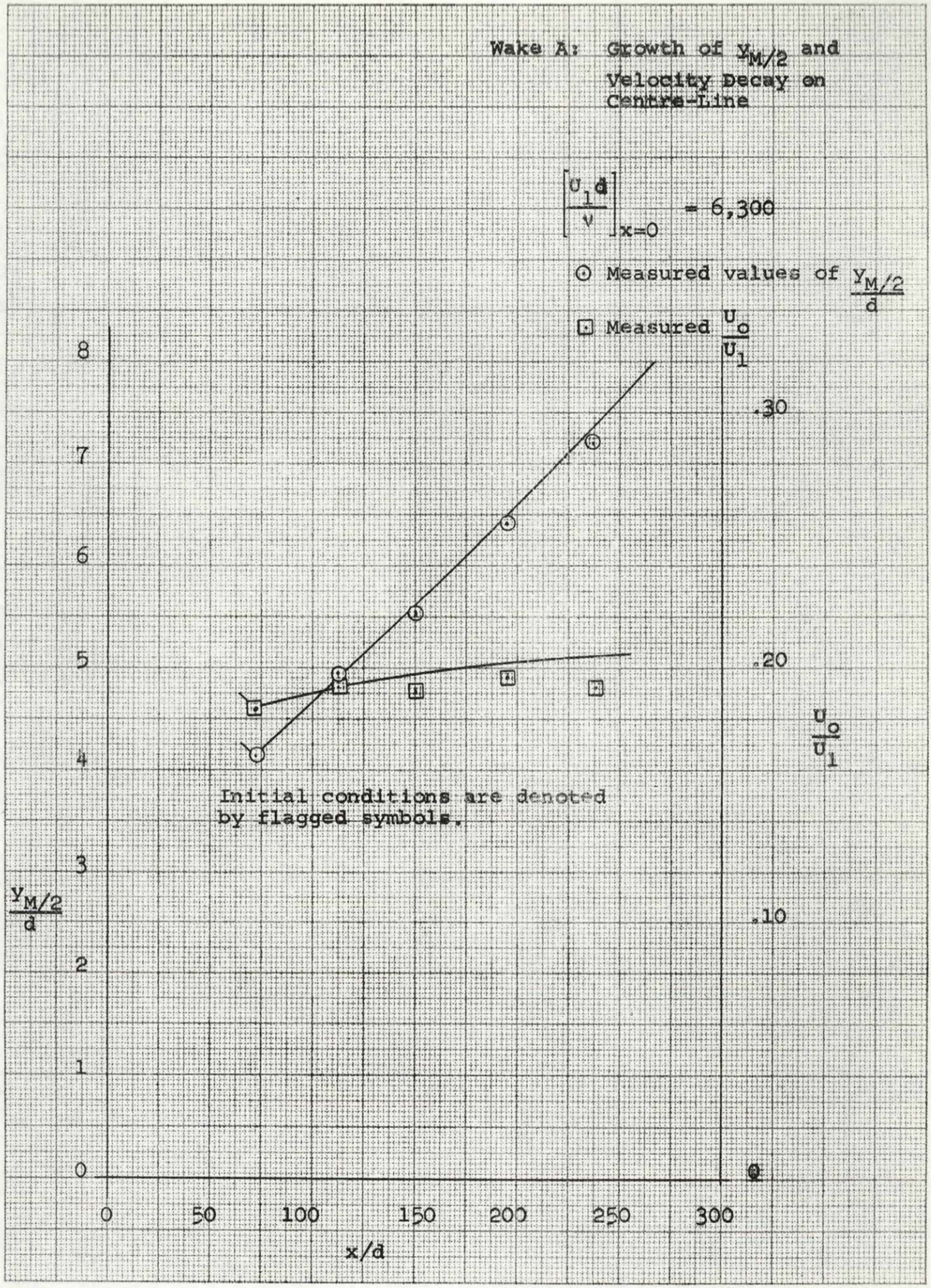
Wake A: Growth of $y_{M/2}$ and Velocity Decay on Centre-Line
$\left[\frac{U_1 d}{\nu}\right]_{x=0} = 6,300$
⊙ Measured values of $\frac{y_{M/2}}{d}$
⊡ Measured $\frac{U_o}{U_1}$
Initial conditions are denoted by flagged symbols.
$\frac{y_{M/2}}{d}$
$\frac{U_o}{U_1}$
0
1
2
3
4
5
6
7
8
.30
.20
.10
0
0
50
100
150
200
250
300
x/d

Fig. 16.

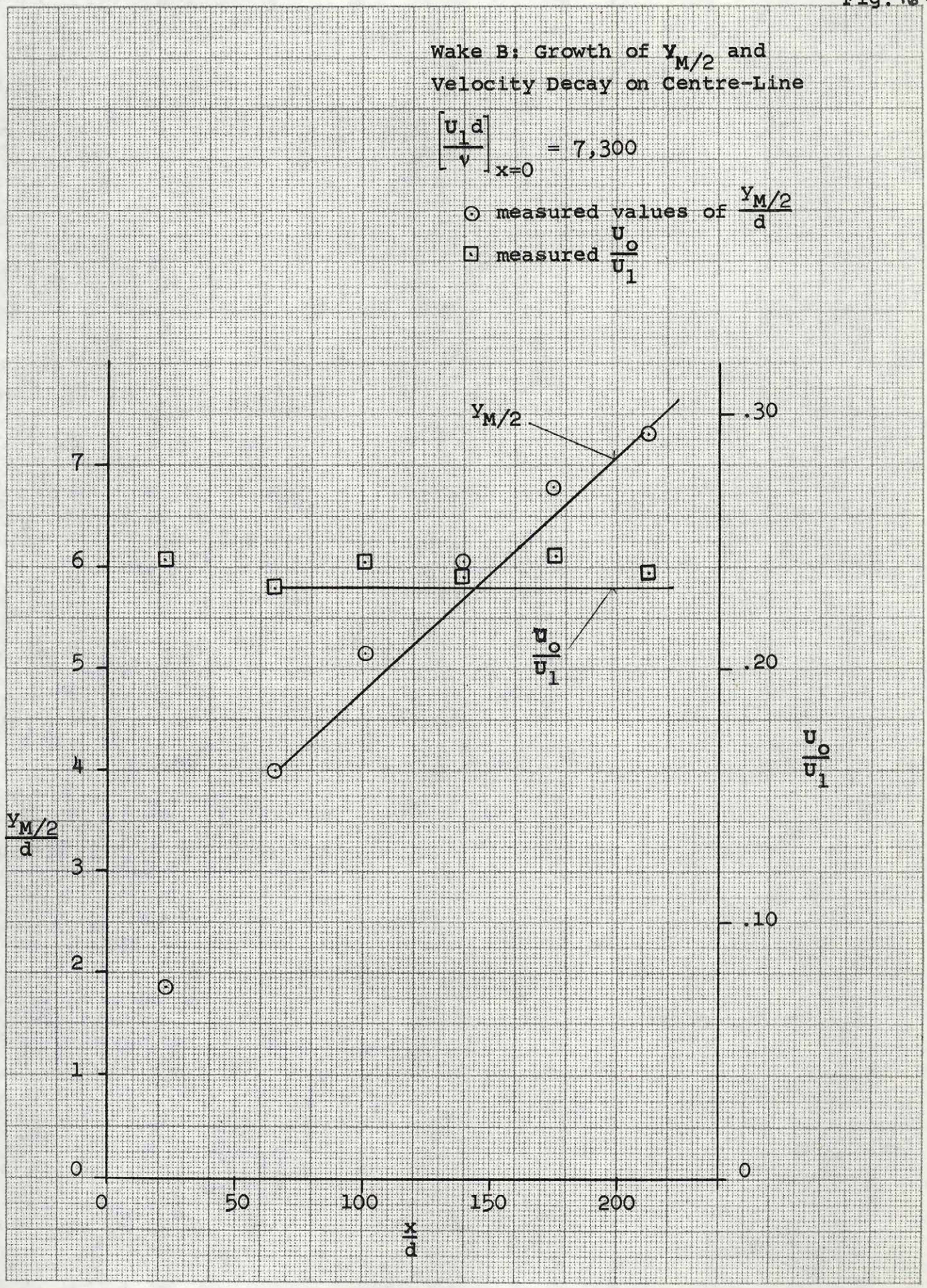
Wake B: Growth of $y_{M/2}$ and Velocity Decay on Centre-Line
$\left[\frac{U_1 d}{\nu}\right]_{x=0} = 7,300$
⊙ measured values of $\frac{y_{M/2}}{d}$
⊡ measured $\frac{U_o}{U_1}$
$y_{M/2}$
$\frac{U_o}{U_1}$
$\frac{y_{M/2}}{d}$
$\frac{U_o}{U_1}$
0
1
2
3
4
5
6
7
.30
.20
.10
0
0
50
100
150
200
$\frac{x}{d}$

Fig. 17.

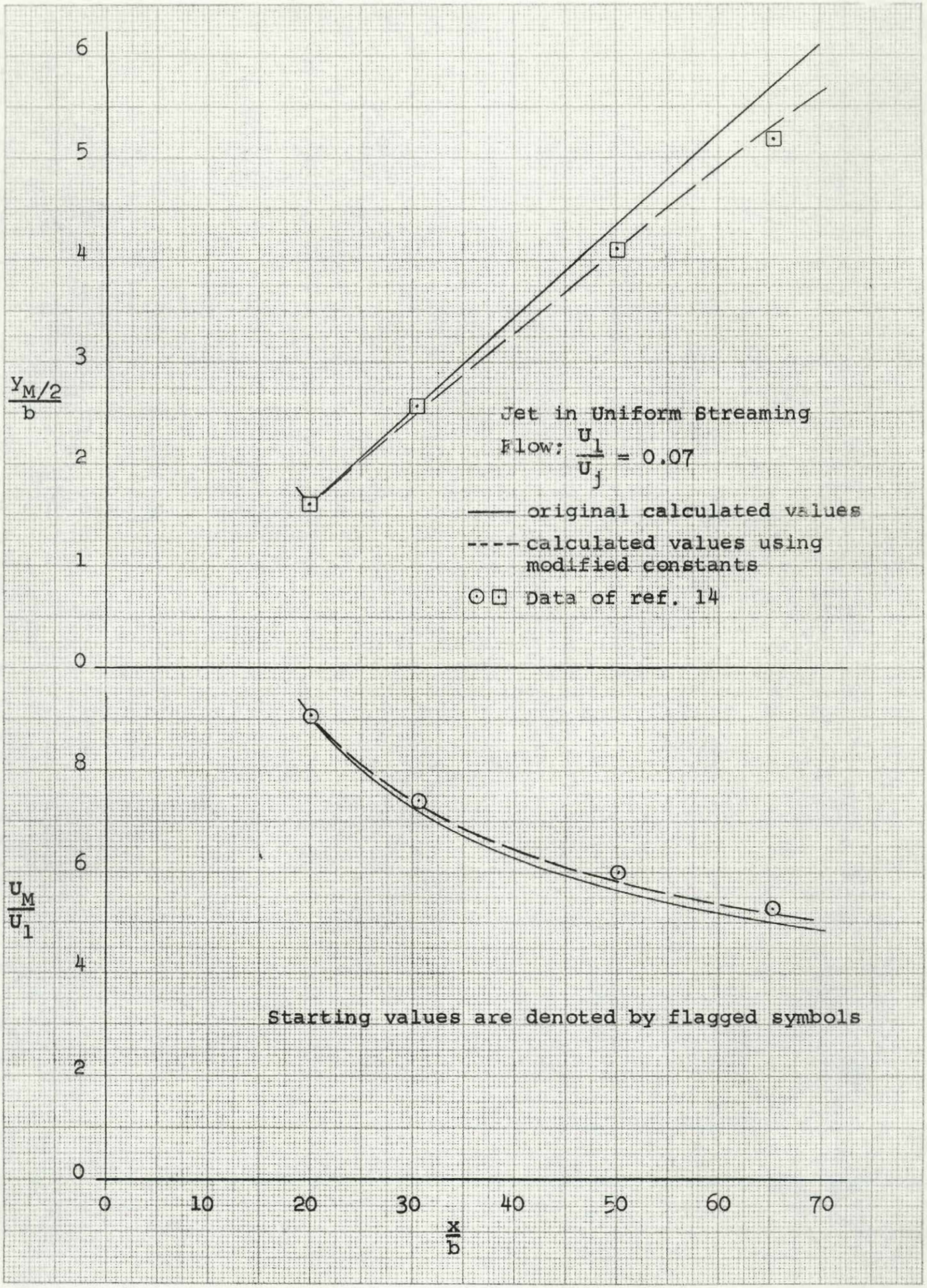
6
5
4
3
2
1
0
$\frac{y_{M/2}}{b}$
Jet in Uniform Streaming Flow: $\frac{U_1}{U_j} = 0.07$
—— original calculated values
---- calculated values using modified constants
⊙⊡ Data of ref. 14
8
6
4
2
0
$\frac{U_M}{U_1}$
Starting values are denoted by flagged symbols
0
10
20
30
40
50
60
70
$\frac{x}{b}$

Fig. 8.

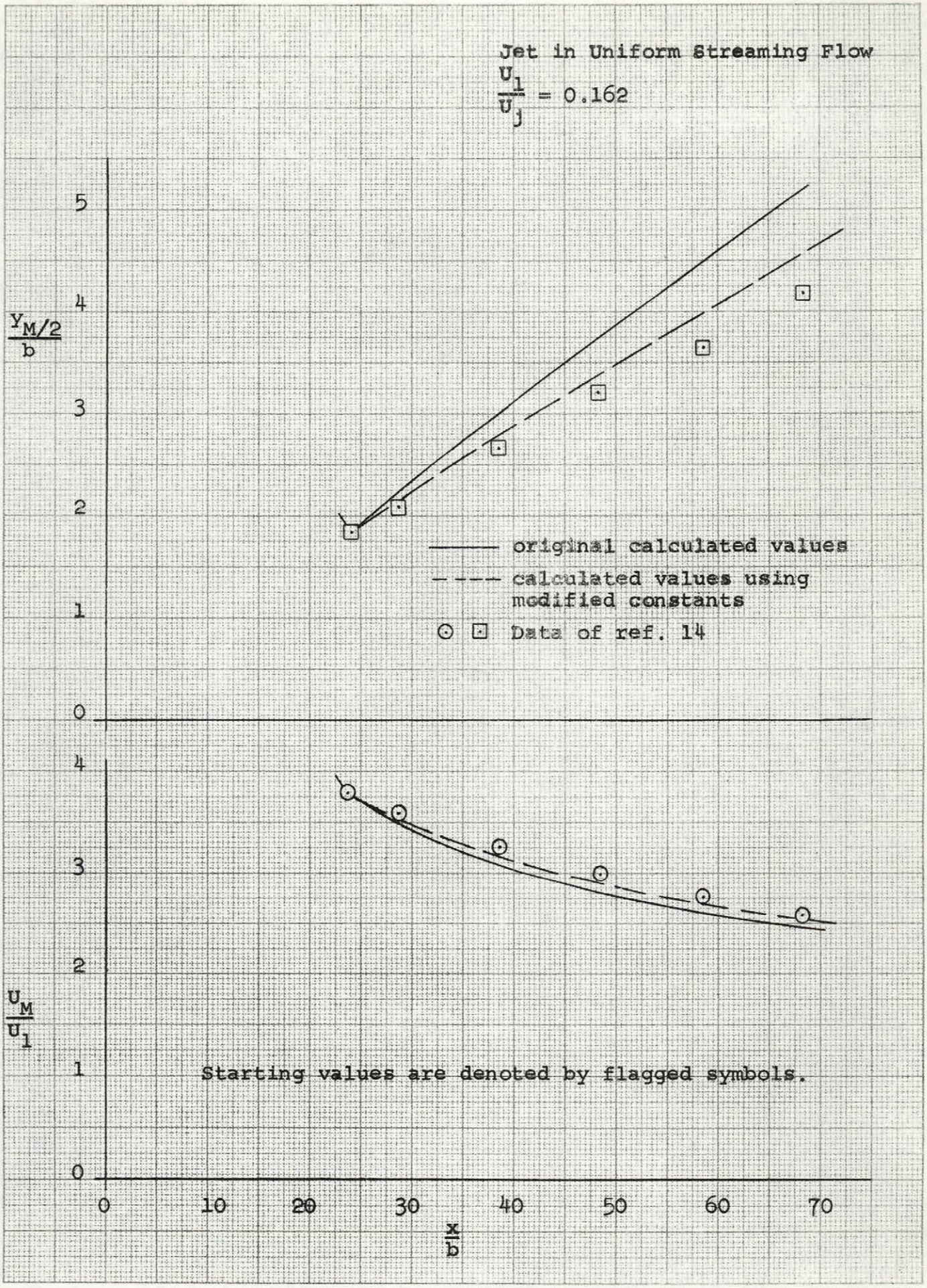
Jet in Uniform Streaming Flow
$\frac{U_1}{U_j} = 0.162$
$\frac{Y_{M/2}}{b}$
5
4
3
2
1
0
original calculated values
calculated values using modified constants
Data of ref. 14
$\frac{U_M}{U_1}$
4
3
2
1
0
Starting values are denoted by flagged symbols.
0
10
20
30
40
50
60
70
$\frac{x}{b}$

Fig. 19.

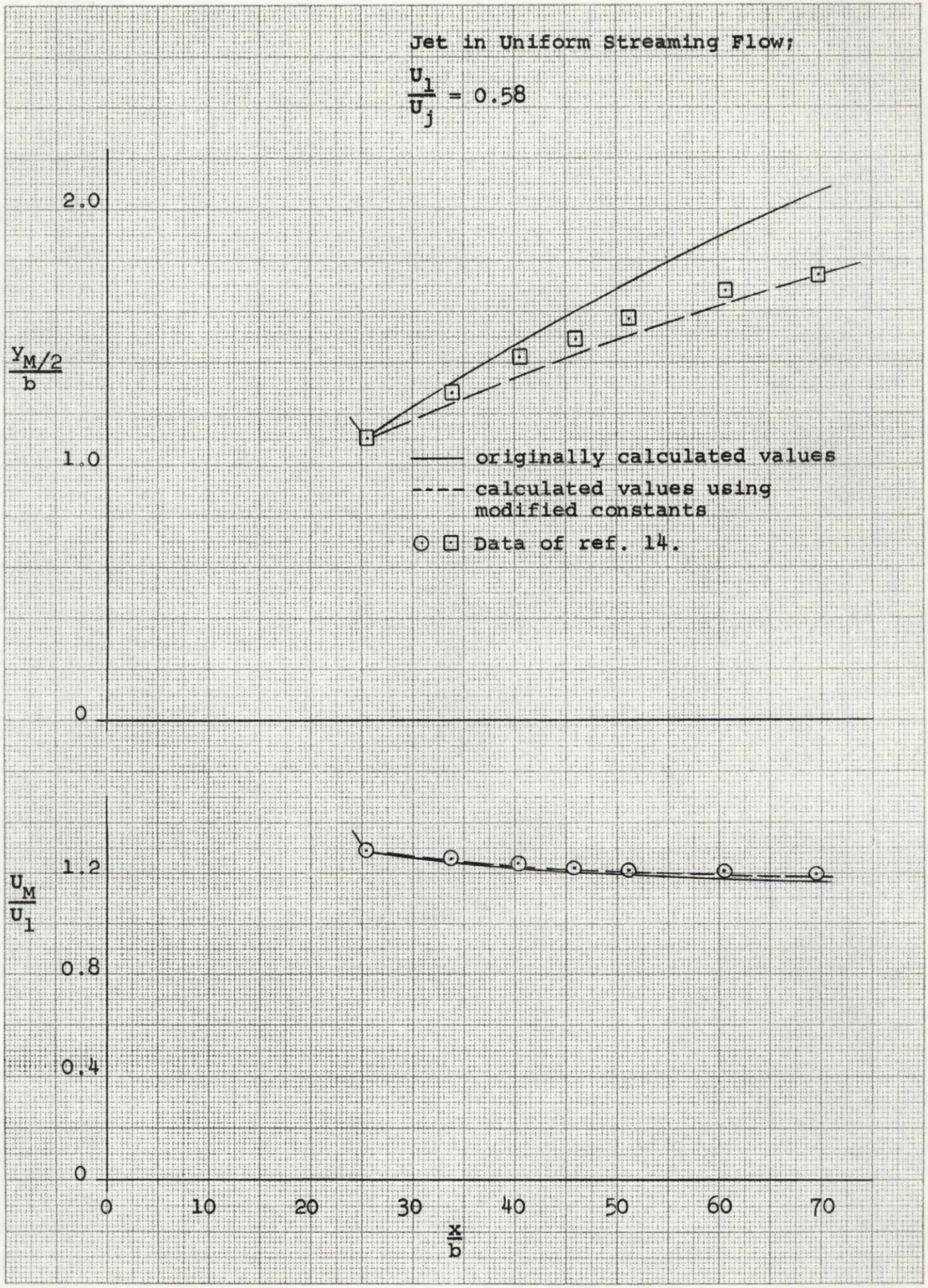
Jet in Uniform Streaming Flow;
$\frac{U_1}{U_j} = 0.58$
$\frac{y_{M/2}}{b}$
2.0
1.0
0
originally calculated values
calculated values using modified constants
Data of ref. 14.
$\frac{U_M}{U_1}$
1.2
0.8
0.4
0
0
10
20
30
40
50
60
70
$\frac{x}{b}$

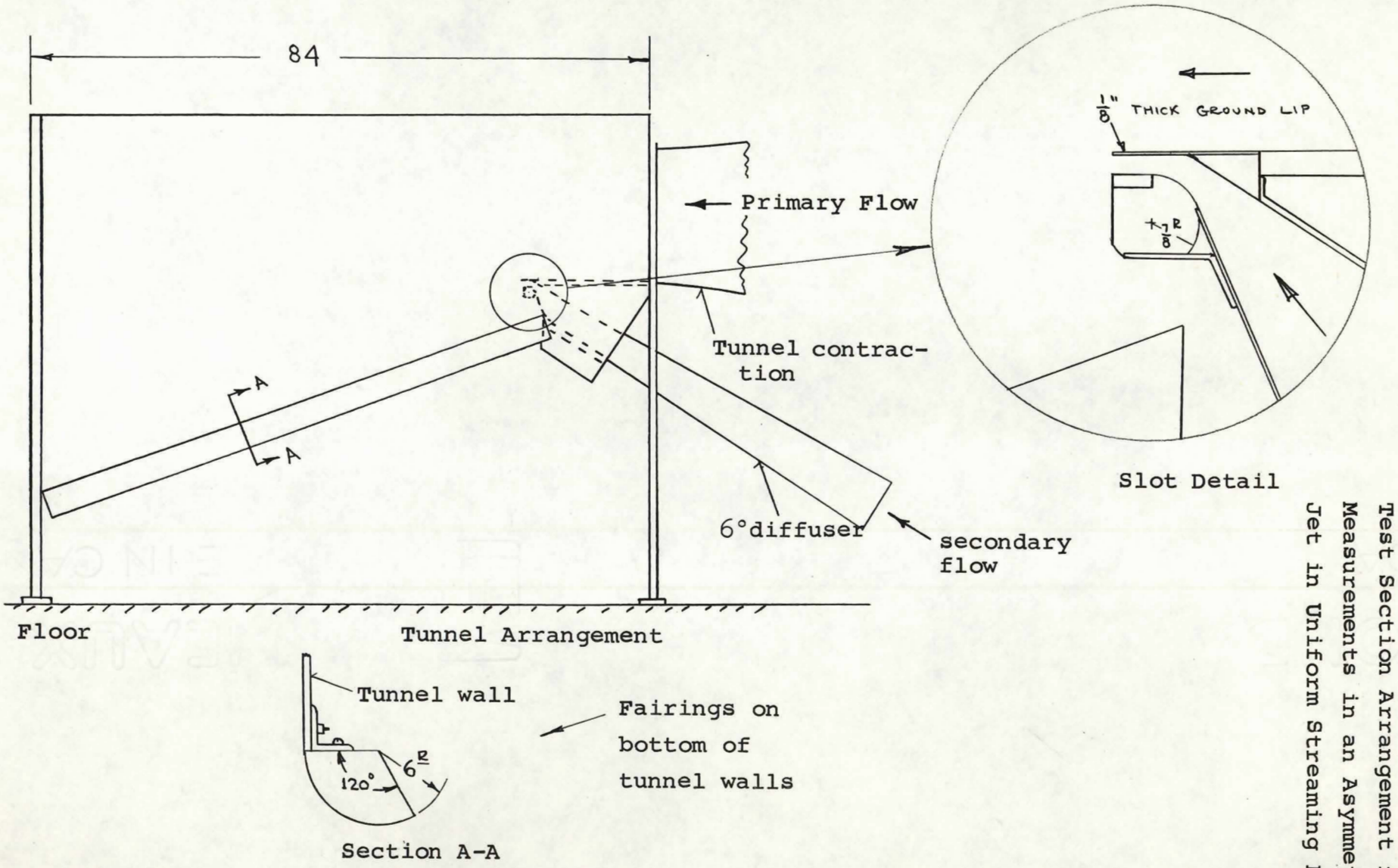

Fig.20

Test Section Arrangement for Measurements in an Asymmetric Jet in Uniform Streaming Flow.

Fig. 21

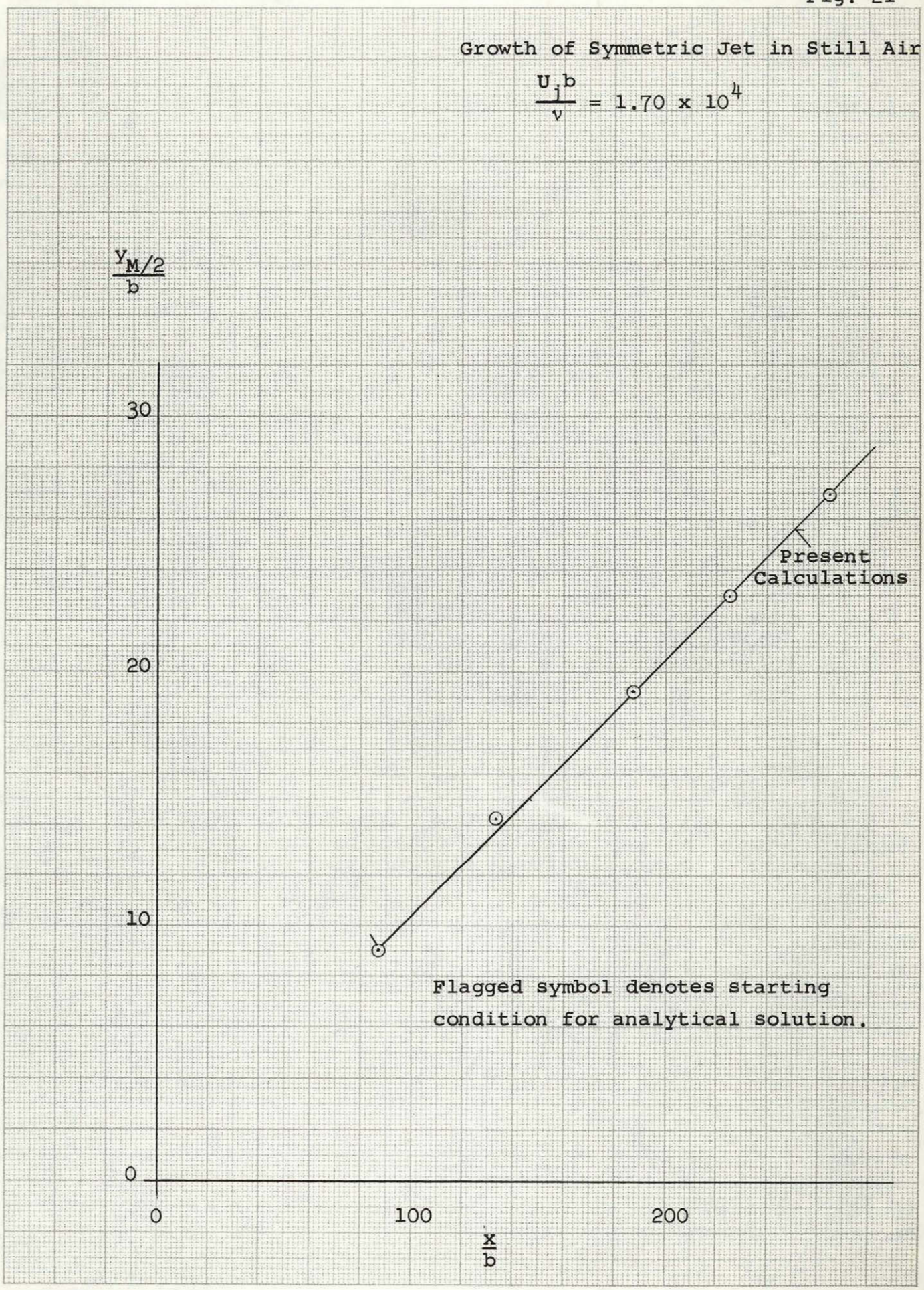
Growth of Symmetric Jet in Still Air
$\frac{U_j b}{\nu} = 1.70 \times 10^4$
$\frac{y_{M/2}}{b}$
30
20
10
0
0
100
200
$\frac{x}{b}$
Present Calculations
Flagged symbol denotes starting condition for analytical solution.

Fig. 22

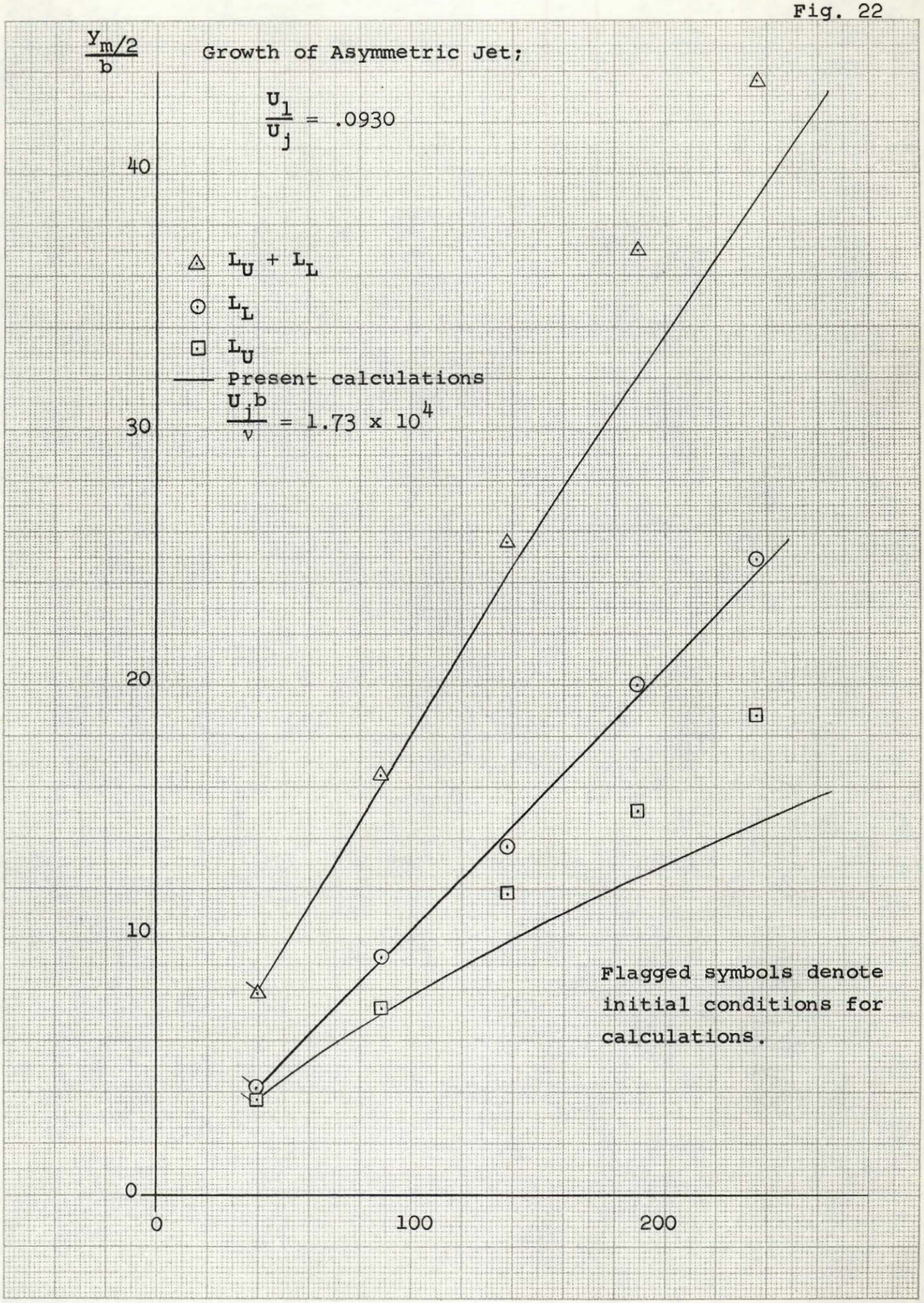
$\frac{y_{m/2}}{b}$
Growth of Asymmetric Jet;
$\frac{U_1}{U_j} = .0930$
40
30
20
10
0
0
100
200
$L_U + L_L$
L_L
L_U
Present calculations
$\frac{U_j b}{\nu} = 1.73 \times 10^4$
Flagged symbols denote initial conditions for calculations.

Fig. 23

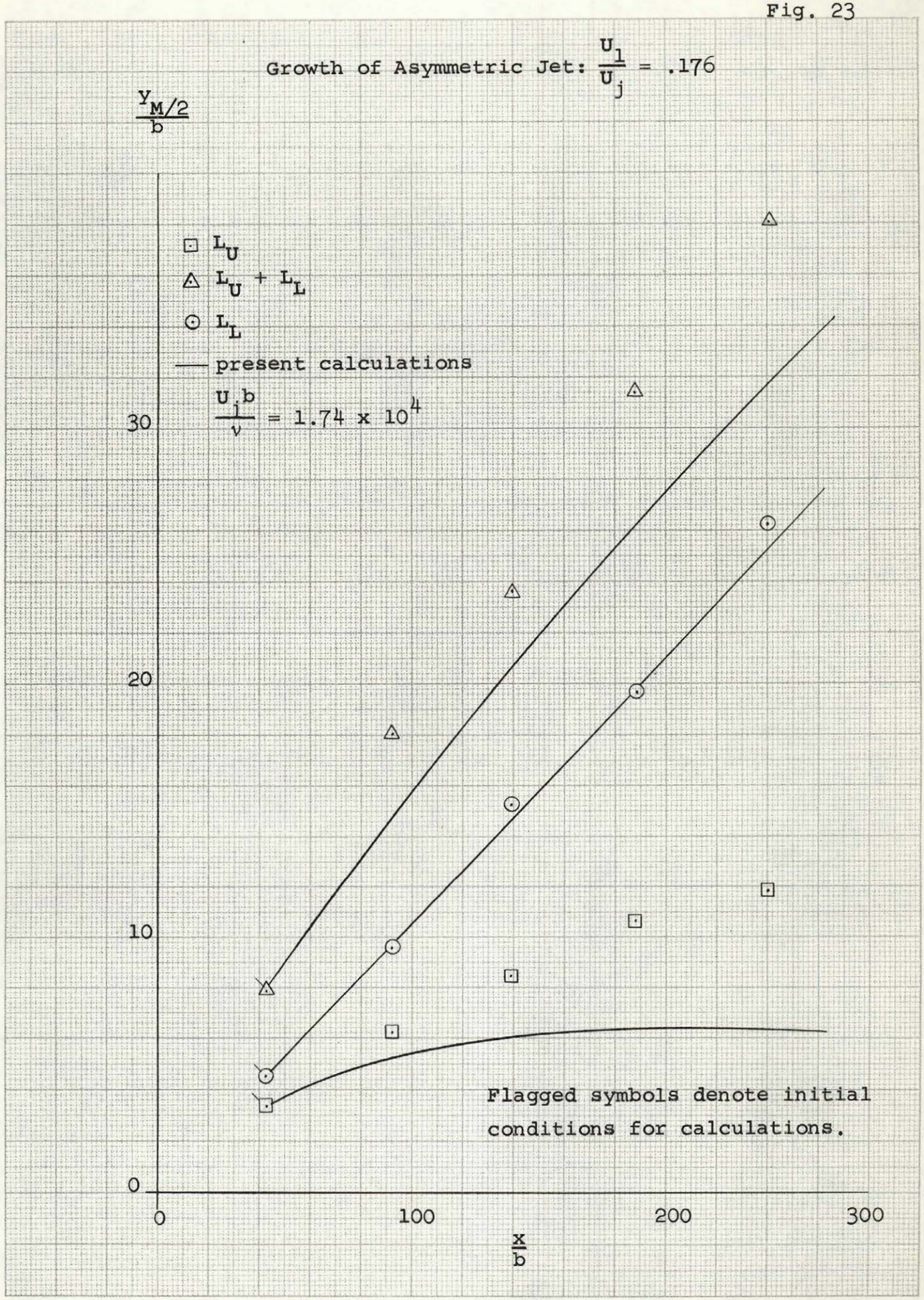
Growth of Asymmetric Jet: $\frac{U_1}{U_j} = .176$
$\frac{y_{M/2}}{b}$
L_U
$L_U + L_L$
L_L
present calculations
$\frac{U_j b}{\nu} = 1.74 \times 10^4$
30
20
10
0
0
100
200
300
$\frac{x}{b}$
Flagged symbols denote initial conditions for calculations.

Fig. 24

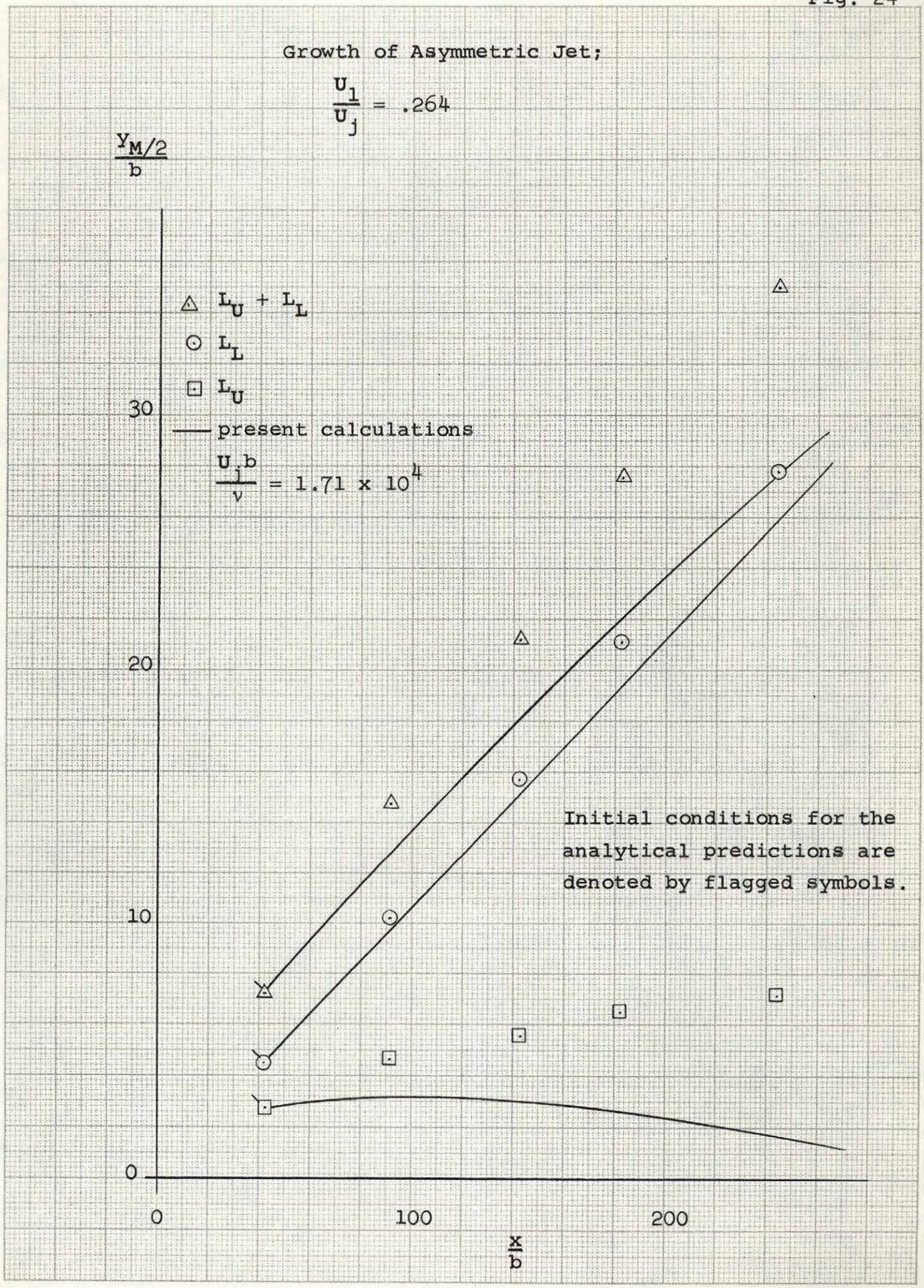
Growth of Asymmetric Jet;
$\frac{U_1}{U_j} = .264$
$\frac{Y_{M/2}}{b}$
$L_U + L_L$
L_L
L_U
present calculations
$\frac{U_j b}{\nu} = 1.71 \times 10^4$
30
20
10
0
0
100
200
$\frac{x}{b}$
Initial conditions for the analytical predictions are denoted by flagged symbols.

Fig. 25

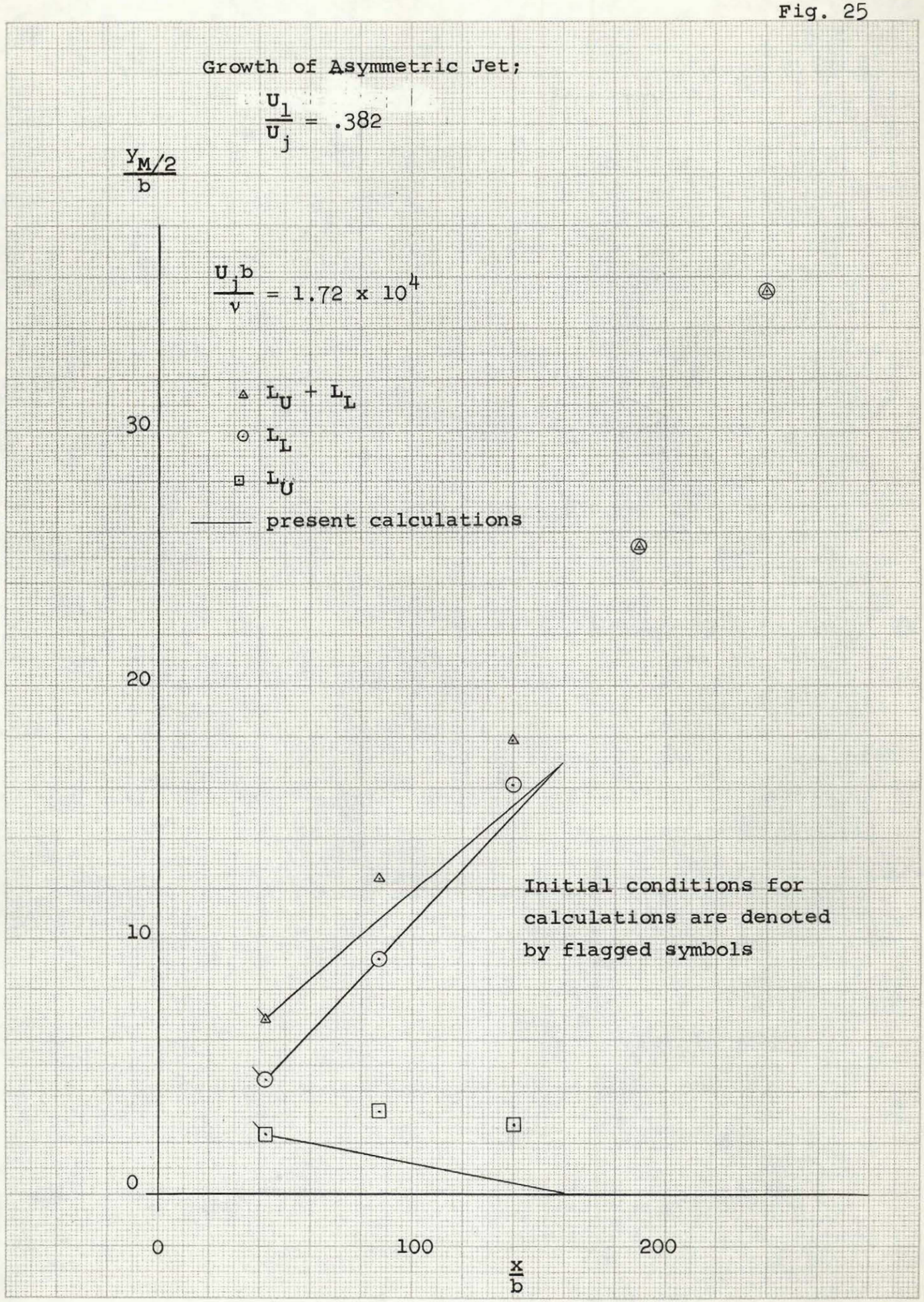
Growth of Asymmetric Jet;
$\frac{U_1}{U_j} = .382$
$\frac{y_{M/2}}{b}$
$\frac{U_j b}{\nu} = 1.72 \times 10^4$
$L_U + L_L$
L_L
L_U
present calculations
30
20
10
0
0
100
200
$\frac{x}{b}$
Initial conditions for calculations are denoted by flagged symbols

Fig. 26

Maximum Velocity Decay for
Asymmetric Jets and Jet in Still Air

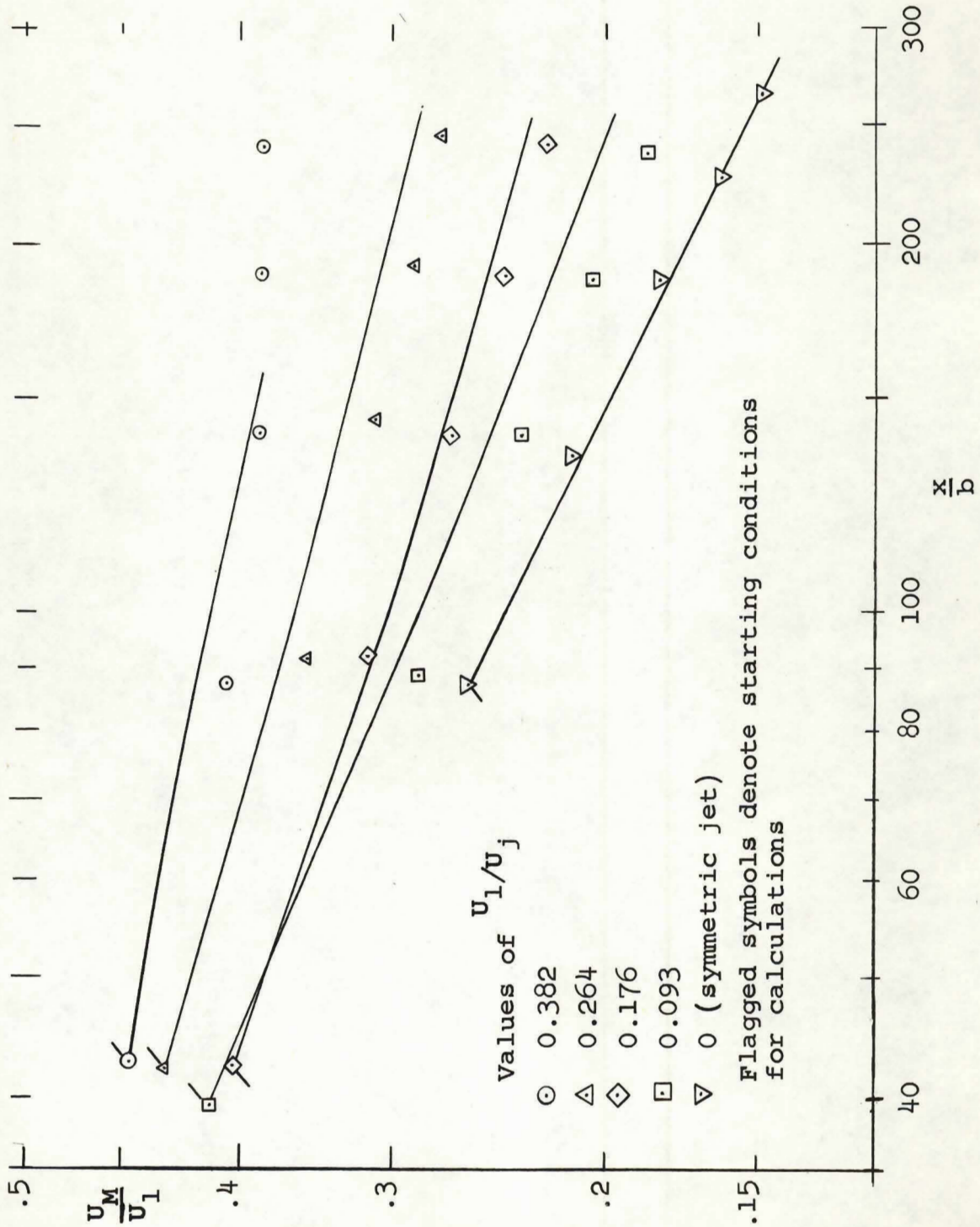

Fig. 27

Streamwise Development of a Plane Mixing Layer

$\frac{U_1}{\nu} = 40.2 \times 10^4 \ FT^{-1}$

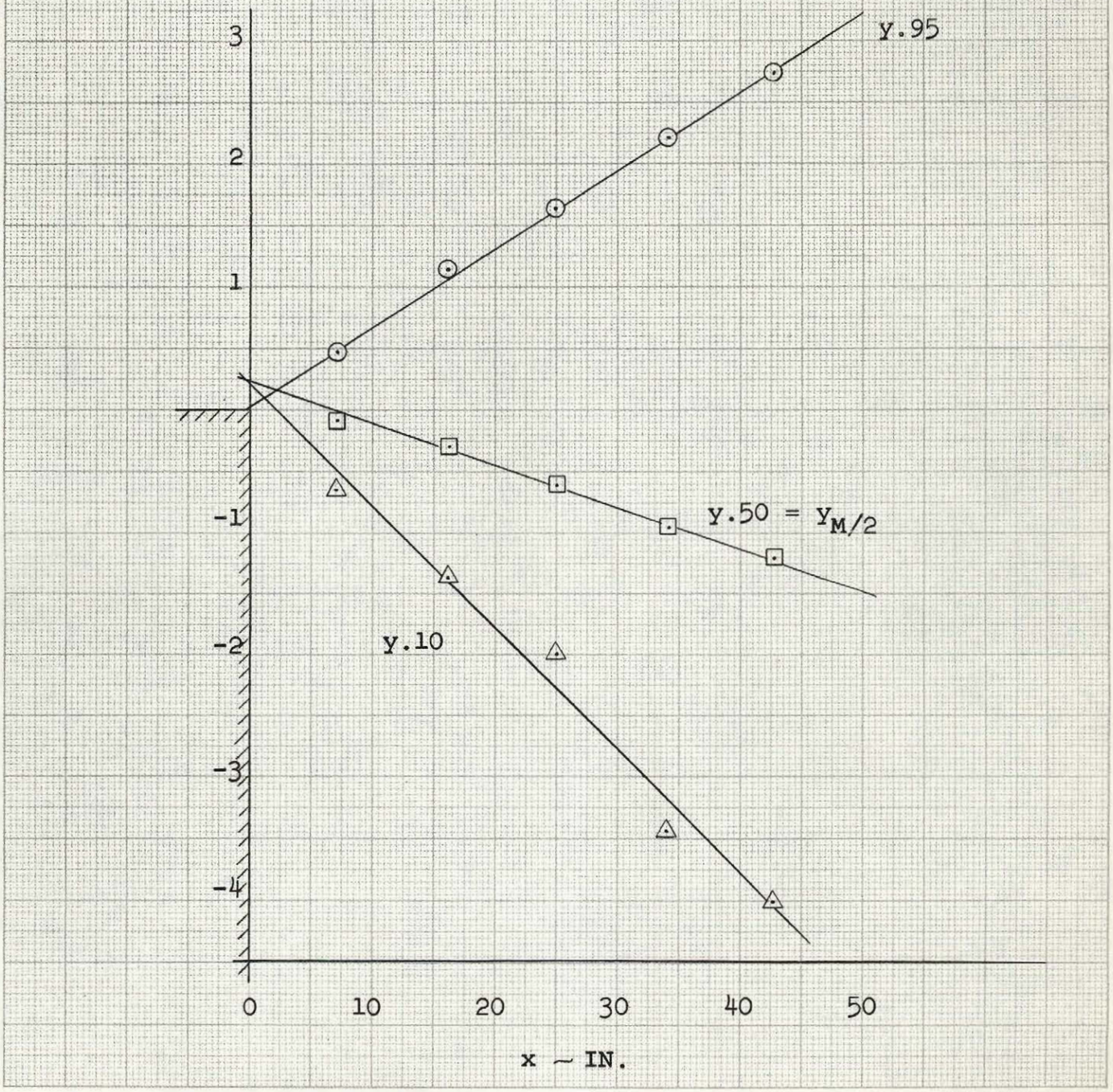

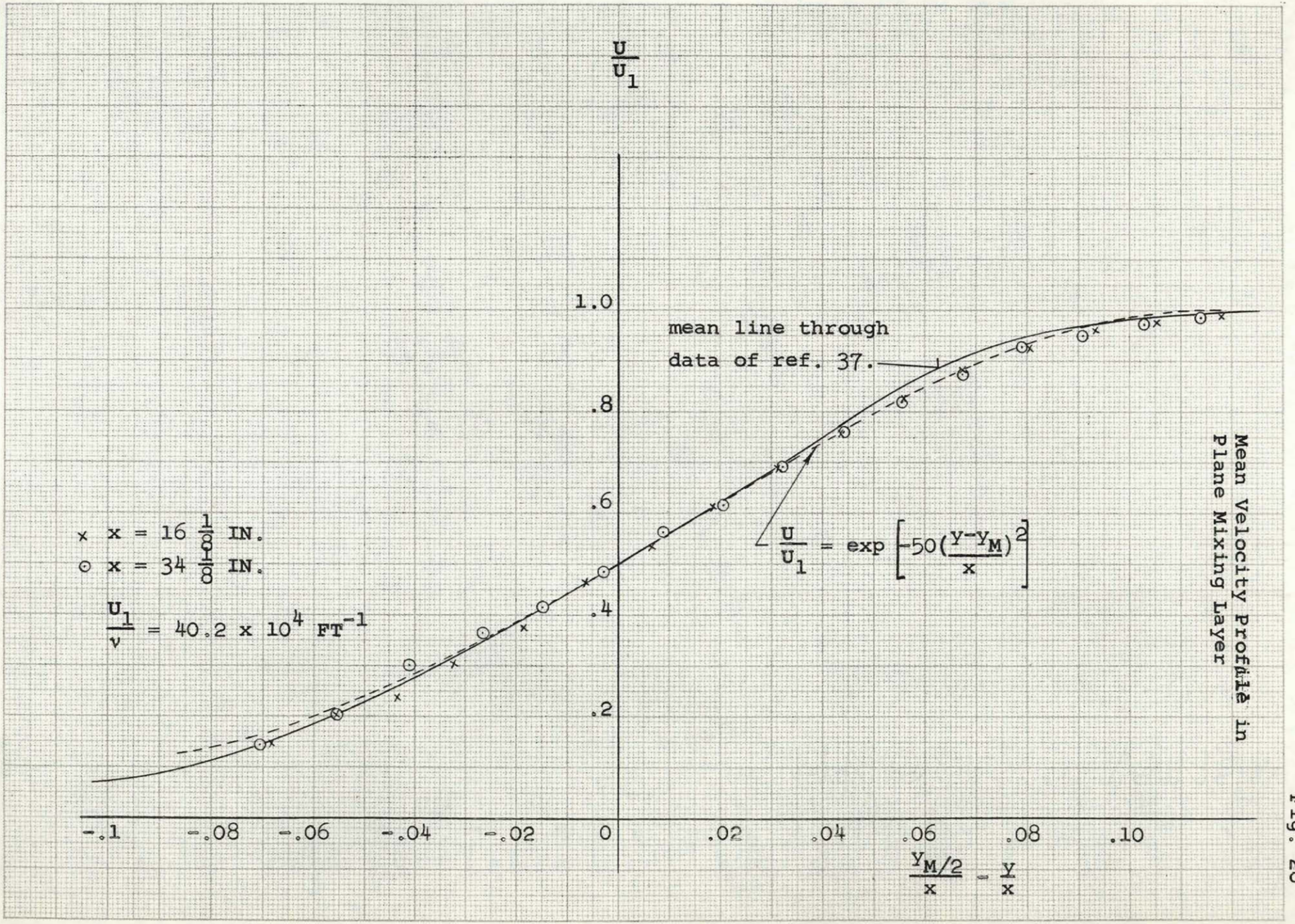

Mean Velocity Profile in Plane Mixing Layer

Fig. 28

Fig. 29

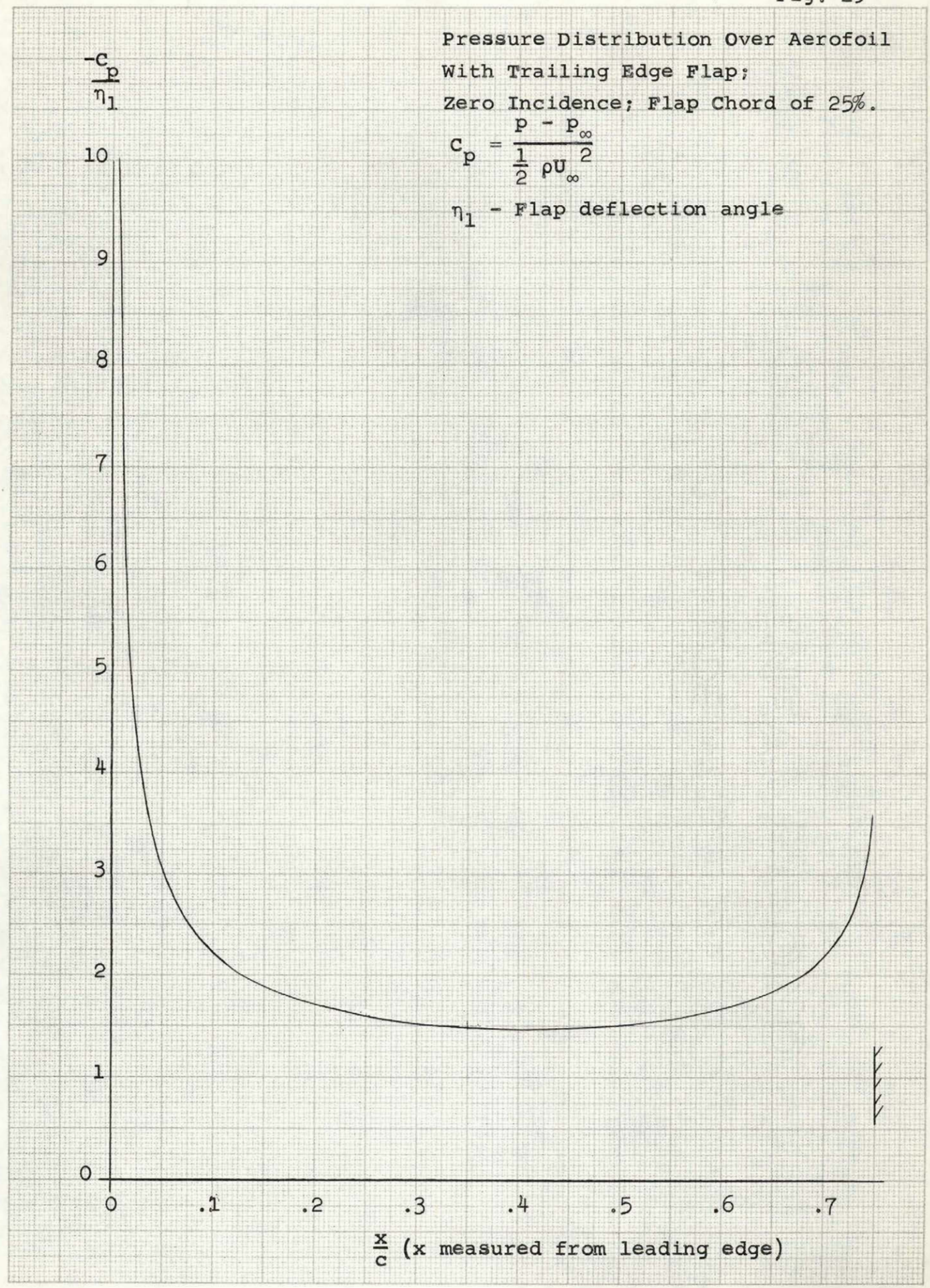
Pressure Distribution Over Aerofoil
With Trailing Edge Flap;
Zero Incidence; Flap Chord of 25%.
$C_p = \frac{p - p_\infty}{\frac{1}{2}\rho U_\infty^2}$
η_1 - Flap deflection angle
$\frac{-C_p}{\eta_1}$
10
9
8
7
6
5
4
3
2
1
0
0
.1
.2
.3
.4
.5
.6
.7
$\frac{x}{c}$ (x measured from leading edge)

Fig. 30

Pressure Distribution Over Trailing Edge Flap

Zero Angle of Attack of Main Chord;

Flap Chord 25%.

$$C_p = \frac{p - p_\infty}{\frac{1}{2}\rho U_\infty^2}$$

η_1 - Flap deflection angle.

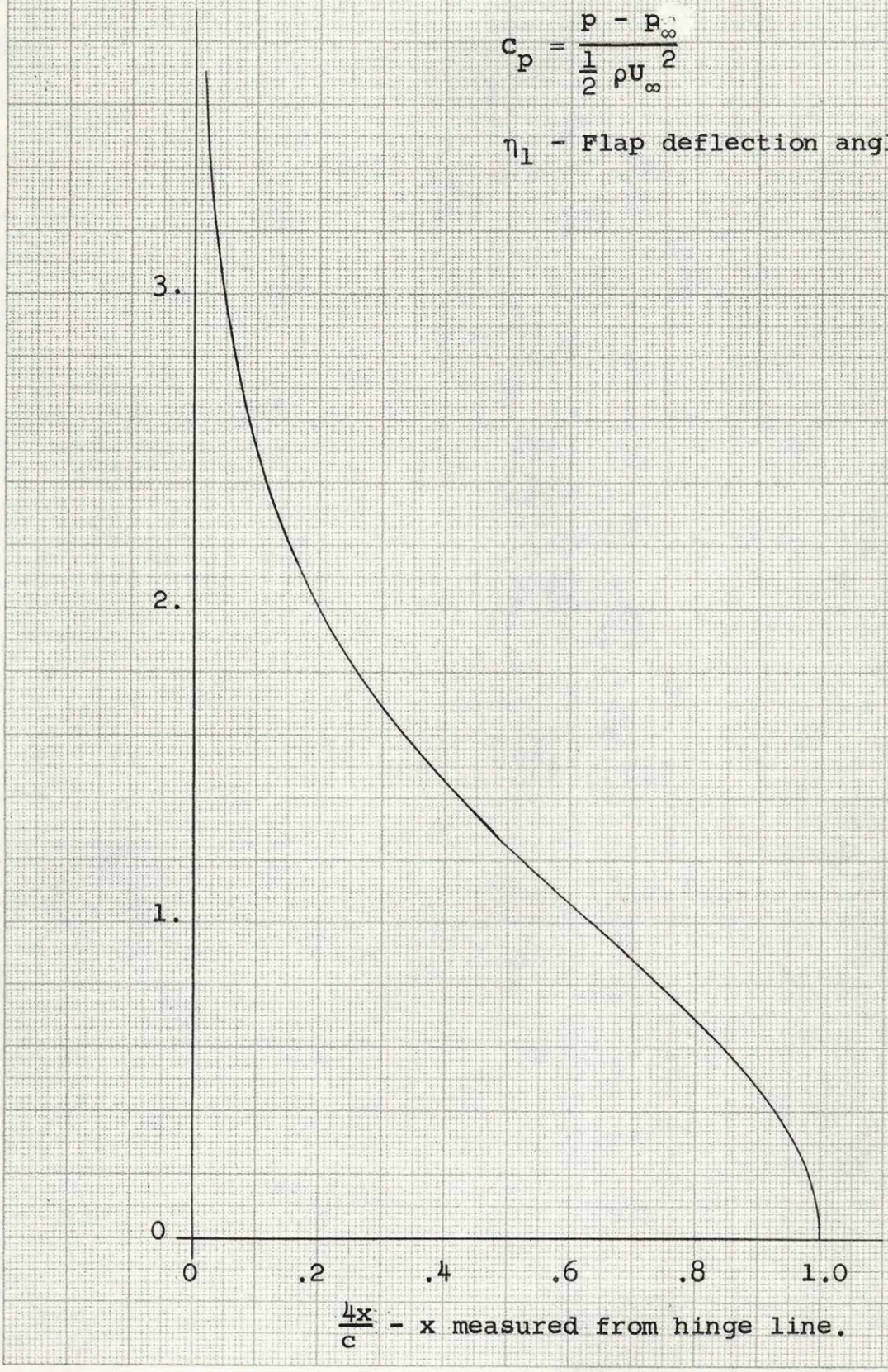

Fig. 31

Initial Conditions at the slot for

$\frac{U_1}{U_j} = 0.5$

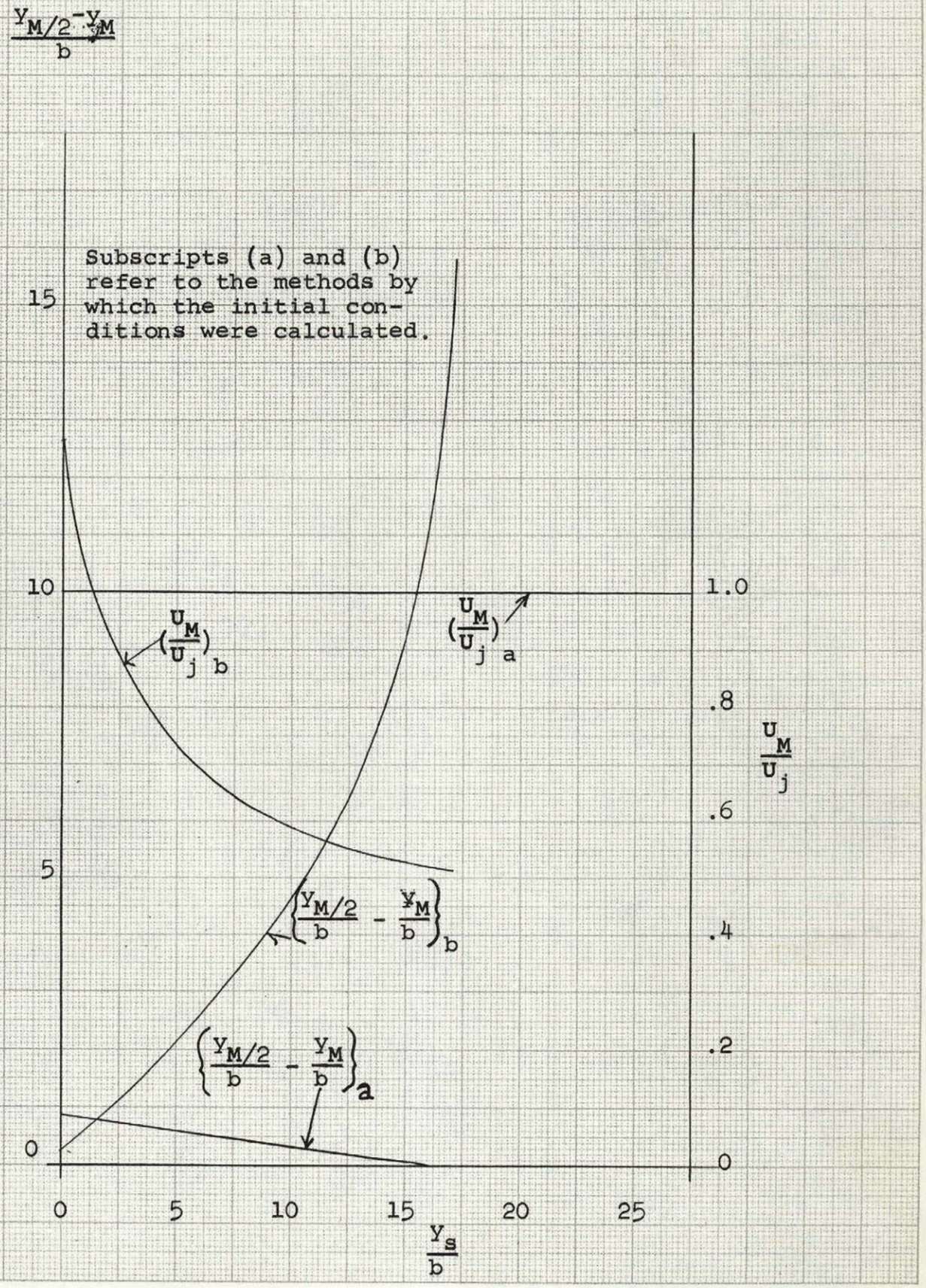

Fig. 32

Shape Factor H in a Boundary Layer Without Blowing; Leading Edge of Flapped Aerofoil.

$\alpha = 0°$, $\eta = 60°$, no upstream boundary layer, $R_e = 5 \times 10^6$.

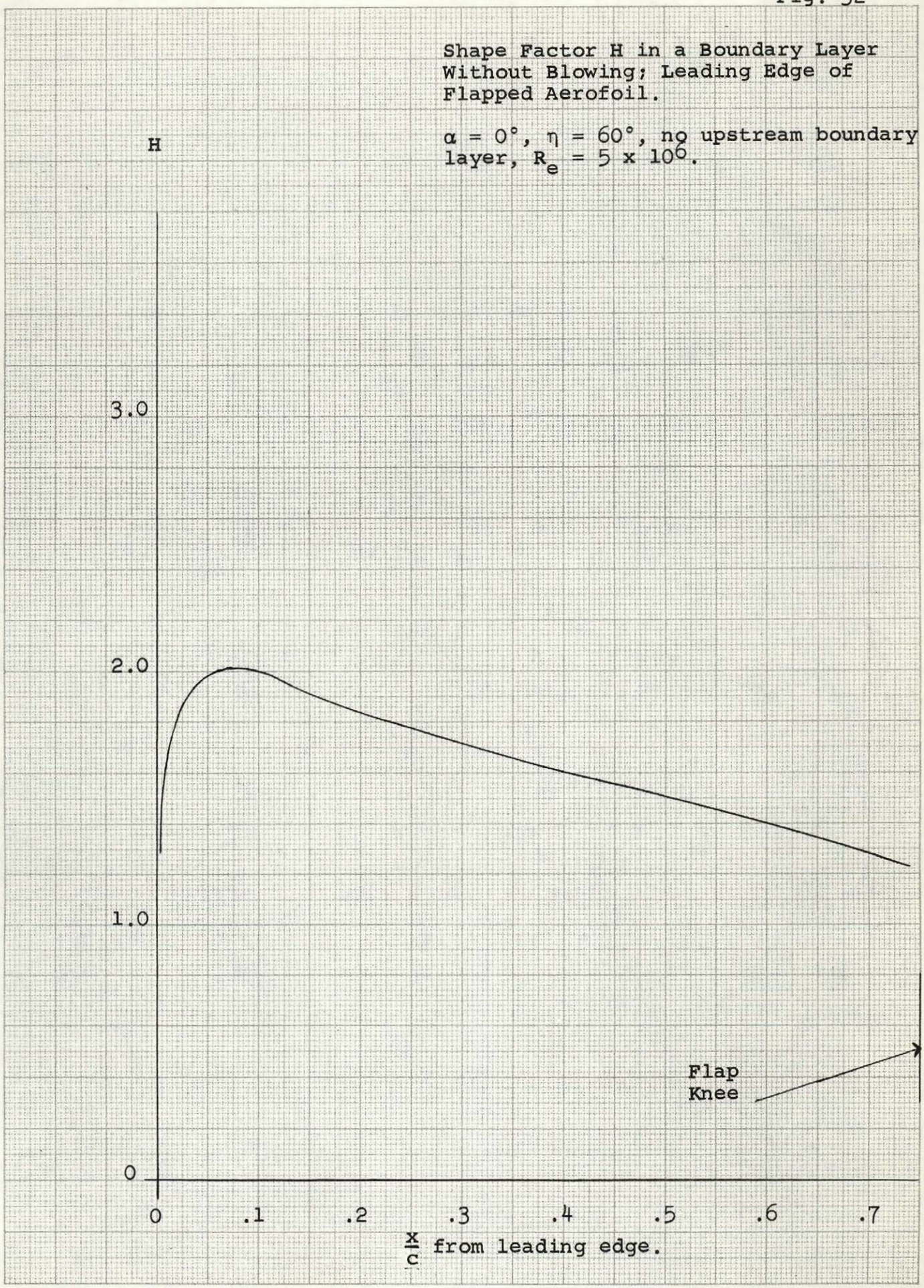

Fig. 33

Critical Values of C_μ for Various Flap Deflection Angles.

$$\frac{c}{b} = 2000, \quad R_e = \frac{U_\infty c}{\nu} = 5 \times 10^6$$

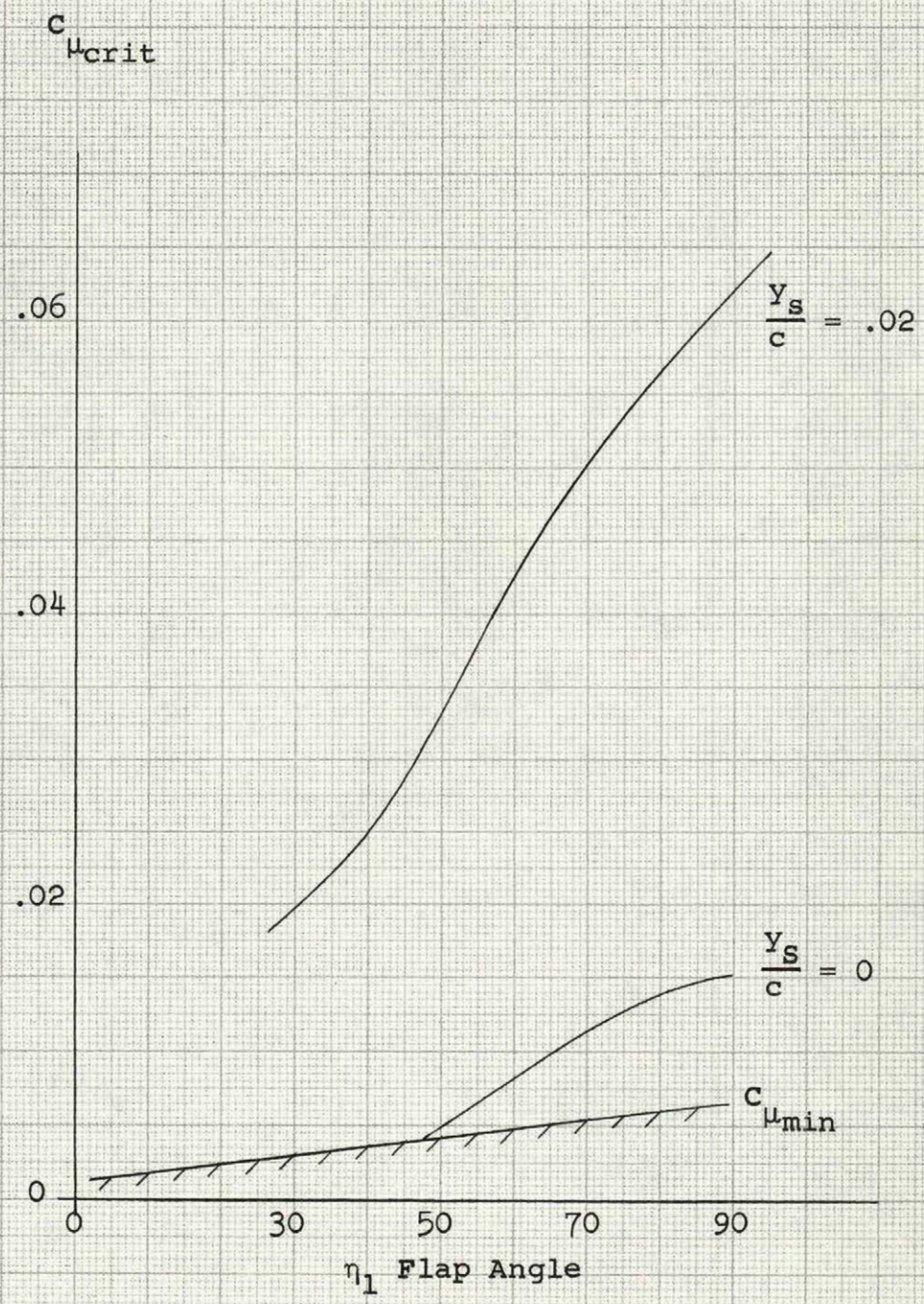

Fig. 34

Shape Factor H in a Boundary Layer Without Blowing; Trailing Edge Flap.

$\alpha = 0°$, $\eta_1 = 60°$, No upstream Boundary layer, $R_e = 10^6$.

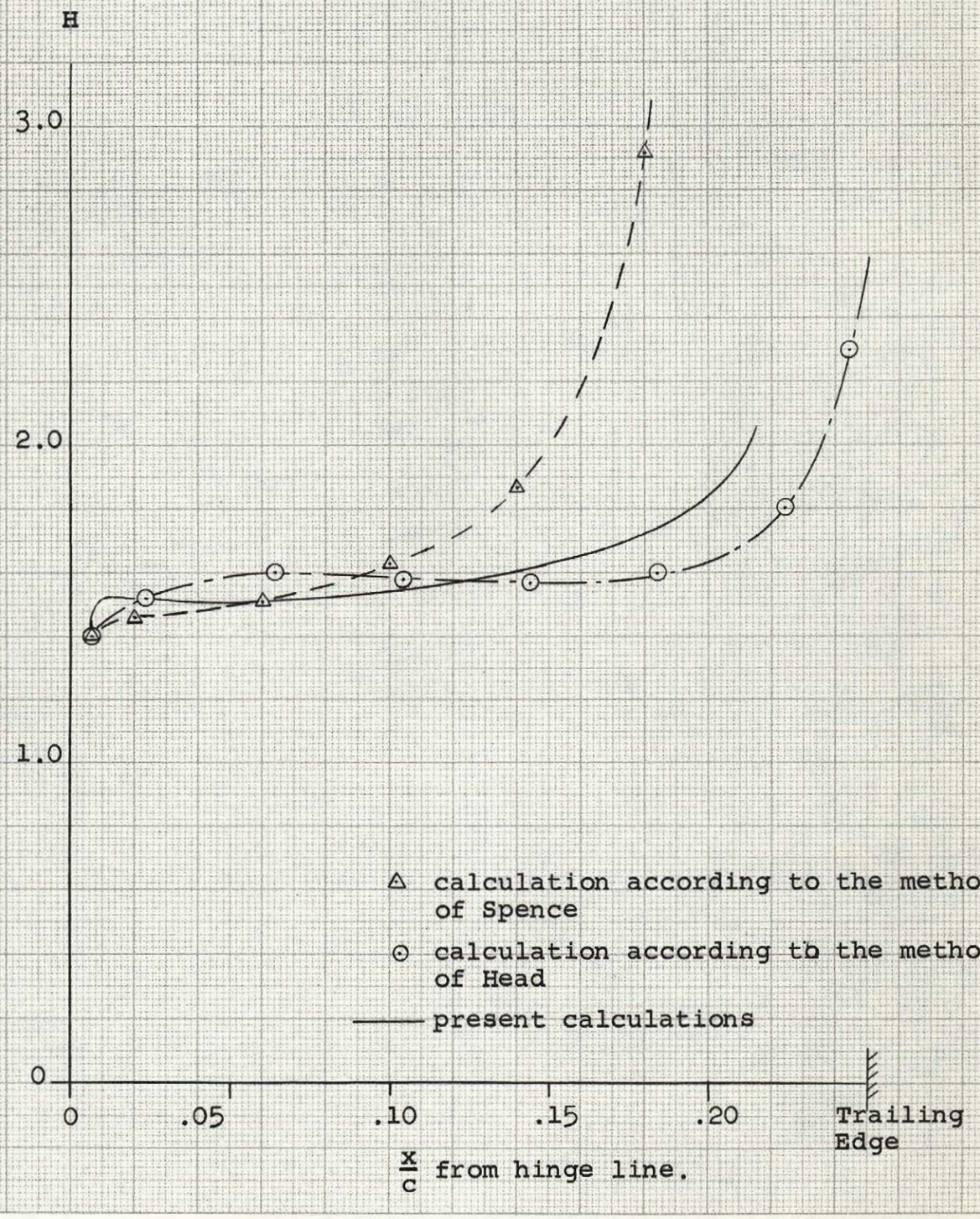

Fig. 35

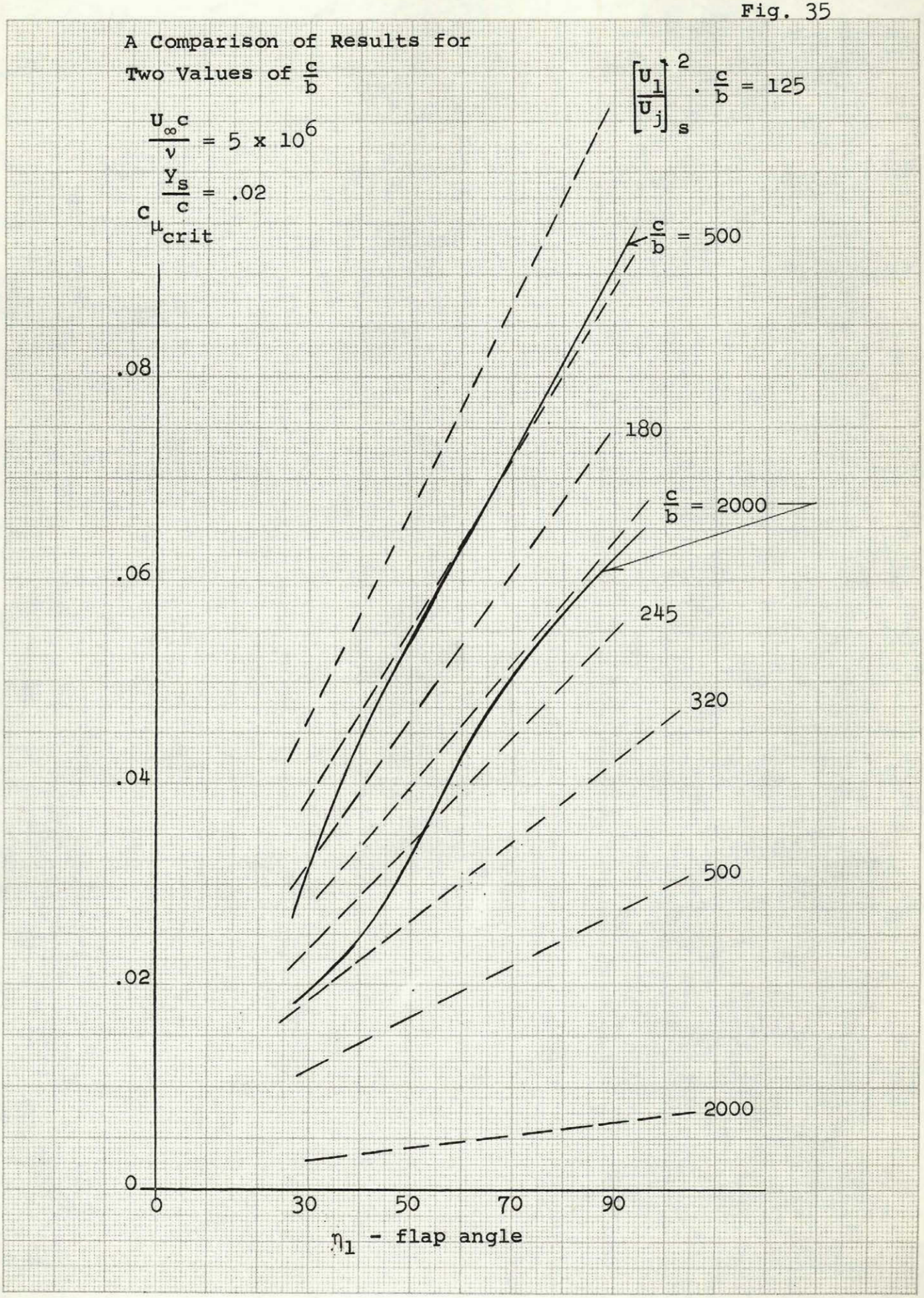
A Comparison of Results for
Two Values of $\frac{c}{b}$
$\frac{U_\infty c}{\nu} = 5 \times 10^6$
$\frac{y_s}{c} = .02$
$C_{\mu_{crit}}$
$\left[\frac{U_1}{U_j}\right]_s^2 \cdot \frac{c}{b} = 125$
$\frac{c}{b} = 500$
180
$\frac{c}{b} = 2000$
245
320
500
2000
.08
.06
.04
.02
0
0
30
50
70
90
η_1 - flap angle

Fig. 36

A Comparison of Results for Two Values of $\frac{c}{b}$ using Kelly's modified coefficient C'_μ.

$$\frac{U_\infty c}{\nu} = 5 \times 10^6$$

$$C'_\mu = C_\mu \left(1 - \left[\frac{U_1}{U_j}\right]_s\right);$$

$$\frac{Y_s}{c} = .02$$

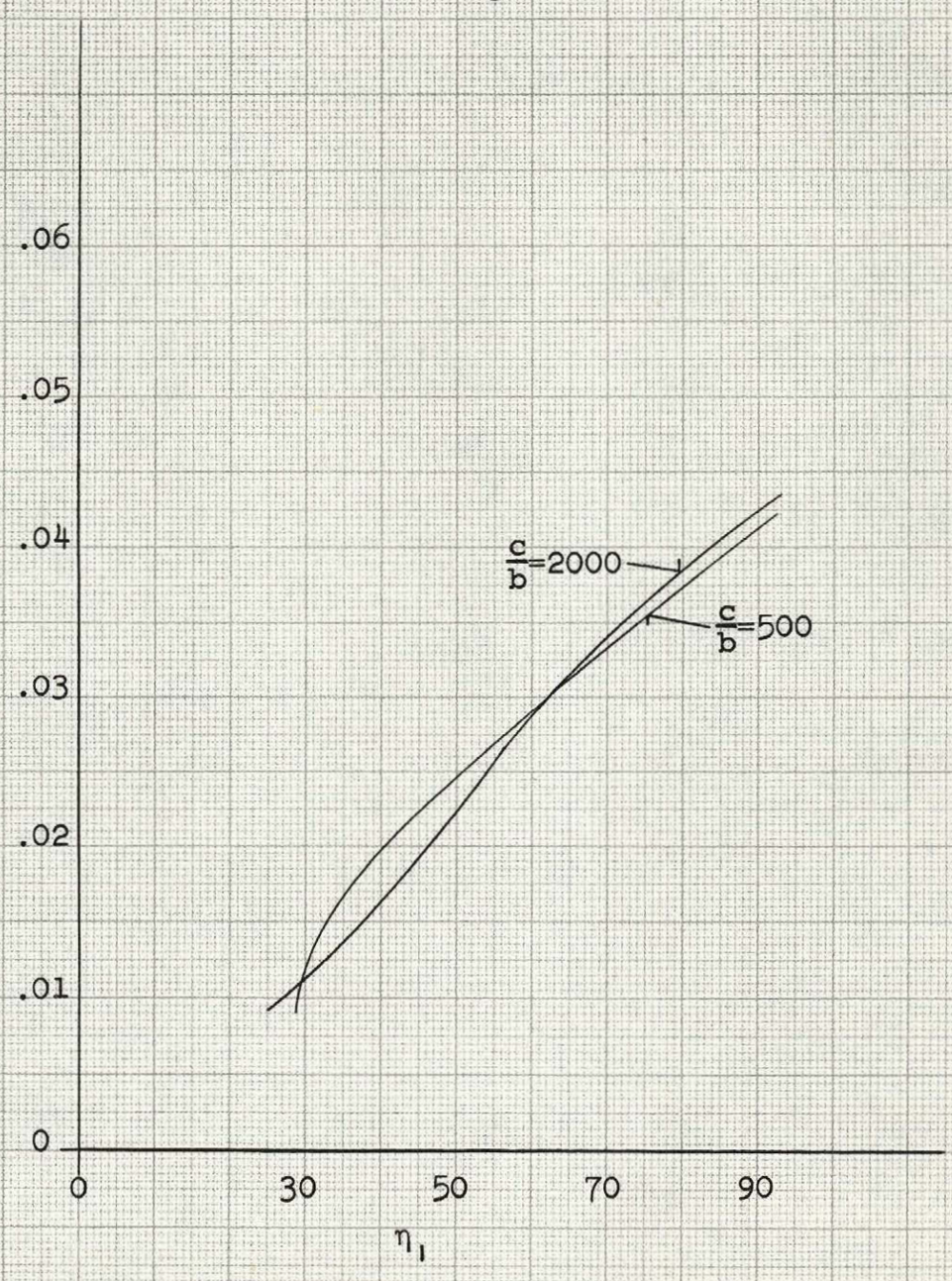

Fig. 37

Experimental and Calculated Variations of $C_{\mu_{crit}}$